The Dynamics of the Initiation of an Oklahoma Squall Line

by

FRANK PARKER COLBY, JR.

B.S., University of Michigan
(May, 1976)

Submitted in Partial Fulfillment
of the Requirements of the
Degree of

Master of Science
at the

Massachusetts Institute of Technology
(February, 1979)

Signature of Author.....
Department of Meteorology, February, 1979

Certified by.....
Thesis Supervisor

Accepted by.....
Chairman, Department Committee

The Dynamics of the Initiation of an Oklahoma Squall Line

by

FRANK PARKER COLBY, JR.

Submitted to the Department of Meteorology
on January 19, 1979 in partial fulfillment of the
requirements for the Degree of Master of Science.

ABSTRACT

The June 8-9, 1966 case from the National Severe Storms Laboratory was used to study the initiation and organization of deep convection into a squall line. This case was outstanding for this study due to its large amount of pre-convection radiosonde data. Strong surface convergence was present at least one to one and a half hours prior to the appearance of echoes on the Norman, Oklahoma radar. This convergence was examined in light of the theory of inertial instability as developed by Emanuel(1978). The results indicated that this theory could not explain the initiation of the mesoscale circulation of which the convergence was a part.

Subsequently, mesoscale analysis was used in conjunction with the calculation of cloud work functions (Arakawa and Schubert, 1974) to develop an understanding of the beginnings of deep convection. It is concluded that a combination of thermodynamic susceptibility to convection (manifested by the behavior of the cloud work functions) coincident with strong frontal surface convergence initiated the deep convection.

ACKNOWLEDGEMENTS

I must give primary recognition to Professor F. Sanders, who has helped me along numerous times, and who has allowed me to proceed at my own speed. I also thank the other members of the MIT Konvection Club, especially John Gyakum for listening to me organize my ideas and suggesting new ones.

Name and Title of Thesis Supervisor:

Frederick Sanders

Professor of Meteorology

TABLE OF CONTENTS

	Page #
Abstract	2
Acknowledgements	3
Table of Contents	4
List of Tables	5
List of Figures	6
Introduction	8
The Data	11
The Synoptic Situation	12
The Mesoscale Situation	13
Evaluation of Inertial Instability	17
Mesoscale Analysis--Cloud Work Functions	20
Summary	28
Appendix	29
Tables	31-33
Figures	34-81
Bibliography	82

LIST OF TABLES

Table #	Description	Page #
1	Corrections made to RH of radiosondes	31
2	Virtual temperature differences across front	32
3	Comparison of CWF in detail for HYB 1530 and HYB 1530 moist	33

LIST OF FIGURES

Figure #	Description	Page #
1	Map of NSSL network for 1966	34
2	Synoptic analysis for June 7, 1966, 1200Z, surface	35
3	500 mb analysis for June 7, 1966, 1200Z	36
4	Synoptic analysis for June 8, 1966, 1200Z, surface	37
5	500 mb analysis for June 8, 1966, 1200Z	38
6	Synoptic analysis for June 9, 1966, 1200Z, surface	39
7	Mesoscale analysis for June 8, 1966, 0800 CST	40
8	Mesoscale analysis for June 8, 1966, 1100 CST	41
9	Mesoscale analysis for June 8, 1966, 1400 CST	42
10	Mesoscale analysis for June 8, 1966, 1500 CST	43
11	Mesoscale analysis for June 8, 1966, 1600 CST	44
12	Mesoscale analysis for June 8, 1966, 1700 CST	45
13	Mesoscale analysis for June 8, 1966, 1800 CST	46
14	Mesoscale analysis for June 8, 1966, 1900 CST	47
15	Sounding for LTS 0548	48
16A	CWFs for SPS 1100	49
16B	Scunding for SPS 1100	50
17A	CWFs for SPS 1400	51
17B	Sounding for SPS 1400	52
18A	CWFs for SPS 1530	53
18B	Sounding for SPS 1530	54
19A	CWFs for CHK 1048	55
19B	Sounding for CHK 1048	56
20A	CWFs for CHK 1400	57
20B	Sounding for CHK 1400	58

LIST OF FIGURES (cont.)

Figure #	Description	Page #
21A	CWFs for CHK 1536	59
21B	Sounding for CHK 1536	60
22A	CWFs for WAT 1105	61
22B	Sounding for WAT 1105	62
23A	CWFs for COR 1400	63
23B	Sounding for COR 1400	64
24A	CWFs for WAT 1526	65
24B	Sounding for WAT 1526	66
25	Sounding for WAT 1257	67
26	Sounding for HYB 1400	68
27	Sounding for HYB 1400 + 1½ hours of lifting	69
28A	CWFs for HYB 1530	70
28B	Sounding for HYB 1530 and HYB 1530 moist	71
28C	CWFs for HYB 1530 moist	72
28D	Cloud tops for HYB 1530 and HYB 1530 moist	73
29A	CWFs for LTS 1527	74
29B	Sounding for LTS 1527	75
30	Schematic of mesoscale circulation of a squall line	76
31A	Stability analysis for 1100, 1400 CST	77
31B	Stability analysis for 1530, 1700 CST	78
32	Sketch of frontal circulation	79
33	Time evolution of CWFs	80
34	Results of divergence calculation at 1500 CST	81

INTRODUCTION

Deep cumulus convection represents the growth of a cloud by a buoyant updraft. The buoyancy is a function of a density difference, manifested as a virtual temperature difference, between the updraft air and the environment air. Given the proper temperature structure and an initial perturbation, a convective cloud can grow to great heights. Generally speaking, one needs a warm moist layer of air near the surface, plus a mechanism to start the activity, in order to get deep convection. Many mechanisms are possible to provide the initial perturbation. Orography can provide a forced ascent, simply by having the flow be upslope. Differential heating can create a mesoscale circulation (sea breeze type) which includes rising warm air. Low level frontal circulation involves a direct thermal circulation which also incorporates rising warm air. Gravity waves have been suggested as mechanisms for setting off convection (Tepper, 1950). Schaeffer (1975) showed that modelling the diffusion of heat and moisture across a dry line could produce convection too.

On June 8-9, 1966, a number of cumulus cells formed in the National Severe Storms Laboratory(NSSL) radiosonde network. After a short while, the cells were deep enough and had become organized into a continuous enough line for the system to be considered a squall line. Upon examination of this case, some of the above mechanisms for initiation can be ruled out. The orography is not strong enough in this area to affect the atmosphere by upslope flow.

Indeed, the flow also appears to be mostly parallel to what topography there is. The moisture gradient in the area is smaller by an order of magnitude than that used by Schaeffer (1975). The differential heating will be dealt with shortly in connection with a theory suggested by Ogura and Chen(1977).

This particular case history from NSSL has been studied by several investigators, including Eisen(1972), Fankhauser(1974), Lewis et al.(1976), and Ogura and Chen(1977). Eisen(1972) used an objective analysis scheme to derive temperature, humidity, pressure, wind, vorticity, mass convergence and moisture convergence fields. He also made time sections of the vertical structure. He was mainly interested in determining the effect the squall line had on the larger scale environment. He did note that the squall line had developed in response to a cold front and moved away from it after it formed. He also noted that the echoes formed near an area of maximum moisture convergence, though not directly on the maximum.

Fankhauser(1974) presented a partly objective, partly subjective technique for deriving a reliable height field using the NSSL data. He demonstrated this using the June 8-9, 1966 case, but looked mostly at later stages (1700 CST and later) after the convection had become organized into a squall line.

Ogura and Chen(1977) used an objective analysis technique to derive various fields of interest. They noted and discussed the fact that significant surface convergence preceeded the initial echoes, but were unable to conclude what was the cause of that

convergence. They concluded that the vertical motion associated with the convergence lifted the top of the mixed layer to saturation, and that this air then was buoyant enough to lead to deep convection. They offered four hypotheses for the convergence: a) inland sea breeze, b) vertical transport of westerly momentum c) Ekman pumping and d) synoptic scale convergence. The inland sea breeze is the result of differential surface heating creating a direct thermal circulation just as in a 'real' sea breeze. This would be seen as a 'sea breeze' front along with its associated surface wind convergence, or if the timing were perfect, as a reinforcement of the existing cold front. The former should have been visible within 4-6 hours after the onset of the heating (Anthes, 1978). As will be seen later, we don't see any convergence that is not associated with the cold front, so the first option is not operating. The second possibility is really indistinguishable from saying that diabatic heating is frontogenetical. Hence, the inland sea breeze does not explain the situation.

The vertical transport mechanism and the Ekman pumping are both dismissed by Ogura and Chen. The transport theory would imply an increase in westerly momentum on the dry side of the convergence line/front. Ogura and Chen(1977) found this was contradicted by the data. The Ekman pumping theory predicts fairly large values of vorticity at the top of the mixed layer, which again were not found. Ogura and Chen concluded that more work on the other theories of initiation was needed.

We pursued one other theory, that presented by Emanuel(1978) in which he suggested that inertial instability could predict the

formation of a mesoscale circulation similar to a frontal circulation. We also did a mesoscale analysis of the state of Oklahoma and a detailed study of the vertical temperature structure, together with its susceptibility to convection. The details will be presented in the rest of this paper.

THE DATA

NSSL is located in western Oklahoma, and in 1966 included a radiosonde network and a surface recording network (see figure 1). The radiosondes were taken on June 8, 1966, at 1100 CST, 1400 CST, and every 1½ hours thereafter until 2300 CST. Two stations also reported at 0600 CST and one station made a sounding at 0030 CST on June 9, 1966. The soundings were plotted at all of the significant levels (about every 300 meters). For 1100, 1400, and 1530 CST the soundings were smoothed by eye to 50 millibar levels (925 mb, 875 mb, 825 mb, etc.). From 1700 CST on, the data was averaged by a computer program written by Brian Reinhold, producing data at the same levels as the eye-smoothing. Data from two soundings was compared using each technique. It was judged that the two were the same within a reasonable error ($\pm$ .5° C. in potential temperature, $\pm$ .5 g/kg in mixing ratio, and $\pm$ .5 m/sec in wind). The winds were rendered into u and v components and also into a natural coordinate system oriented to give components normal and parallel to the line of convection. The relative humidities were corrected for their low bias as suggested by Teweles (1970). See table 1 for details. The standard radiosonde was redesigned be-

tween 1970 and 1974 to correct this problem.

As seen on figure 1, the surface system was not extended as far to the northwest as the radiosonde network. As a result, although the front and associated convergence penetrated the radiosonde network, the surface network was undisturbed until 1800 CST, two hours after initiation of deep convection. Consequently the data did not play a direct role in the understanding of the initiation of the convection. The data consisted of copies of time records from the various instruments showing wind, temperature, relative humidity and rainfall. A series of maps showing these variables was drawn beginning at 1800 CST, but the series was used mainly to derive a mean orientation for the line of convection and so determined the natural coordinate system described previously.

THE SYNOPTIC SITUATION

Although others have discussed the synoptics, the situation is recounted briefly here to orient the reader who has not seen the previous work.

At 1200 Z (0600 CST), June 7, 1966, a developing low pressure center can be seen over station 72363 in Oklahoma, and a surface front can be identified just west of station 72267 in Texas on the surface map, figure 2. The low apparently developed in response to the short wave trough discernible on figure 3 over Nevada. By 1200 Z, June 8, 1966, one can see in figure 4 that the low has deepened and developed a stronger circulation. The surface front on figure 2 now shows fairly marked convergence across

it. The 500 mb trough, as seen on figure 5, is now almost on top of the low center. By June 9, 1200 Z, figure 6 shows the surface low has filled, although the circulation has strengthened, and it has moved rapidly east-northeast leaving a long cold front trailing west through Oklahoma, Note that the front has become nearly stationary in Texas.

THE MESOSCALE SITUATION

A mesoscale analysis was made using the hourly station data from the stations in Oklahoma and one in Texas. The series for times from 0800 CST to 1900 CST is shown in figures 7 through 14. Where needed, reference is made to Eisen's(1972) analysis which includes a somewhat larger area.

The wind field behaved similarly to what could be seen on the synoptic scale. Initially, winds were mainly from the south. As the front moved into the area northerly components could be seen northwest of the front and an area of surface convergence could be seen centered about the front. This convergence line/front proceeded southeastward and at 1800 CST could be shown to be the same wind shift which was subsequently tracked through the NSSL surface network. Note, however, that between 1500 and 1600 CST the front stagnated near Altus (LTS), and actually retreated northward in the area south of LTS. After this time, the situation became noticeably more complex. The squall line appeared to have moved away from the front, which is frequently observed. However, the NSSL surface network analysis (not shown) indicated that a sharp wind shift moved ahead of the line of deep convection

itself as judged by the rainfall amounts. Was this the gust front? A gust front is air which has been carried downwards from higher levels in a cloud through evaporative cooling, and has spread out in a pool beneath the cloud. Hence this air is cooler(not buoyant) and more moist (through the cooling agent, evaporation) than the air around it. Given time enough, this pool can cut off the supply of warm moist air which was the fuel for the buoyant updraft, thus ending the growth of the cell. However, this wind shift in the surface network propagated as much as 30-40 km ahead of the rain shield, which appeared to be quite a large distance. In addition, the largest temperature change appeared to lag the wind shift, implying a complexity of structure. This area will not be addressed in this paper, but should be examined in the future.

The cloud history was taken from the ceiling reports and periodic synoptic reports made by the hourly stations. Early in the day, many stations reported a high thin overcast. Between 0600 and 1100 CST, many stations reported a lower stratus layer (or alto-stratus) which broke up in the next couple of hours. Some stations then reported broken stratus or scattered cumulus. By 1400 CST, the reported clouds were few and scattered. At 1500 CST, stations began reporting cumulus and towering cumulus, especially in the vicinity of the convergence line/front. By 1600 CST, the reports all pointed to the line of cells which formed along the convergence line.

The surface temperatures showed an interesting and important behavior. During the morning, general surface heating occurred

in most of Oklahoma, with the strongest occurring in a narrow tongue as shown in figures 8 and 9. This heating produced by 1500 CST a tongue of 100° F. air reaching from Altus (LTS) to near Watonga (WAT) as seen on figure 10. This strong heating at the surface had the effect of destabilizing the boundary layer. Note here that the 1400 CST map (figure 9), 6 hours at least after the onset of heating, shows only convergence of the surface wind due to the cold front. Hence, as previously mentioned, the inland sea breeze effect does not show up in the data.

The radar history was taken from a 35 mm film taken of the PPI display at Norman, Oklahoma. The echoes were traced at fifteen minute intervals starting as soon as they appeared shortly before 1600 CST. From various cloud models and a few observations, this implies that significant cumulus clouds did not exist prior to 1530 CST at the earliest (Silverman and Glass, 1973), or at least those which finally produced precipitation sized particles were absent. Note, however, that various stations reported seeing cumulus and towering cumulus at 1500 CST. Apparently many non-echo producing cumulus were forming by this time, implying that conditions were becoming less stable. From figure 10, it is clear that the stations were viewing clouds mostly along the convergence line/front where the echoes later appeared. The lessened stability was concentrated mostly in the convergence zone.

Through the many soundings, we discovered much about the pre-squall line environment in the vertical. In the morning, all of

the soundings exhibited a mixed boundary layer structure with potential temperature and mixing ratio approximately constant with height. It is even possible to see the conditions which were responsible for the low level stratus cloud in the morning. The early morning unsmoothed soundings showed high relative humidity at the 910 mb level which was nearly the level of the reported ceiling for the stratus deck. (Figure 15 shows one of the early soundings). Evidently the early morning heating created an adiabatic (probably super-adiabatic) boundary layer (shallow and near the surface) and turbulence saturated the top of this layer. As the boundary layer warming continued the temperature of the mixed layer rose as well, thereby implying a higher saturation mixing ratio. However, the mixing ratios themselves remained constant. Hence the air became unsaturated, and the clouds dispersed.

The morning heating previously referred to was not limited to the surface but extended in some cases at a lesser degree with increasing height, to 700 mb. Apparently this heating was from diffusion and eddy transport from the surface layer. One effect of this was a growth in the height of the mixed layer with time especially in the northwestern and central stations in the radiosonde network. The other effect was that the small stable layer visible in all the soundings at the top of the mixed layer was destabilized until by 1530 CST a situation developed such as figure 21B, which shows only a conditional instability at the top of the mixed layer, rather than the absolutely stable layer visible at 1100 CST (figure 19).

While the boundary layer was heating, the layer just above the boundary layer cooled by about 1^{o} C. up to about 600 to 500 mb. So, the entire atmosphere was destabilized, the sounding pivoting at the top of the boundary layer. The moisture was not very consistent. Indeed, in the northwest, the surface front moved into the network by 1400, so that part dried out at that time.

EVALUATION OF INERTIAL INSTABILITY

We considered as a possible explanation of the surface convergence the theory of inertial instability as recently presented by Emanuel(1978). In this paper, Emanuel derived stability characteristics for perturbations in a rotating Boussinesq fluid. A zonal current with horizontal and vertical shear is assumed for the equilibrium state, and thermal wind balance is assumed too. The fluid is stratified vertically as well. One result is that for values of the Richardson number ($Ri \triangleq N^2/u_z^2$) small enough, a convective circulation sets in oriented in a line parallel with the vertical shear, just as is seen in a typical squall line. (See figure 30.) We then used this result in a modified way to examine the stability of the atmosphere in the NSSL case of June 8-9, 1966.

If solutions to the linearized perturbation equations are assumed to take the form $\exp(\sigma t)$, then if σ = a real number or $\sigma^2 > 0$, growth of the perturbation will occur. σ^2/f^2 can be (assuming hydrostatics) expressed as $\sigma^2/f^2 = 1/Ri - \eta/f$, for a fluid with Prandtl number ($\triangleq \nu/\kappa$, dynamic viscosity/thermometric viscosity)= 1, and $\eta \triangleq f - u_y$. (Emanuel, 1978 and Raymond, 1977). This can be

related to q, the potential vorticity as follows:

$$q \overset{d}{=} (\nabla \times \underset{\sim}{V} + \hat{k}f) \cdot \nabla \ln \theta$$

Take $\underset{\sim}{V} = u\hat{i}$ (zonal current) where $u = u_z(z) + u_y(y)$

$$\nabla \times \underset{\sim}{V} = u_z\hat{j} - u_y\hat{k}$$

$$q = \left[u_z\hat{j} + (f-u_y)\hat{k} \right] \cdot \left(\hat{j}\frac{\partial \ln\theta}{\partial y} + \hat{k}\frac{\partial \ln\theta}{\partial z} \right)$$

$$= \left[u_z\hat{j} + \eta\hat{k} \right] \cdot \left(\hat{j}\frac{\partial \ln\theta}{\partial y} + \hat{k}\frac{\partial \ln\theta}{\partial z} \right)$$

$$= u_z\frac{\partial \ln\theta}{\partial y} + \eta\frac{\partial \ln\theta}{\partial z} \qquad (*)$$

$N^2 \overset{d}{=} g\frac{\partial \ln\theta}{\partial z}$ or $\frac{\partial \ln\theta}{\partial z} = N^2/g$

The assumed thermal wind balance implies as follows:

$\underset{\sim}{V} = (g/f)\hat{k} \times \nabla_p z$ geostrophic wind

if $\hat{i}u = \underset{\sim}{V}$ then $u = -(g/f)\left(\frac{\partial z}{\partial y}\right)_p$

$\frac{\partial u}{\partial p} = -(g/f)\frac{\partial}{\partial y}\left(\frac{\partial z}{\partial p}\right)_p$ hydrostatics implies $\frac{\partial z}{\partial \rho} = -\rho g$

or $\frac{\partial z}{\partial p} = -(1/\rho g)$

so, $\frac{\partial u}{\partial p} = (g/f)\frac{\partial}{\partial y}(1/\rho g)_p$

$= (1/f)\frac{\partial}{\partial y}(1/\rho)_p$

an ideal gas is assumed, so $p/\rho = RT$ or $1/\rho = (RT)/p$

so, $\frac{\partial u}{\partial p} = (1/f)\frac{\partial}{\partial y}\left(\frac{RT}{p}\right)_p$

$= \frac{R}{fp}\left(\frac{\partial T}{\partial y}\right)_p$

$u_z \overset{d}{=} \frac{\partial u}{\partial z} = \frac{\partial u}{\partial p}\frac{\partial p}{\partial z} = \frac{R}{fp}\left(\frac{\partial T}{\partial y}\right)_p \frac{\partial p}{\partial z}$

using hydrostatics again

$$u_z = \frac{-R\rho g}{fp}\left(\frac{\partial T}{\partial y}\right)_p$$

and using $\rho/p = (1/(RT))$ (ideal gas again)

$$u_z = \frac{-Rg}{fRT}\left(\frac{\partial T}{\partial y}\right)_p = \frac{-g}{f}\left(\frac{\partial \ln T}{\partial y}\right)_p$$

potential temperature $\Theta \overset{d}{=} T\left(\frac{1000}{p}\right)^{\kappa}$

so $\ln\Theta = \ln T + \kappa \ln 1000 - \kappa \ln p$

or $\left(\frac{\partial \ln\theta}{\partial y}\right)_p = \left(\frac{\partial \ln T}{\partial y}\right)_p$ so, $u_z = \frac{-g}{f}\left(\frac{\partial \ln\theta}{\partial y}\right)_p$

$\left(\frac{\partial \ln\theta}{\partial y}\right)_p = \left(\frac{\partial \ln\theta}{\partial y}\right)_z + \frac{\partial \ln\theta}{\partial z}\frac{\partial z}{\partial y}$. Assuming $\frac{\partial z}{\partial y}$ is small implies

$\left(\frac{\partial \ln\theta}{\partial y}\right)_p = \left(\frac{\partial \ln\theta}{\partial y}\right)_z$ and (*) implies $q = u_z\left(\frac{\partial \ln\theta}{\partial y}\right)_z + \eta\frac{\partial \ln\theta}{\partial z}$

$$= \frac{-f u_z^2}{g} + \eta\frac{N^2}{g}$$

implying $$\frac{qg}{f N^2} = \frac{-u_z^2}{N^2} + \frac{\eta}{f}$$

and since $Ri \stackrel{d}{=} N^2/u_z^2$

then $$-q\left(\frac{g}{fN^2}\right) = 1/Ri - \eta/f = \nabla^2/f^2$$

Hence, by evaluating the sign of q, we can evaluate the sign of ∇^2. This was done by a graphical procedure. The nine radiosonde stations were oriented in roughly three parallel lines, which themselves were oriented roughly parallel to the mean orientation of the line of convection. (see figure 1). The smoothed soundings were then averaged along each line, producing a mean cross section for the network, normal to the line of convection. Components of the wind parallel and normal to the line had been computed already. The data was plotted in cross sections for each time. q was then measured graphically along constant theta surfaces as detailed in the appendix. The results are shown in figures 31A,B.

Notice that even at 1530 CST, just before the outbreak of convection as seen on radar that only a very small part of the net-

work indicates an inertial instability. This can hardly be construed as a synoptic scale instability as required by Emanuel's introduction, "It is the premise of this paper that the intensity and persistence of organized convection are determined by the susceptibility of the synoptic scale temperature, moisture and wind fields to mesoscale circulations..." (Emanuel, 1978). Indeed, all that can really be postulated on the basis of this analysis is that strong vertical shear was present in the vicinity of the place where convection ensued. It should also be noted that this corresponds to the top of a mixed boundary layer, where one would expect strong shear. This is not to say that the mechanism of inertial instability was inoperative, but merely that its intensity was too low to be considered as an important part of the initiation of the convection.

MESOSCALE ANALYSIS--CLOUD WORK FUNCTIONS

If we suppose that the synoptic scale front is responsible for the convergence, then we need to make sure that the details are consistent with that structure. Notice that the virtual temperature was not the same across the front as seen on the figures 7 - 11 and also table 2. Southeast of the front, the air was warmer and wetter than that northwest of the front, which implied a density difference across the front. Given a frontal discontinuity, plus horizontal deformation, one expects to find a direct thermal circulation across the front, as manifested by convergence (Hoskins and Bretherton, 1972). That too was present here. This frontal cir-

culation is characterized by a zone of stronger horizontal temperature gradient and stronger vertical shear (locally stronger than the surrounding area). (See figure 32 for sketch). This is exactly what the analysis of the previous section showed especially near 1530 CST. Remembering finally that diabatic heating of the warm air is frontogenetical, we can easily see that the frontal circulation was enhanced by 1500 CST after the morning heating. It appears then, that frontal circulation is sufficient to explain the surface convergence.

In an attempt to analize the susceptibility to convection of the soundings in an objective manner, cloud work functions (CWF) were calculated for representative soundings at each time. Arakawa and Schubert(1977) (hereafter denoted AS) developed the CWF as it was used in our analysis. Briefly, AS used a one dimensional entraining cloud model which included variable rainout via a rain conversion coefficient ($\stackrel{d}{=}C\emptyset$) with units of 1/meters. Entrainment was also explicitly rendered by specifying fractional mass entrainment $\frac{1}{m}\frac{dm}{dz}=\lambda$, with similar units. Consequently, plots of CWF versus $C\emptyset$ are shown as a family of curves, one for each λ. The range of lambdas bracketed accepted values (Johnson et al., 1977). Little is really known about $C\emptyset$, so the values were taken directly from AS. The CWF is really an integral between cloud base and cloud top of the difference in virtual dry static energy (modified by water loading) of the cloud and the environment. The cloud top was determined as the level where the CWF was maximum and positive. So, when contributions became negative (negatively buoyant) the cloud was assumed to end.

A computer program was written by John Gyakum which took data at the levels where our smoothed sounding data existed. The program then interpolated hydrostatically between levels, and wrote out the contribution to CWF at each level for each combination of lambda and CØ. The cloud base was determined by computing the lifting condensation level (LCL) of a layer near the surface (900mb) which was an average of the two lowest levels in our smoothed soundings. The mixing ratio was then adjusted to produce condensation at a 25 mb level--a practical method allowing simplicity of programming. The mixing ratio was always adjusted upwards, if at all, a maximum of 1 g/kg. This value was judged to be a reasonable estimation of the magnitude of variation in mixing ratio under these conditions. One comparison was made between using two different values for the mixing ratio at cloud base leaving the rest of the sounding unchanged. The sounding used was HYBrid 1530. (The origin of this sounding will be explained below). Initially, a value of 11.5 g/kg was used. This implied an LCL of 700 mb. The CWFs are shown in figure 28A. The second run used 13.8 g/kg for the mixing ratio, and this was just enough to lower the LCL to 725 mb. The CWFs are shown in figure 28C. Two changes occurred. One was that the moist sounding produced cloud tops slightly higher, as seen in figure 28D. The second was that the values were quite a lot larger in magnitude, by as much as a factor of two. Upon examination of the contributions to CWF (see table 3), it is clear that the difference was not due to the lower cloud base alone. The contribution by the extra layer was slight compared with the magnitude of the total difference, and

the "moist" values were greater at every level. Hence, the change must have been due to the moisture content. One thing did not change, however. The behavior of the CWFs was the same--less variability with lambda and CØ than for other soundings. We have allowed a variability in the other soundings of less that 1 g/kg, less than half the change used in this example. So, there is some uncertainity in the values of the CWFs, but the general behavior of the CWFs should remain unaffected.

Lambda, as discussed by Johnson et al. (1977) and others can be regarded as a size parameter = constant/cloud radius. So, different lambdas can imply simply different sized clouds. One of the main differences between soundings was the effect of lambda and CØ on CWF. For soundings very near the echo producing area, lambda and CØ had a much smaller impact on CWF (see figure 21A). Evidently, for some soundings, clouds of any size could grow, whereas other soundings needed very large clouds, (small lambda) (see figure 18A). This is not to say that small clouds did not appear, or that large clouds grew more easily than small ones. All this means is that deep convection could only occur for large clouds, but deep convection need not have occurred at all. The requirement stated in the introduction still held, namely that both the environment must be conducive, and there must exist a lifting mechanism to start things off. Small scale turbulence and small inhomogeneities in moisture and temperature could and did produce many small cumulus. However, these small scale clouds did not grow very deep. What is being said here, then, is that for those

soundings which could grow only large clouds, it meant that larger scale perturbations were required to produce deep convection. For those soundings which were not sensitive to lambda, small inhomogeneities could lead to deep convection.

The second major difference between soundings was more obvious. Many soundings indicated that the air was negatively buoyant for some distance above cloud base. To suppose clouds to grow under such conditions implied strong vertical motion forcing the air to rise through the stable layer. So, the behavior of the CWFs indicated something about the stability above cloud base and sensitivity to cloud size. (This second point can be seen best on the soundings, figures 16B through 25B).

Before going on, it should be noted that as Warner(1970) pointed out, assuming a constant lambda implies that there is no such thing as an undilute tower growing inside a cumulonimbus cloud. Indeed, the one-dimensionality itself prevents this, as long as lambda $\neq 0$. However by choosing a range of lambdas, it seems that statistically, the model is reproducing reality in some average sense. And, even if that vague assumption is not true, it is at least true that the CWF represents a measure of susceptibility to convection, whether or not the model accurately depicts reality.

Due to time limitations, all of the soundings could not be run through the CWF program. So, one sounding was chosen for each of the three lines described above and shown in figure 1 at each time prior to 2000 CST. The stations were chosen to represent a cross-section through the echo area but consideration was also given to

time continuity, trying as much as possible to keep the same station at each time.

Looking at the results in time series, it can be seen that as the heating destabilized the atmosphere, the negative buoyancy decreased and the variability in CWF became less as well, as long as the moisture level cooperated. WAT 1526 showed a remarkable temperature profile--very unstable--but could not grow large sized clouds (see figures 24A,B). CHK 1536, however, exhibited a stable layer, but had a low CWF variability and high CWF values once the negative buoyancy was overcome (figures 21A,B). Another view of the time sequence appears in figure 33. Although only one choice of CØ and lambda is given, the indications are rather dramatic. SPS and CHK showed the rises mainly due to destabilization due to surface heating and 700-500 mb cooling, and also to some extent due to an increase in moisture ($\frac{1}{2}$ to 1 g/kg) near the top of the mixed boundary layer. For CHK from 1100 to 1400 CST moisture above the boundary layer increased greatly. This mitigated the effect of destabilization, yielding CWF of not greatly higher value. However the moisture increase in the environment lessened the effect of entrainment as seen in comparing figures 19A and 20A. From 1400 to 1530 CST the boundary layer moisture increased, which worked to increase CWF values just as destabilization did.

WAT from 1100 to 1530 CST showed destabilization, but marked moisture redistribution. Its boundary layer became much dryer and the air from above the boundary layer to 550 mb showed increased moisture by as much as 2 times. Hence, the moisture did

not cooperate and the behavior is as seen in figure 33.

The echoes which appeared at 1600 CST were located almost midway between WAT and CHK (see figure 11), and were almost on the axis of high temperature. In an attempt to make a guess at what a sounding between CHK and WAT would have been like, a hypothetical HYBrid was constructed. The temperature was set at 100°F. at the ground, and presumed adiabatic up to 700 mb (average of WAT and CHK). The sounding above that was the average of WAT and CHK, though WAT and CHK were quite similar above 700 mb. The moisture was taken as an average between the two, though presumably the convergence line/front represented a discontinuity in moisture and the cells formed on the moist side implying that the moisture in HYB might have been too low. The sounding for HYB 1530 is shown in figure 28B. To lend some credence to the existence of HYB, LTS 1527 is plotted next (figure 29B). LTS is located very nearly on top of the front at 1530 CST. The two soundings were remarkably similar, and both yielded CWFs quite similar (figures 28A,29A), though LTS's were lower in value (remember the caution about the numbers). Also noteworthy is that both LTS and HYB exhibited no negative buoyancy. However, no echoes appeared in the vicinity of LTS until after 1700 CST. What was the difference if it was not the sounding?

A look at the 1500 CST surface analysis (figure 10) indicates a region of strong surface convergence, nicely defined by six wind reports. We calculated the divergence in the box defined by the six stations, and found its value to be -4.3×10^{-4} sec^{-1}. Assuming a value of -4.0×10^{-4} at 965 mb (ground), a linear

increase in divergence with pressure, going to zero at 800 mb, and using continuity in pressure coordinates, we obtained the omega profile shown in figure 34. Using $\omega = \frac{\partial p}{\partial t}$ which implies $\partial t = \frac{\partial p}{\omega}$, we calculated time from 900 mb to 700 mb. The time involved was on the order of 2 hours, which indicated only that this magnitude of convergence was sufficient to change the environment on a short time scale. An earlier HYB sounding is shown in figure 26 for 1400 CST. This was constructed by averaging boundary layer top, boundary layer potential temperature (one temperature for the whole layer, assumed constant in the whole layer), and averaging potential temperature above the boundary layer for WAT 1357 (figure 25) and CHK 1400 (figure 20B). The moisture was assumed to be that of CHK 1400, as the surface front had already passed WAT by 1400 (see figure 9), and WAT had dried out significantly in the boundary layer. If we apply lift for 1½ hours according to the divergence calculation shown above, we have a sounding like figure 27 in the boundary layer. Clearly, this ignores the fact that the convergence was not acting on HYB at that magnitude for that length of time. Also heating of about 1°C., as seen at CHK, would change the sounding too, destabilizing it but raising the LCL. However, it is apparent that convergence of the magnitude shown could indeed have saturated the air in the vicinity of HYB.

So, in the HYBrid sounding we have the most unstable boundary layer coupled with sufficient moisture to produce significant CWFs for all lambdas and CØs. LTS 1527 does something similar, but what LTS doesn't have is the surface convergence. Although our analysis

does not show data south of LTS, Eisen's (1972) did. He showed that while there was strong convergence where we found it, the divergence near LTS was on the order of 10^{-5} sec^{-1}. Therefore, it appears that the convection started only when both the convergence and associated vertical motion and the proper thermodynamic environment coincided.

SUMMARY

Our findings indicate that the line of convection was initiated by frontally produced (and diabatically enhanced) convergence and the diabatically destabilized boundary layer structure as demonstrated by the behavior of the CWF. Of secondary importance was the increase of moisture in the upper parts of the boundary layer. The convection was organized into a squall line because its initiation was due to linear elements. There is still much to understand about the subsequent history of this squall line, especially its behavior as it passed through the NSSL surface network. Much also remains to assessing the value of the cloud work function as a measure of the susceptibility of the environment to convection. We have, at least, shed some light on the initiation and organization of convection in this case.

APPENDIX

The method used for deriving the sign of q, and therefore ∇ is as follows:

Assume a situation for a stable atmosphere as shown below

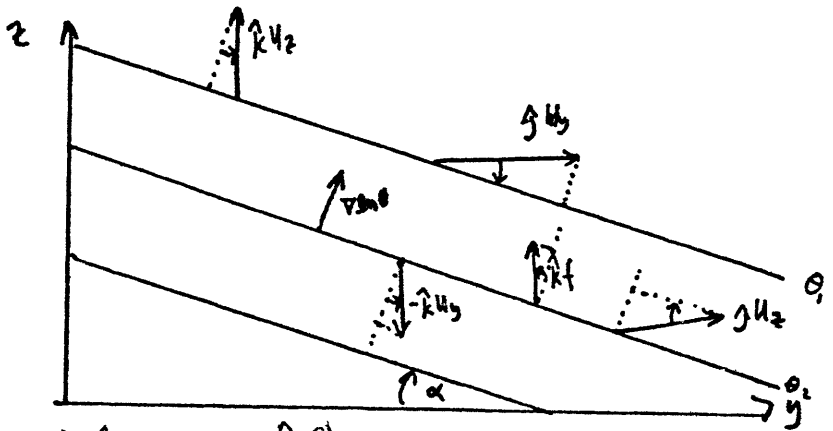

$$q = (-\hat{k}u_y + \hat{\jmath}u_z + \hat{k}f)\cdot\nabla\ln\theta = -\hat{k}u_y\cdot\nabla\ln\theta + \hat{\jmath}u_z\cdot\nabla\ln\theta + \hat{k}f\cdot\nabla\ln\theta$$

so we have contributions from each term, and each contribution can be written as the projection of the component along $\nabla\ln\theta$. We also make the approximation that the magnitude of $\nabla\ln\theta = \frac{\partial\ln\theta}{\partial z}$

from the diagram, each is expressed as follows:

$$-\hat{k}u_y\cdot\nabla\ln\theta = -u_y\cos\alpha\,\frac{\partial\ln\theta}{\partial z}$$

$$\hat{\jmath}u_z\cdot\nabla\ln\theta = u_z\sin\alpha\,\frac{\partial\ln\theta}{\partial z}$$

$$\hat{k}f\cdot\nabla\ln\theta = f\cos\alpha\,\frac{\partial\ln\theta}{\partial z}$$

$$\text{So } q = \frac{\partial\ln\theta}{\partial z}\left(-u_y\cos\alpha + u_z\sin\alpha + f\cos\alpha\right)$$

Notice from the diagram, the compnnent of the shear of U (zonal wind, with horizontal and vertical shear) along a constant theta surface in the +y direction is:

$$= (\hat{k}u_z + \hat{\jmath}u_y)_{\theta,+y} = -\sin\alpha\,u_z + u_y\cos\alpha$$

$$\text{So, } q = \frac{-\partial\ln\theta}{\partial z}(\text{shear})_{\theta,+y} + f\cos\alpha\,\frac{\partial\ln\theta}{\partial z}$$

We let $f\cos\alpha = f$

So $$q = -\frac{\partial \ln\theta}{\partial z}(\text{shear})_{\theta,ty} + f\frac{\partial \ln\theta}{\partial z}$$

$$\frac{q}{fN^2} = \frac{q}{f}\frac{1}{\frac{\partial \ln\theta}{\partial z}} = -\frac{(\text{shear})_{\theta,ty}}{f} + 1$$

$$\frac{\sigma^2}{f^2} = -\frac{g}{fN^2}q = \frac{(\text{shear})_{\theta,ty}}{f} - 1$$

For $\frac{\sigma^2}{f^2} > 0 \Rightarrow (\text{shear})_{\theta,ty} > f$

Note that the direction of tilt does not affect the result.

The diagrams are drawn for a constant two m/sec interval in u. Hence, by measuring the distance between contours of u along a constant theta line, we can measure the shear.

When measuring distance, we use the fact that the vertical scale is much exaggerated.

For neutral stability, $\frac{\partial\theta}{\partial z} = 0$, the assumptions made break down, and, indeed $N^2 \to 0$ implying $q/N^2 \to \infty$. So, the whole problem breaks down. Therefore, the diagrams should not be considered below the 313 isotherm, as the soundings provide considerable evidence that the boundary layer was neutrally stable in the radiosonde network.

Table 1

Corrections made to the relative humidity as set forth by Teweles (1970). The day correction was used for 1100, 1400, 1530, 1700, and 1830 CST, and the night correction was used for 2000 CST.

pressure (mb)	day factor	night factor
1000-701	1.18	1.06
700-501	1.28	1.09
500-250	1.61	1.20

RH(true) = RH(measured) x factor

Table 2

Virtual Temperature Difference Across the Front
taken from figures 7 through 14

Time	NW of the front			SE of the front		
0800	GUY	296.0	⟷	GAG	300.2	
1100	GAG	302.5	⟷	VAN	304.9	
				CSM	306.7	higher elevation
1400	GAG	305.6	⟷	VAN	308.9	
	CSM	308.5	⟷	HOB	312.4	
				LTS	311.7	
1500	VAN	309.5	⟷	END	311.3	
	CSM	310.1	⟷	HOB	312.5	

Table 3

Contributions to CWF λ = 10% per km $C\emptyset = 1 \times 10^{-3}$ per meter

HYBrid 1530 LCL * base = 700 mb	p(mb) above base	HYBrid 1530 LCL* moist base = 725 mb
16.9	25	17.3
24.0	50	37.4
31.2	75	46.5
37.0	100	55.9
50.3	125	61.7
78.7	150	77.4
90.2	175	115
80.0	200	132
72.8	225	123
82.7	250	120
88.2	275	136
101	300	148
106	325	169
125	350	184
128	375	214
128	400	232
101	425	245
37.3	450	233
negative	475	188
"	500	70.2
Total 1380		2610

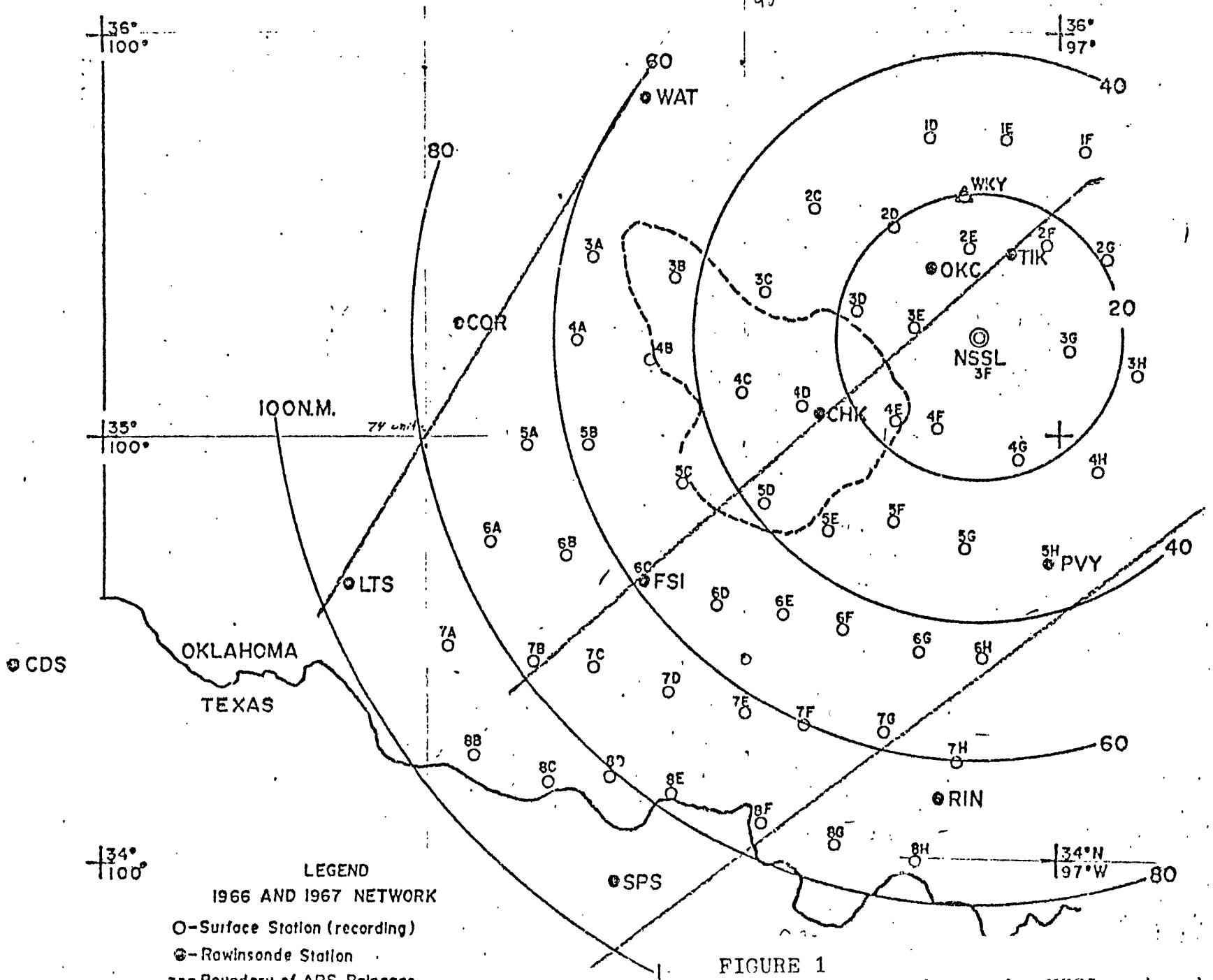

FIGURE 1
This map shows the NSSL network as it existed in 1966 for this case. Taken from Barnes, et.al. (1971).

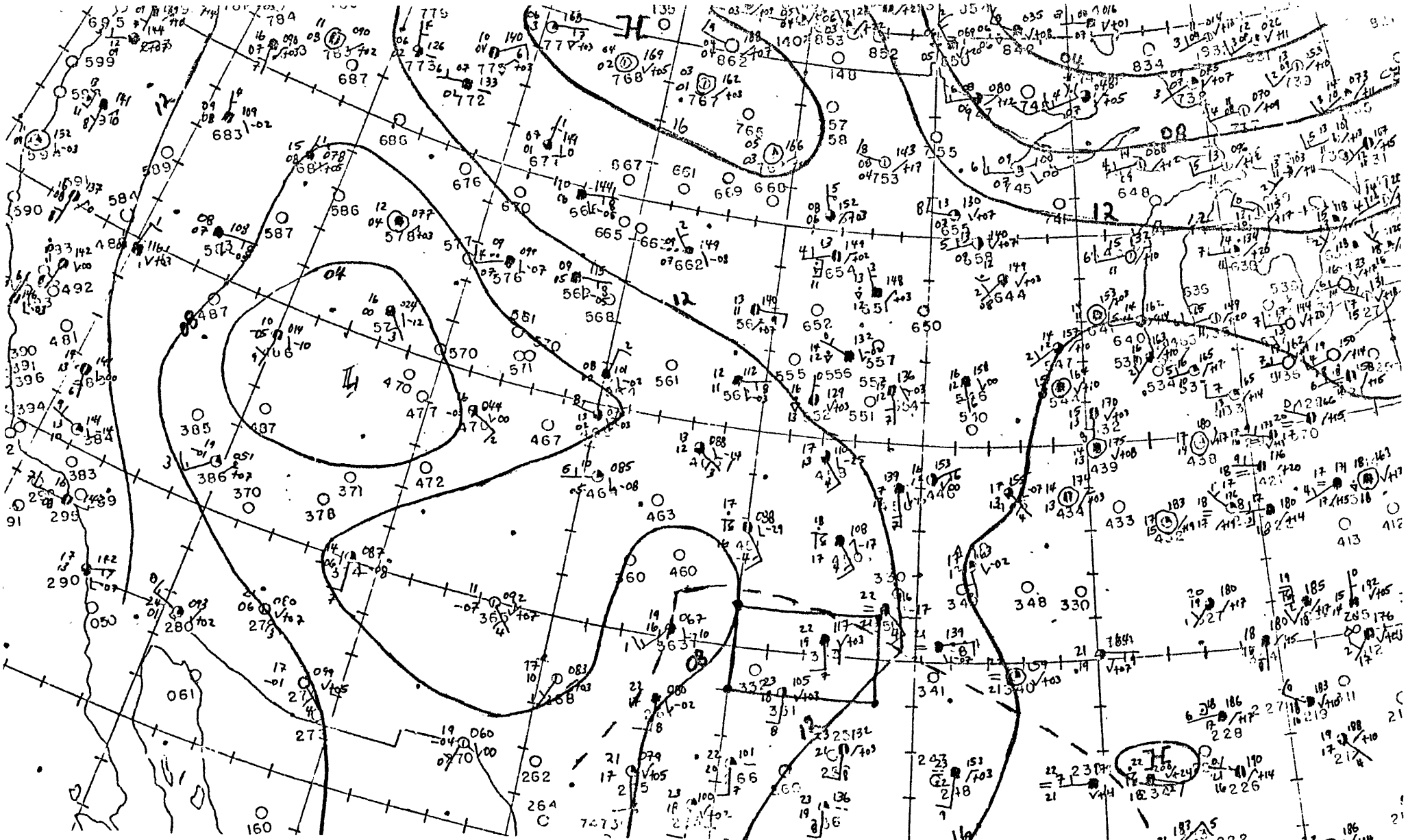

FIGURE 2

Surface synoptic analysis for June 7, 1966, 1200 Z (0600CST). Solid lines are isobars at 4 mb intervals. Each station has plotted pressure, wind speed and direction, temperature and dew point, sky cover, current weather and 3 hour pressure change. Winds are in knots, temperatures in °C. Plotting model follows US standard (abbriev.) form. Dashed lines show fronts. The approximate location of the NSSL area is shown by a box with dots at the corners.

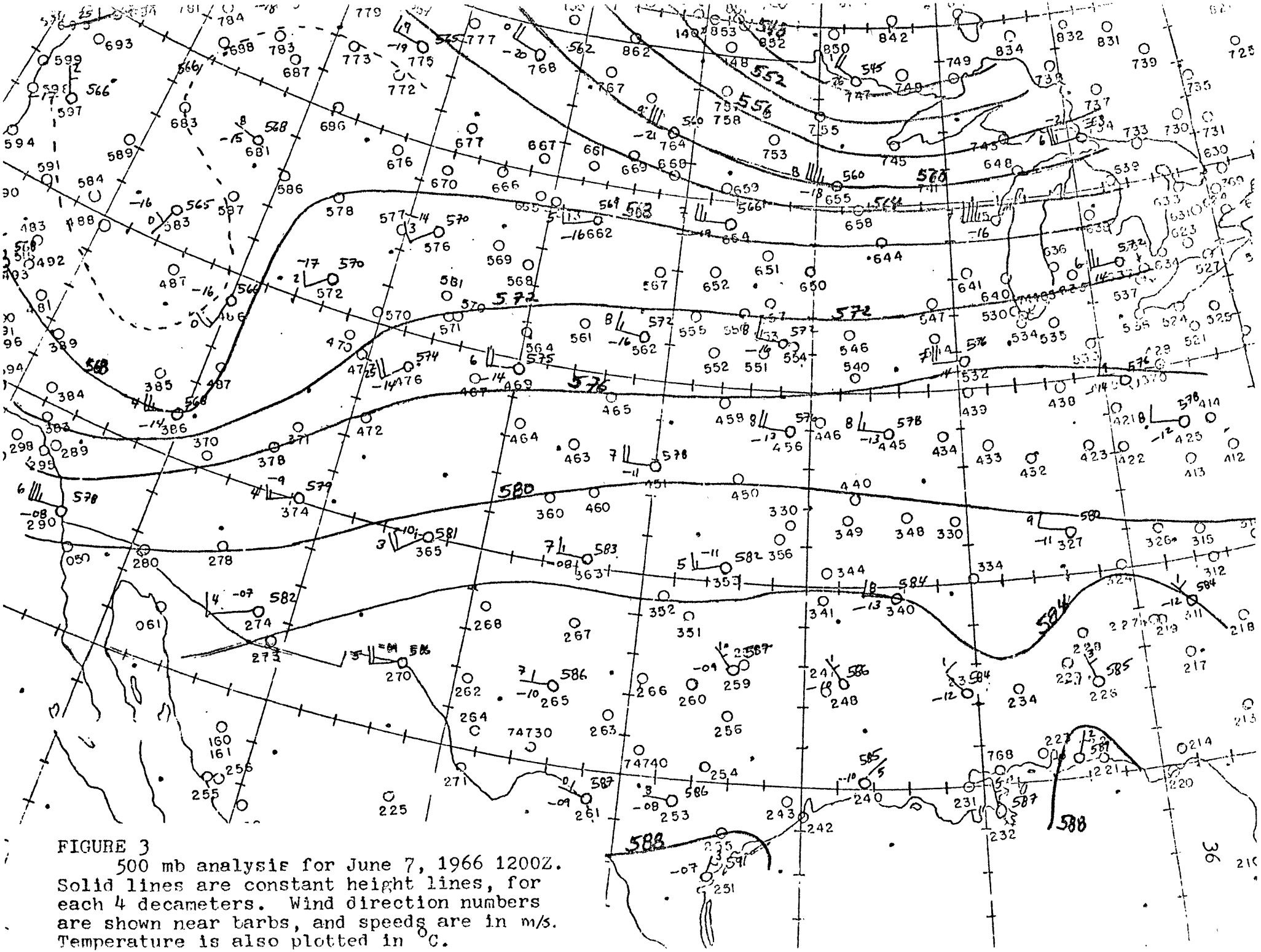

FIGURE 3

500 mb analysis for June 7, 1966 1200Z. Solid lines are constant height lines, for each 4 decameters. Wind direction numbers are shown near barbs, and speeds are in m/s. Temperature is also plotted in °C.

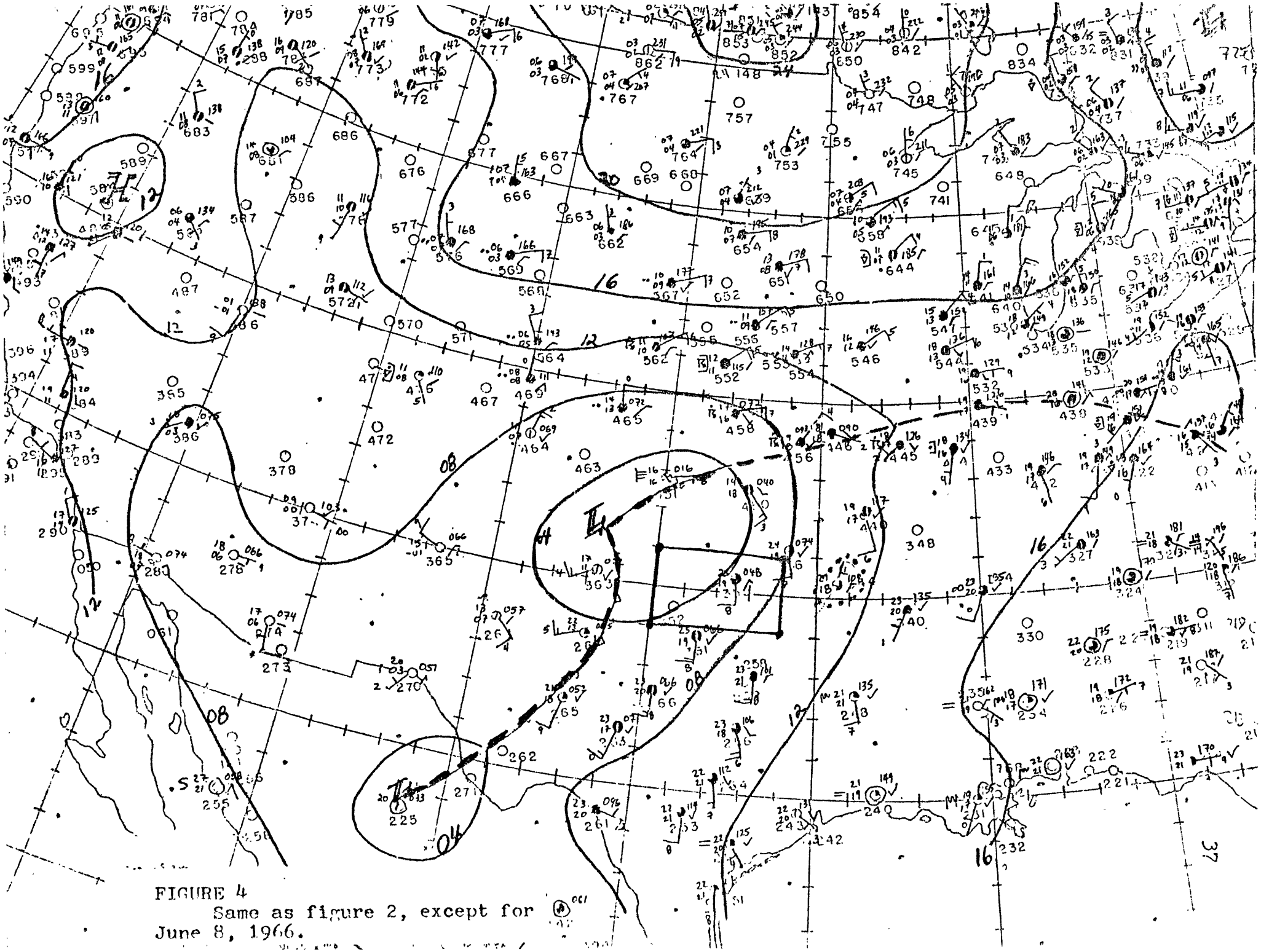

FIGURE 4

Same as figure 2, except for June 8, 1966.

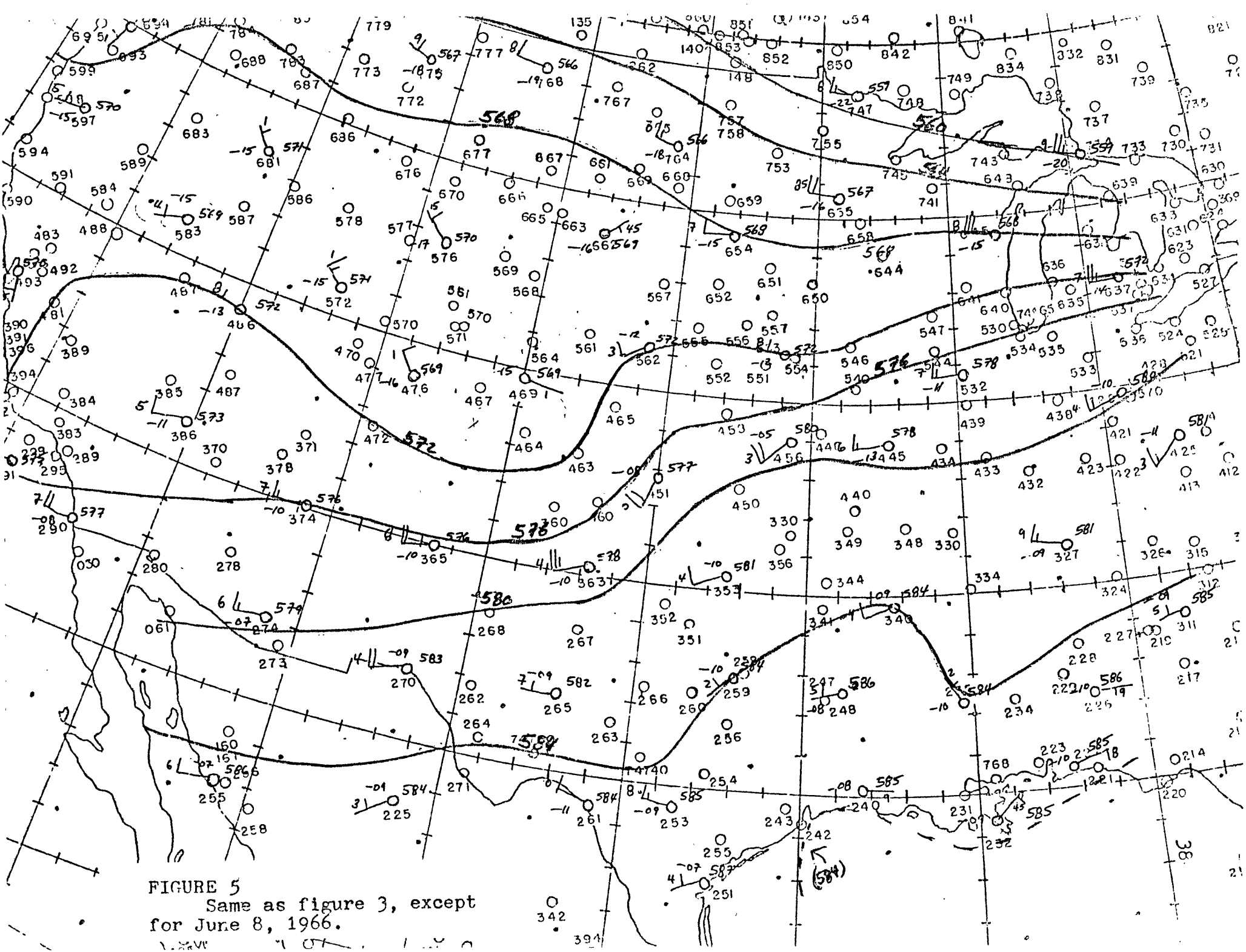

FIGURE 5
Same as figure 3, except for June 8, 1966.

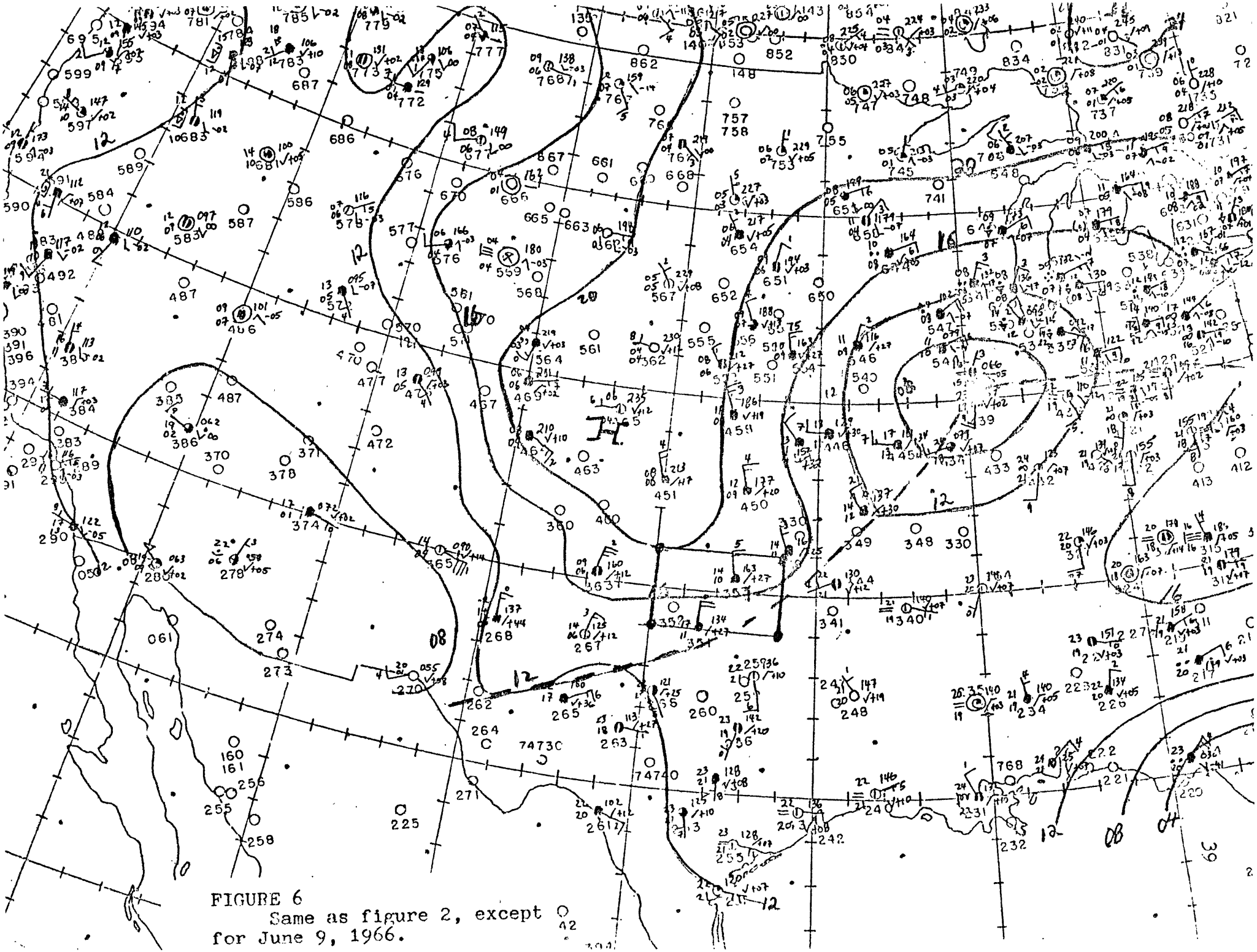

FIGURE 6
Same as figure 2, except for June 9, 1966.

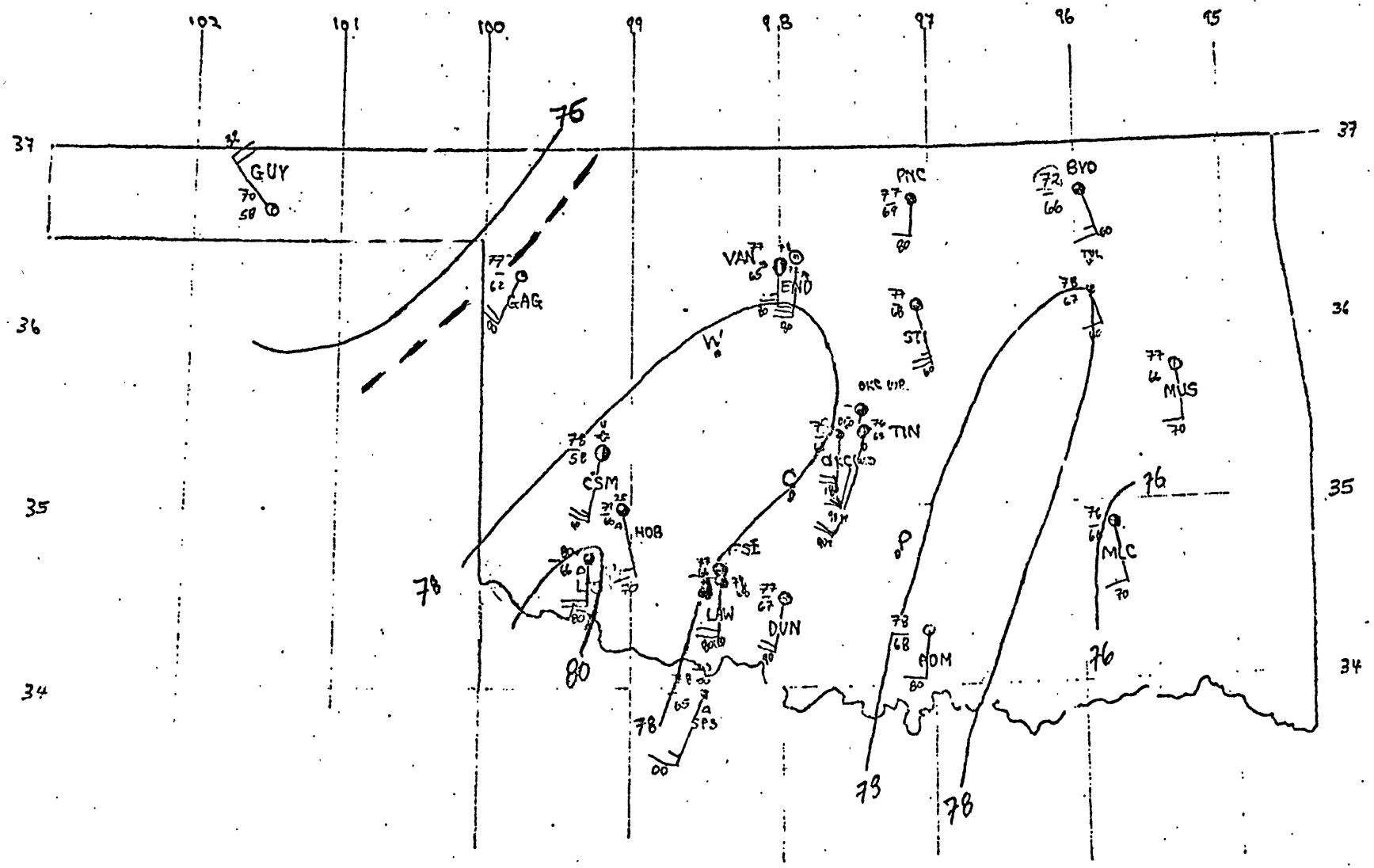

FIGURE 7

Mesoscale analysis of Oklahoma at 0800 CST. Each station has plotted wind speed (knots) and direction, temperature and dew point (^{o}F.), sky cover, current weather, and high, middle and low cloud types where available, following standard US form. Temperature is analyzed for each 2^{o}F. and surface wind shift/cold front is dashed.

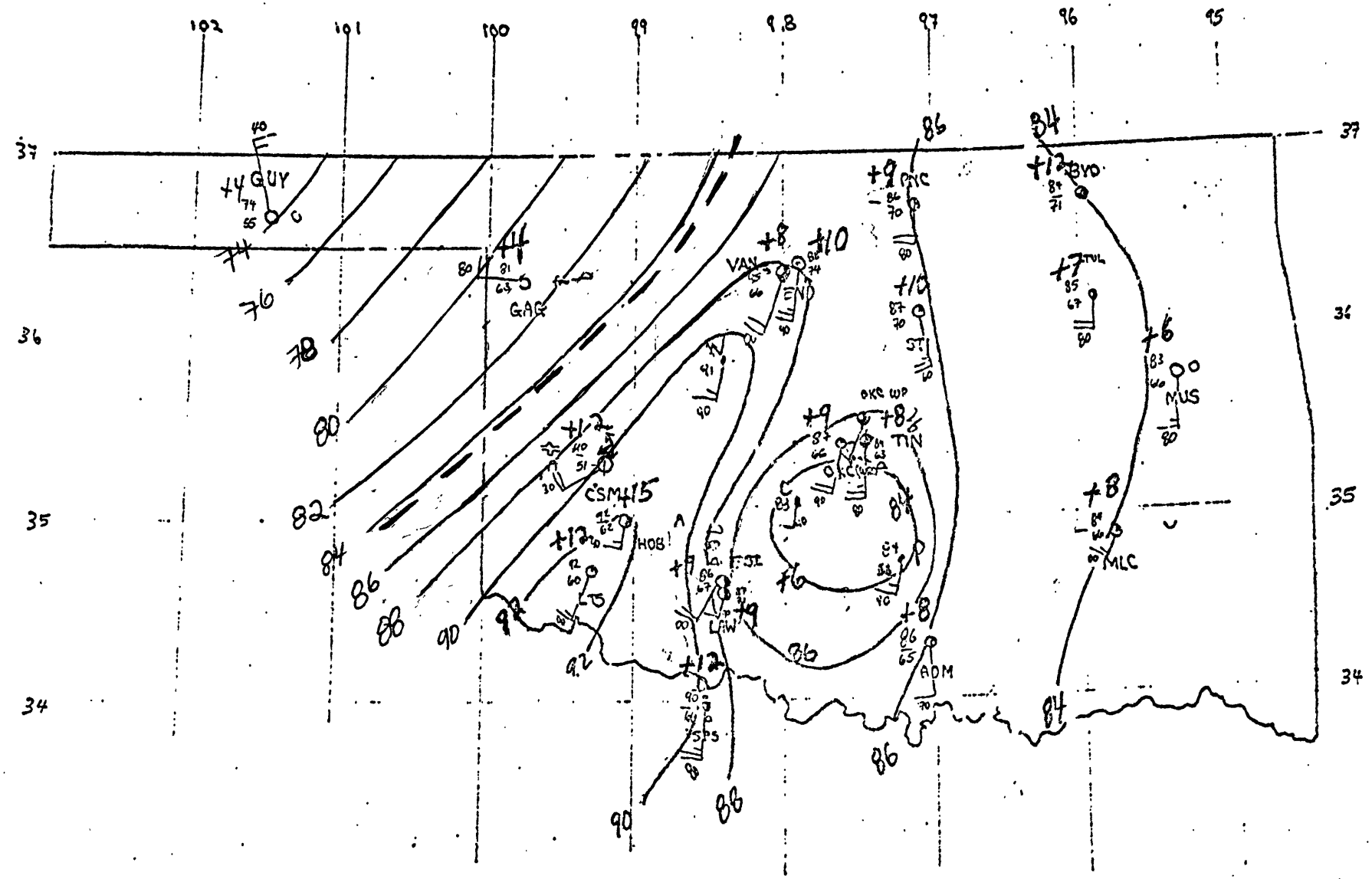

FIGURE 8

Same as for figure 7, except for 1100 CST. Cloud types from comments are plotted to the right of station. Large numbers with plus (+) sign indicate 3 hour temperature change.

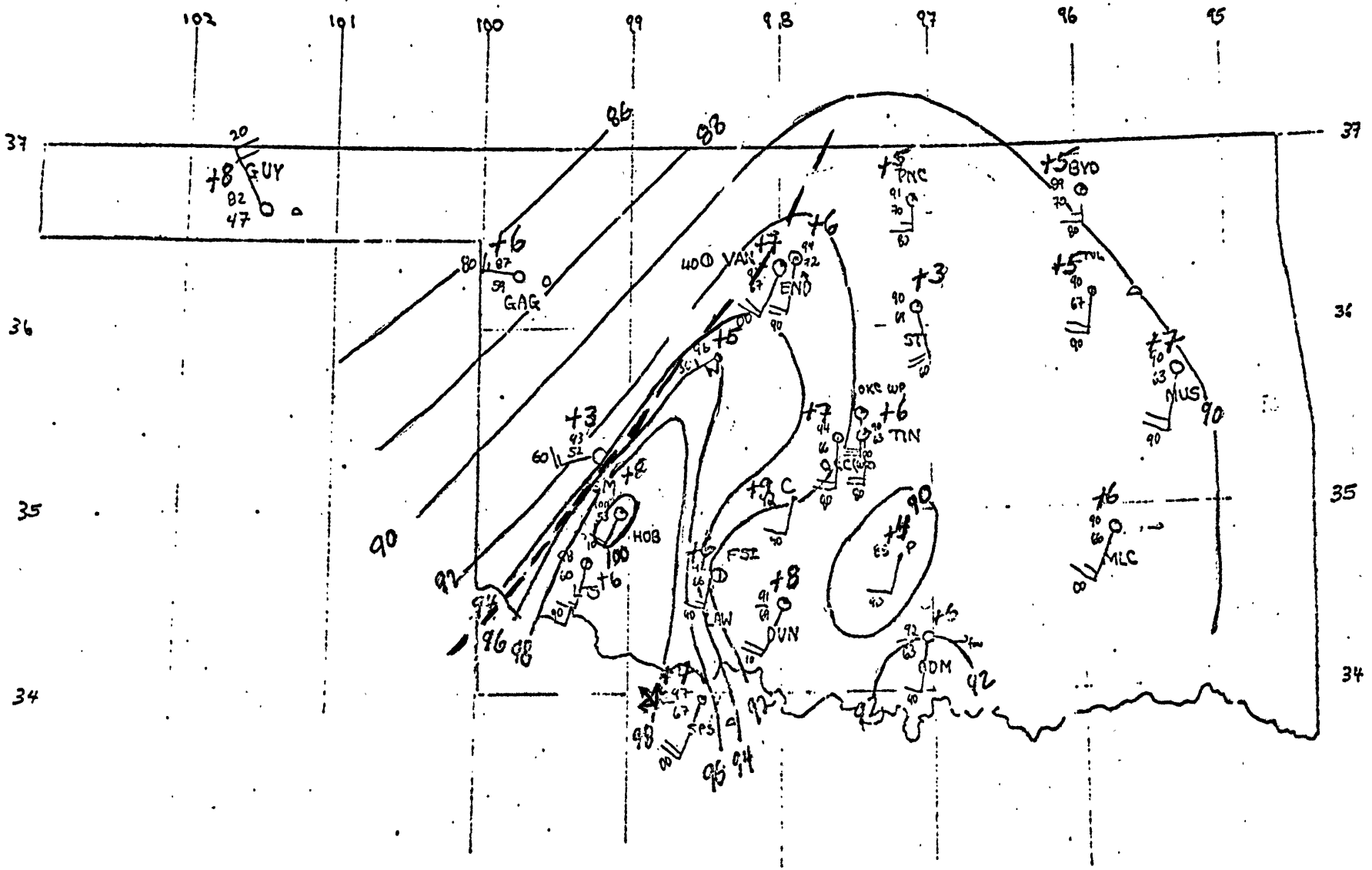

FIGURE 9
Same as figure 8, except for 1400 CST.

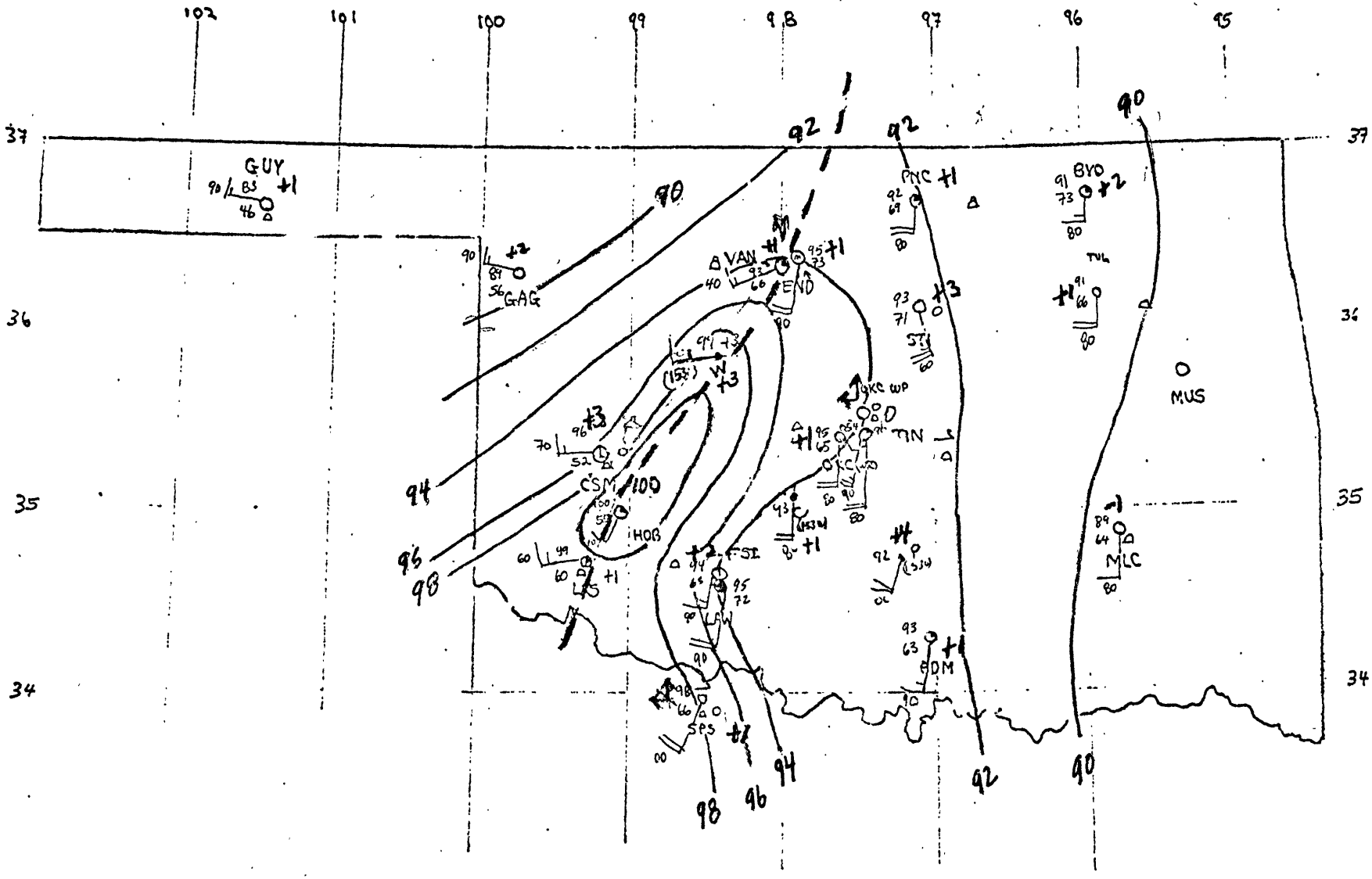

FIGURE 10
Same as figure 9, except for 1500 CST. Where cumulus were sighted, the direction is plotted by arrows. Temperature changes are for 1 hour. Off hour observations are designated by time (1530).

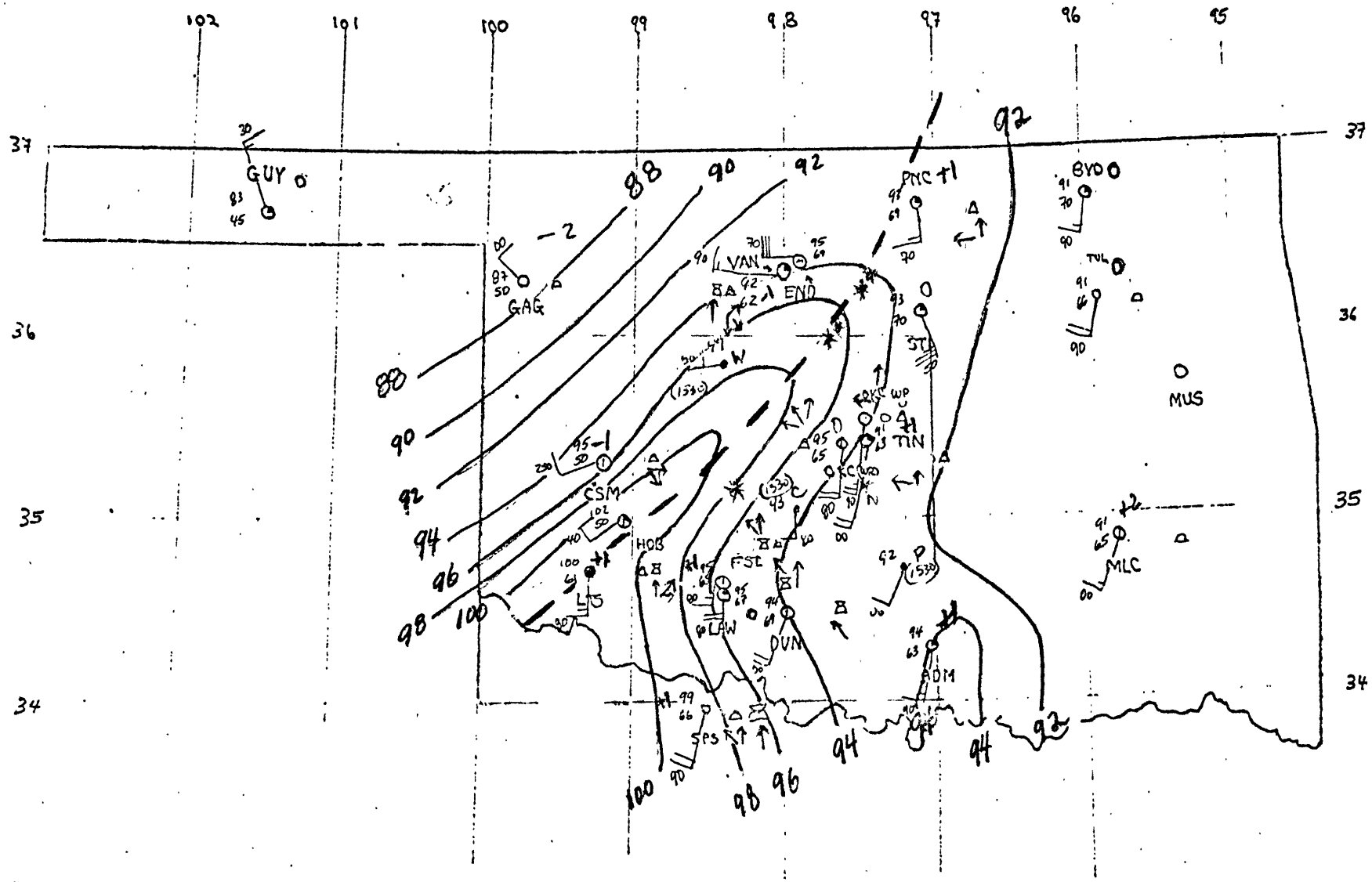

FIGURE 11

Same as figure 10, except for 1600 CST. Asterisks represent radar echoes as seen at Norman, Oklahoma *N = Norman site.

1700 CST JUNE 8, 1966

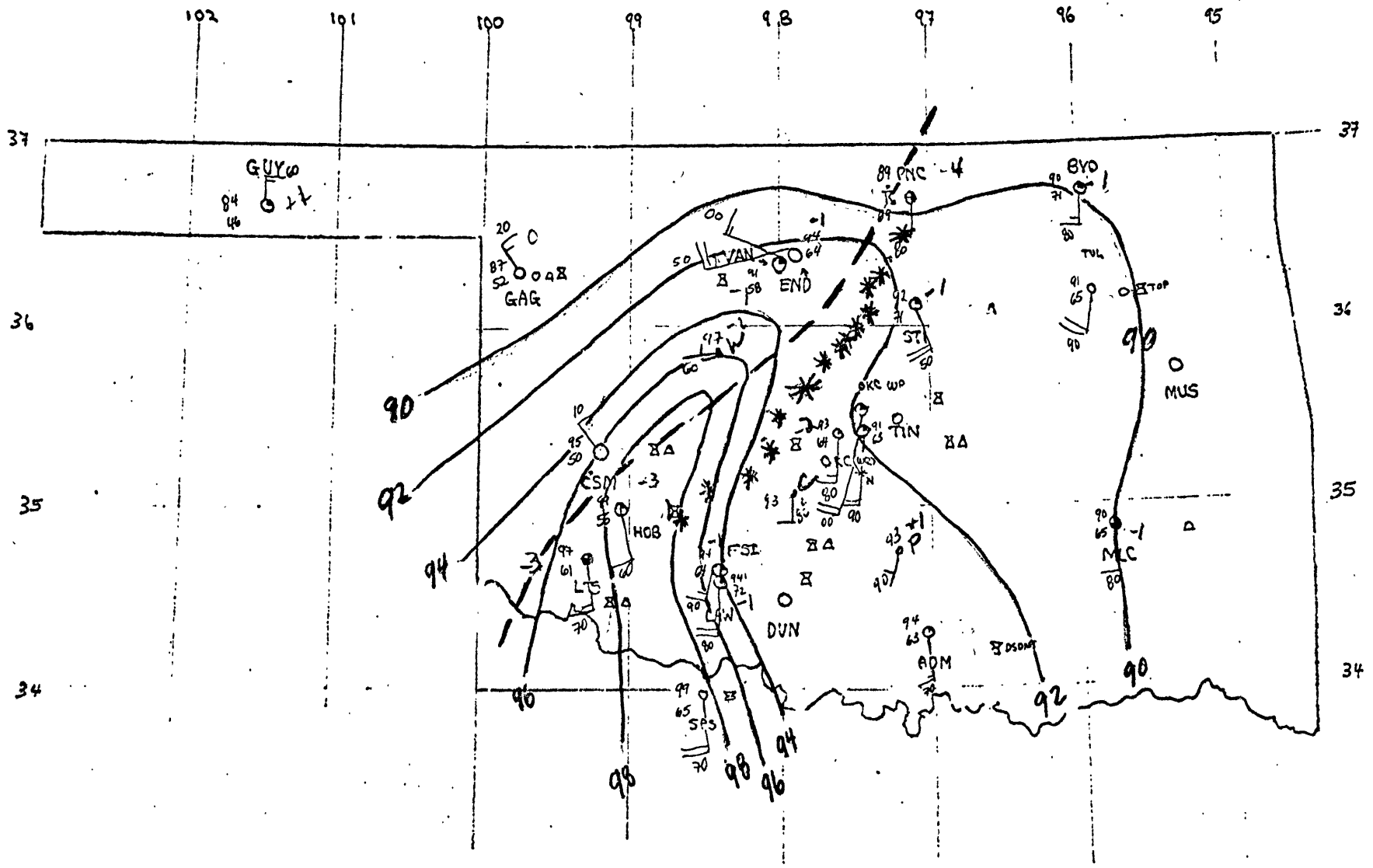

FIGURE 12
Same as figure 11 except for 1700 CST. Arrows not drawn anymore.

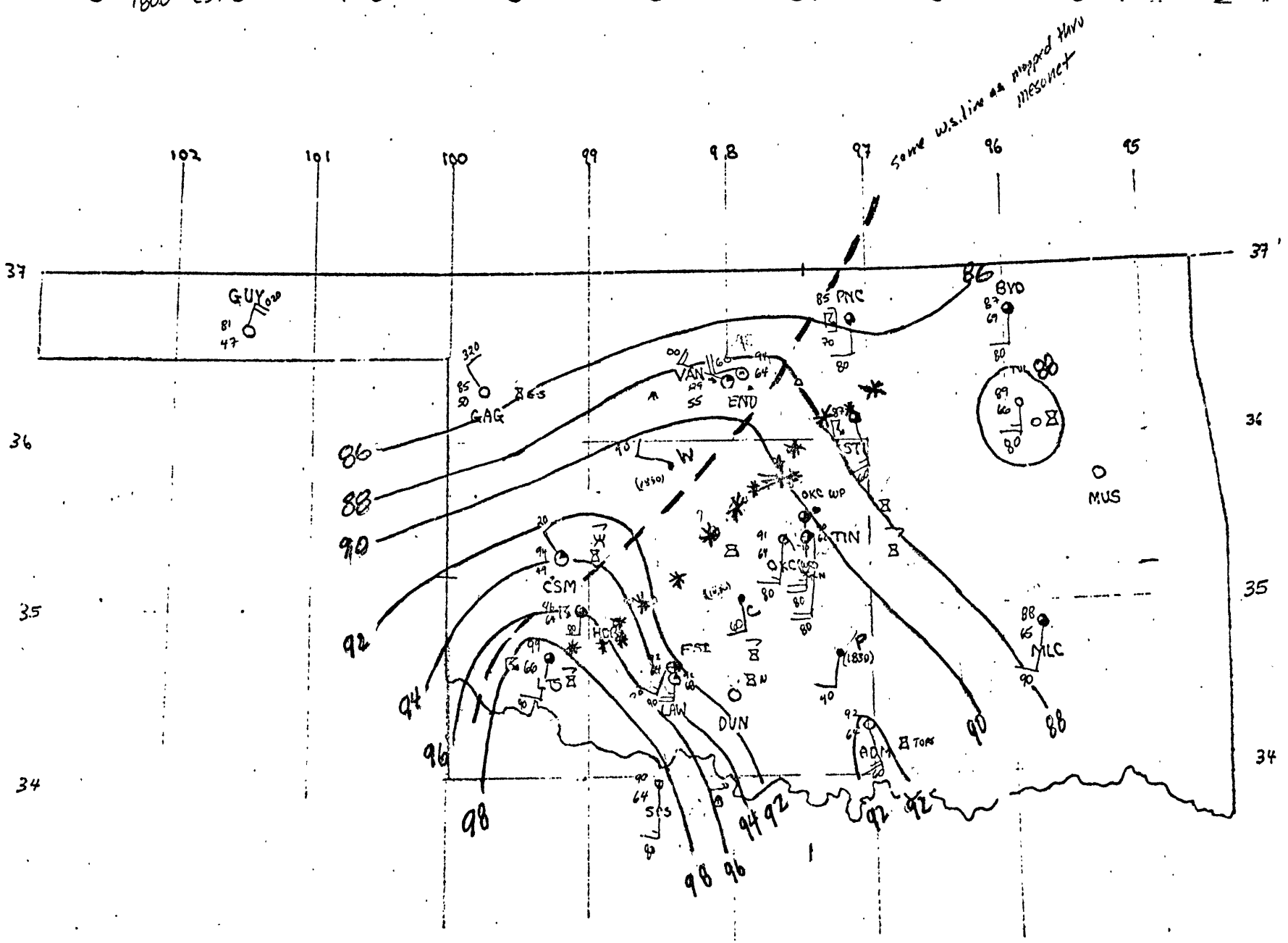

FIGURE 13
Same as figure 12, except for 1800 CST.

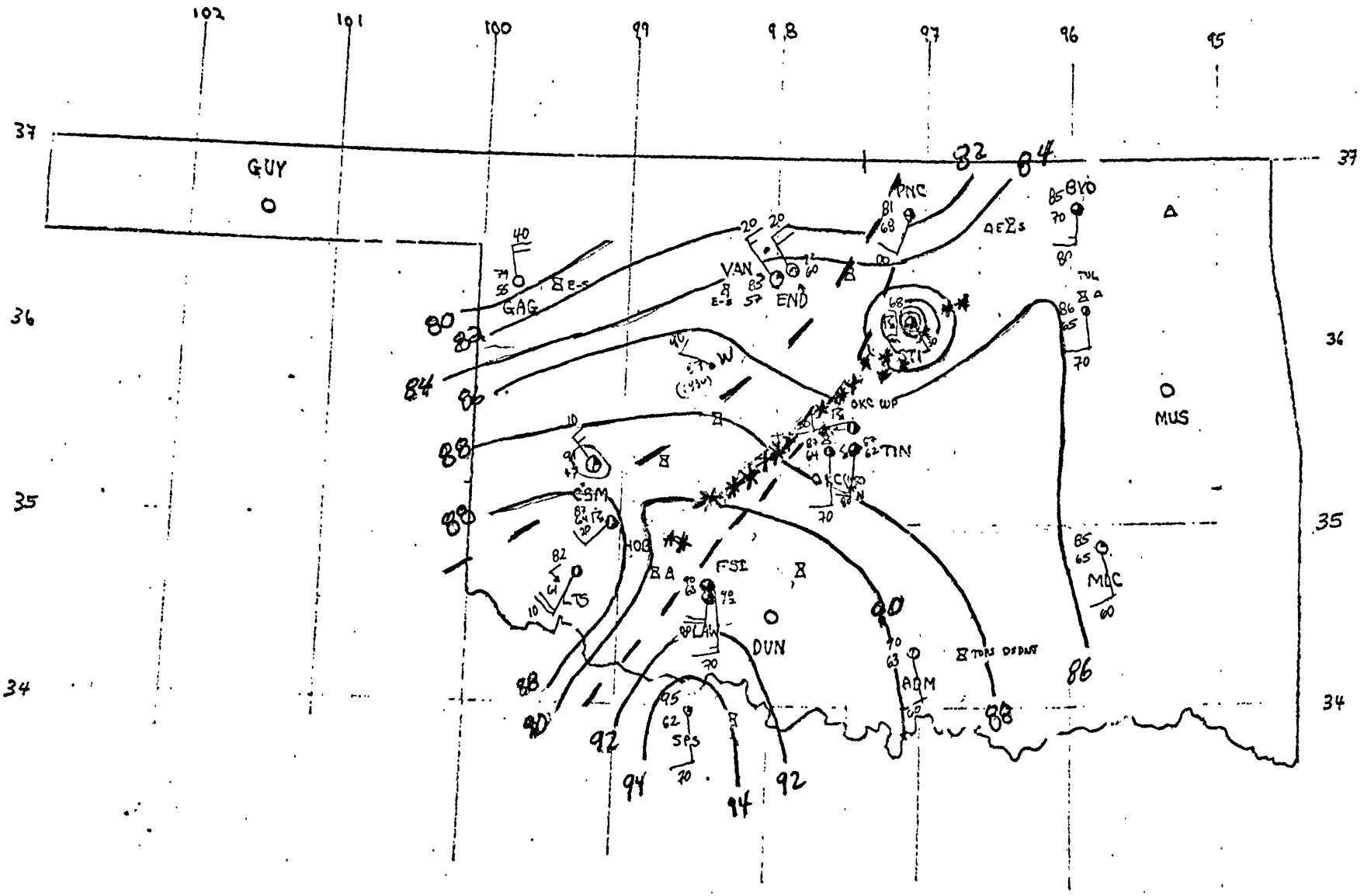

FIGURE 14
Same as figure 13, except for 1900 CST. Isotherms around STI were not resolvable.

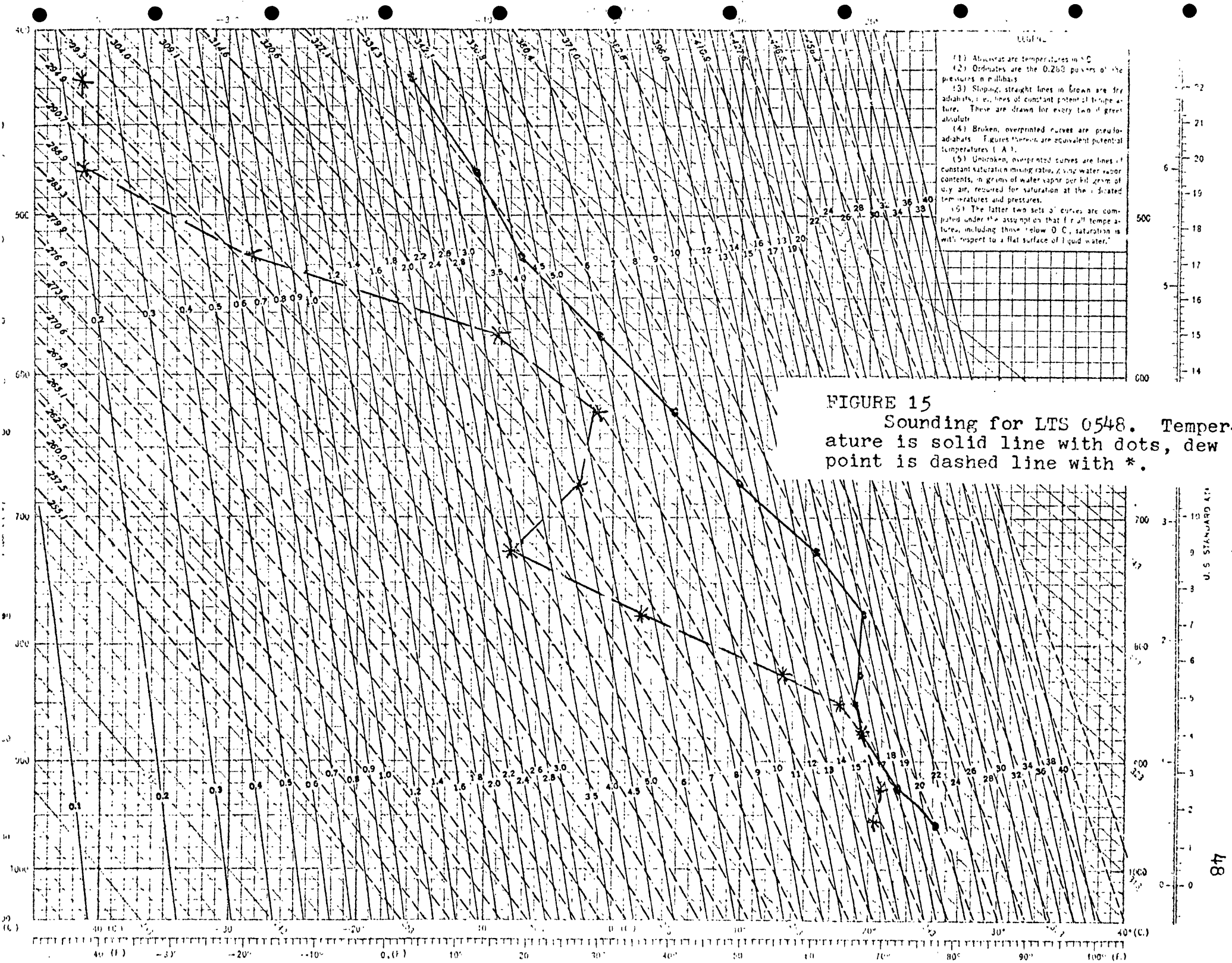

FIGURE 15
Sounding for LTS 0548. Temperature is solid line with dots, dew point is dashed line with *.

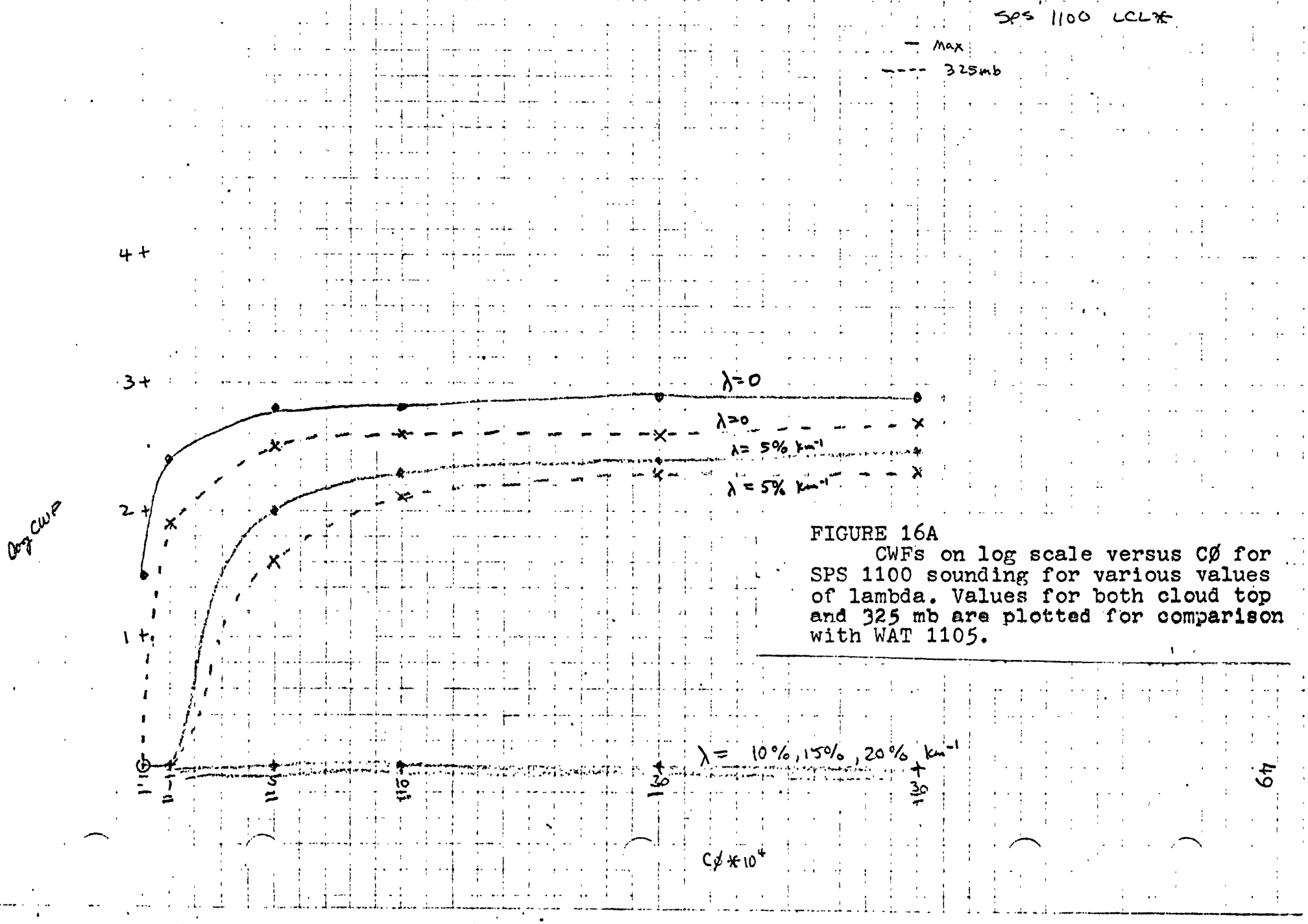

FIGURE 16A
CWFs on log scale versus Cø for SPS 1100 sounding for various values of lambda. Values for both cloud top and 325 mb are plotted for comparison with WAT 1105.

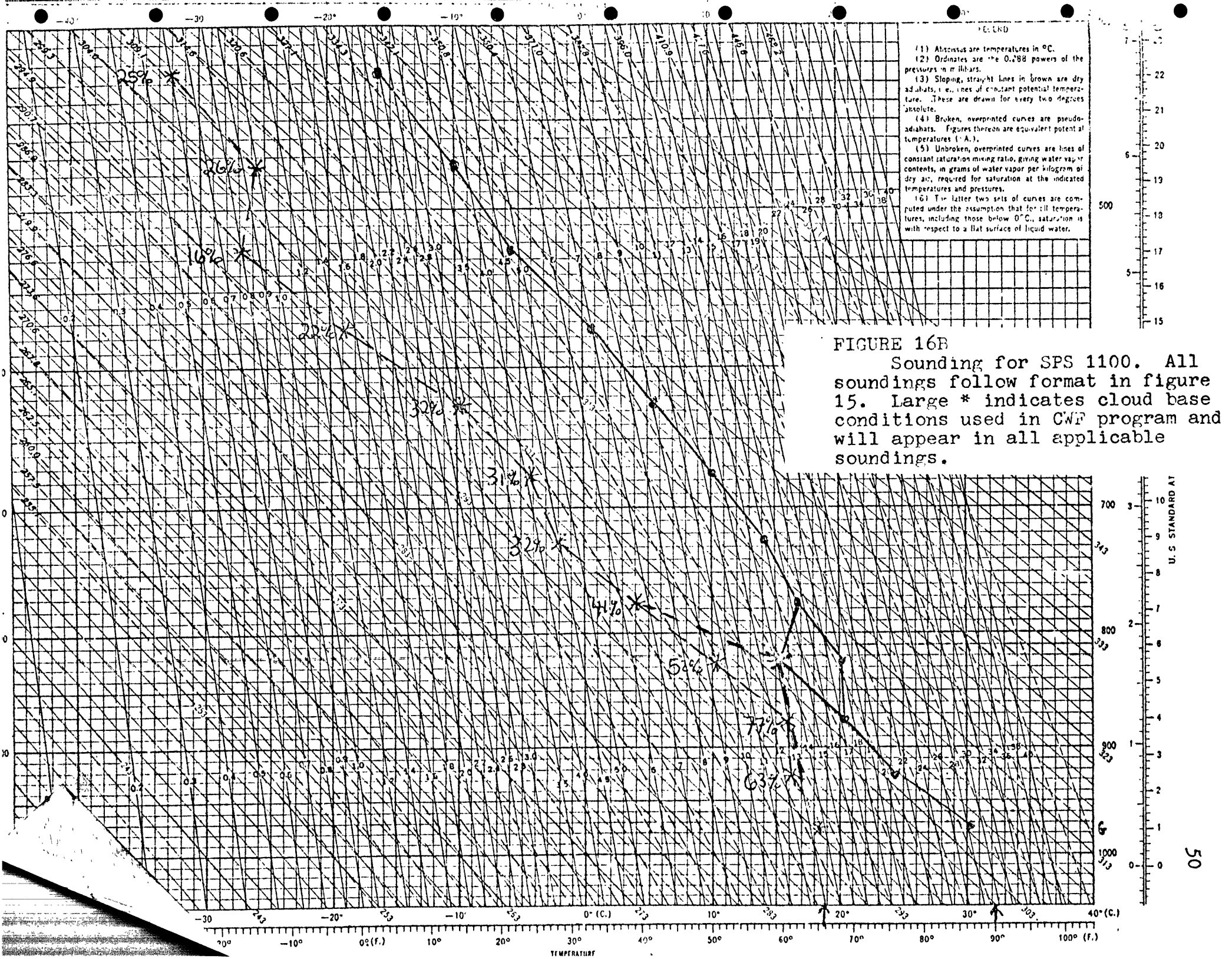

FIGURE 16B

Sounding for SPS 1100. All soundings follow format in figure 15. Large * indicates cloud base conditions used in CWF program and will appear in all applicable soundings.

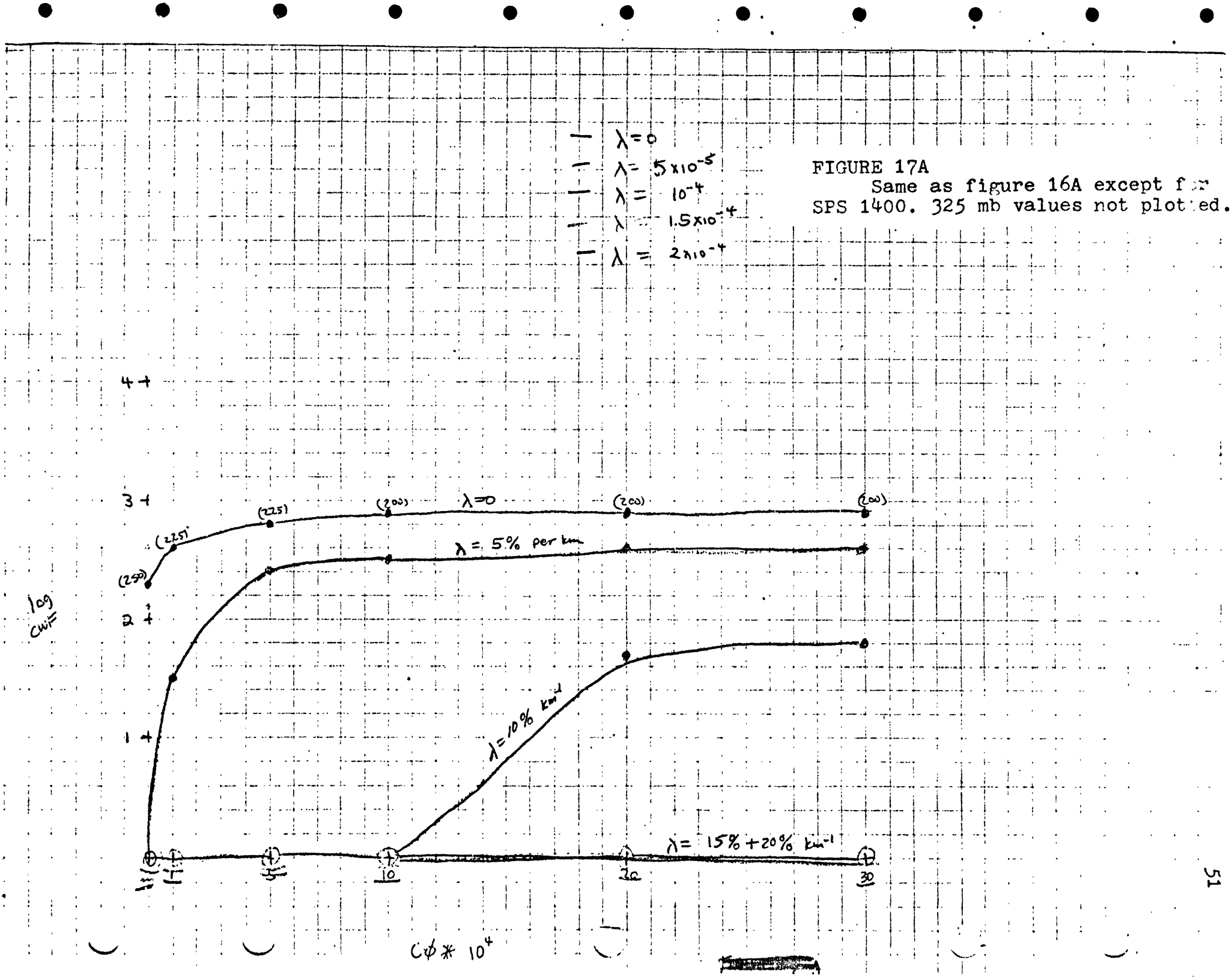

FIGURE 17A
Same as figure 16A except for SPS 1400. 325 mb values not plotted.

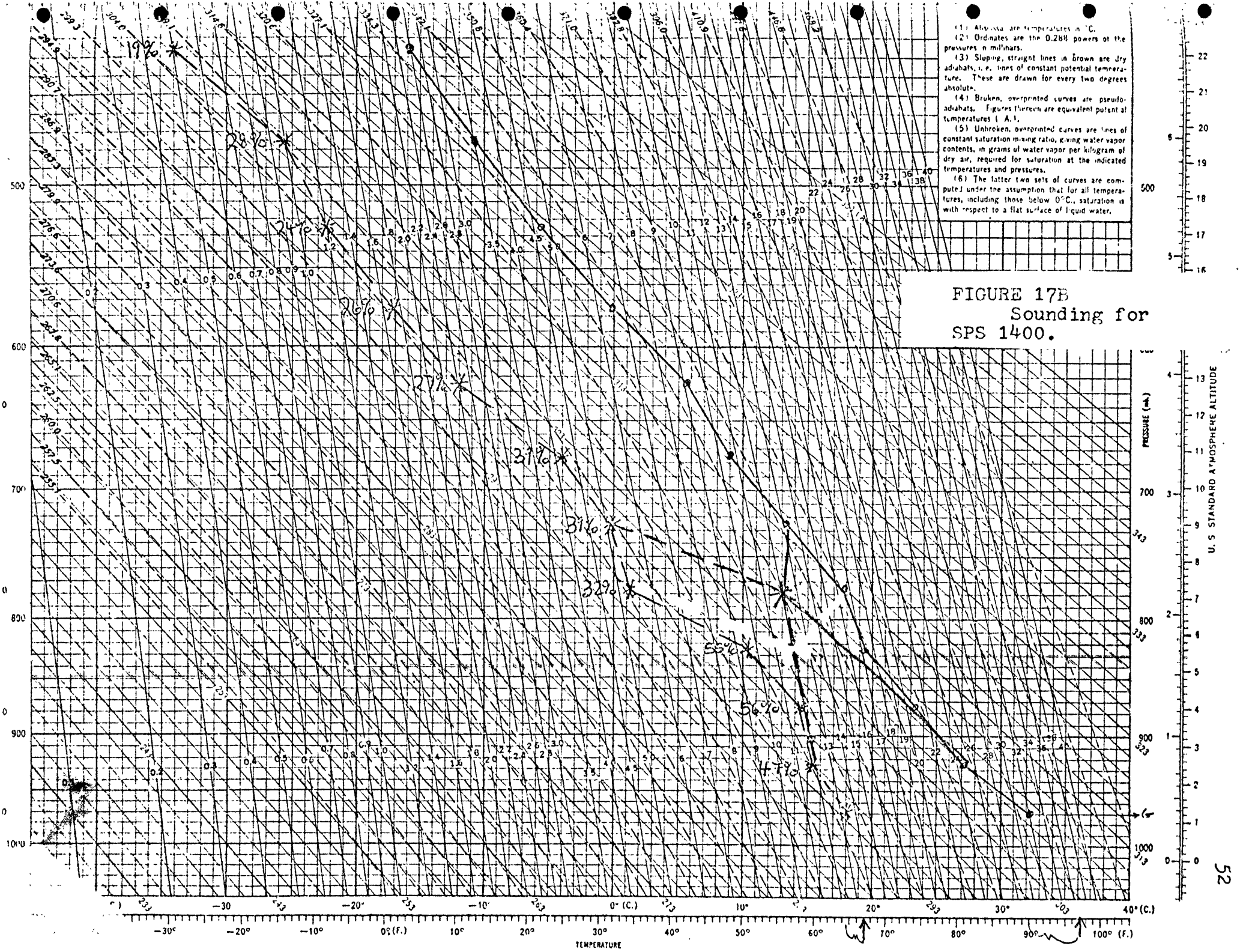

FIGURE 17B
Sounding for
SPS 1400.

FIGURE 18A
Same as figure
17A except for SPS 1530.

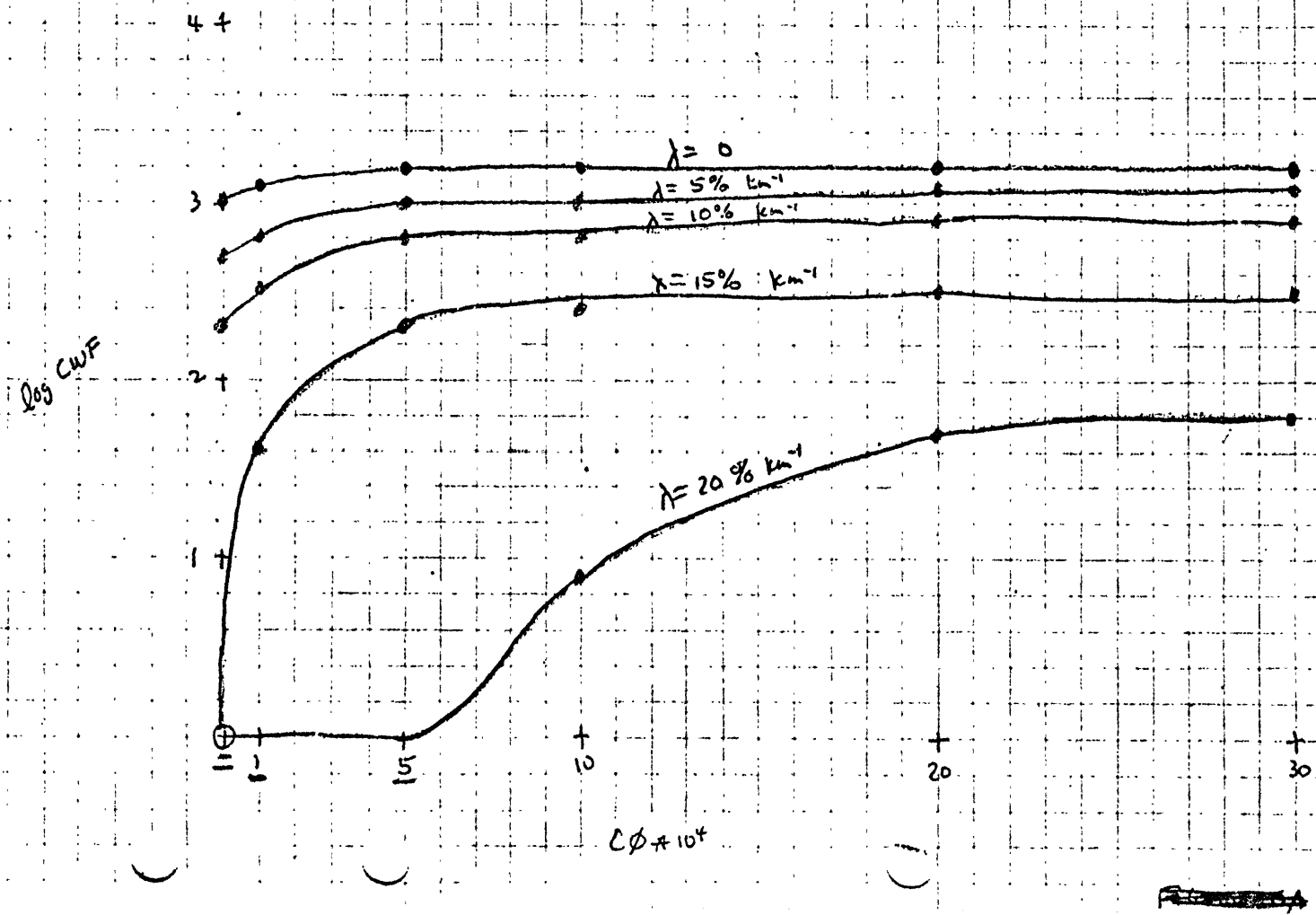

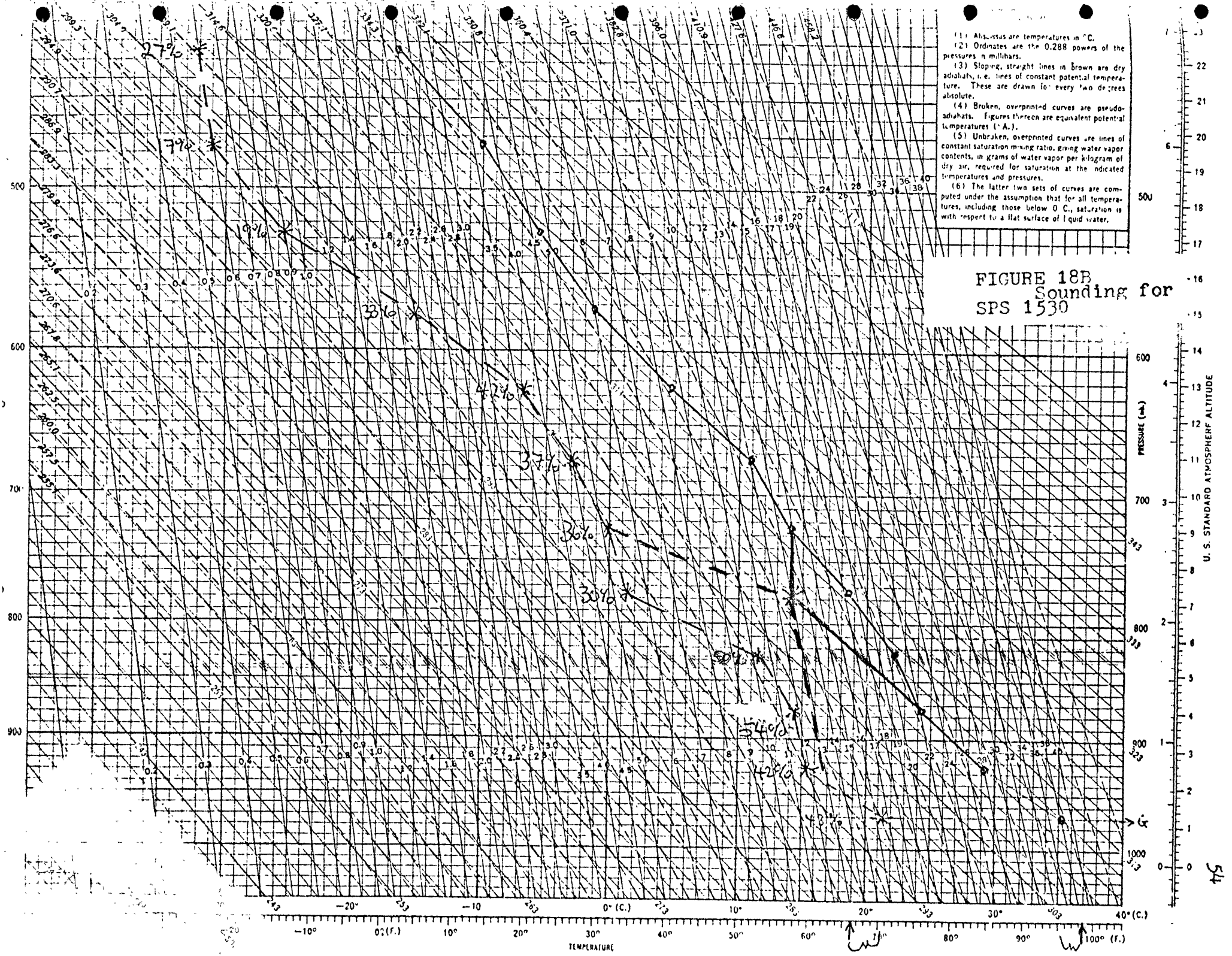

FIGURE 18B Sounding for SPS 1530

FIGURE 19A
Same as figure 16A except for CHK 1048.

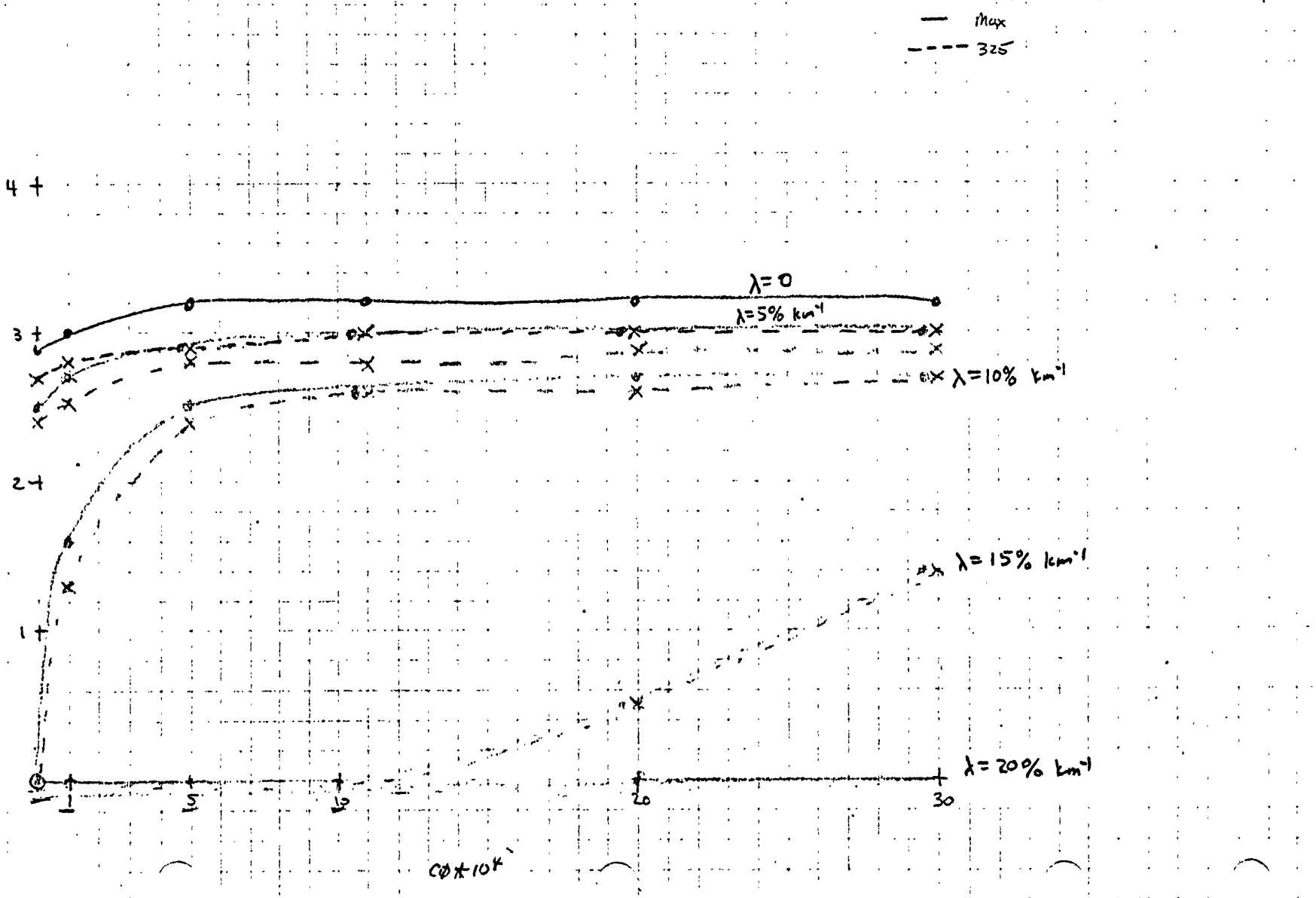

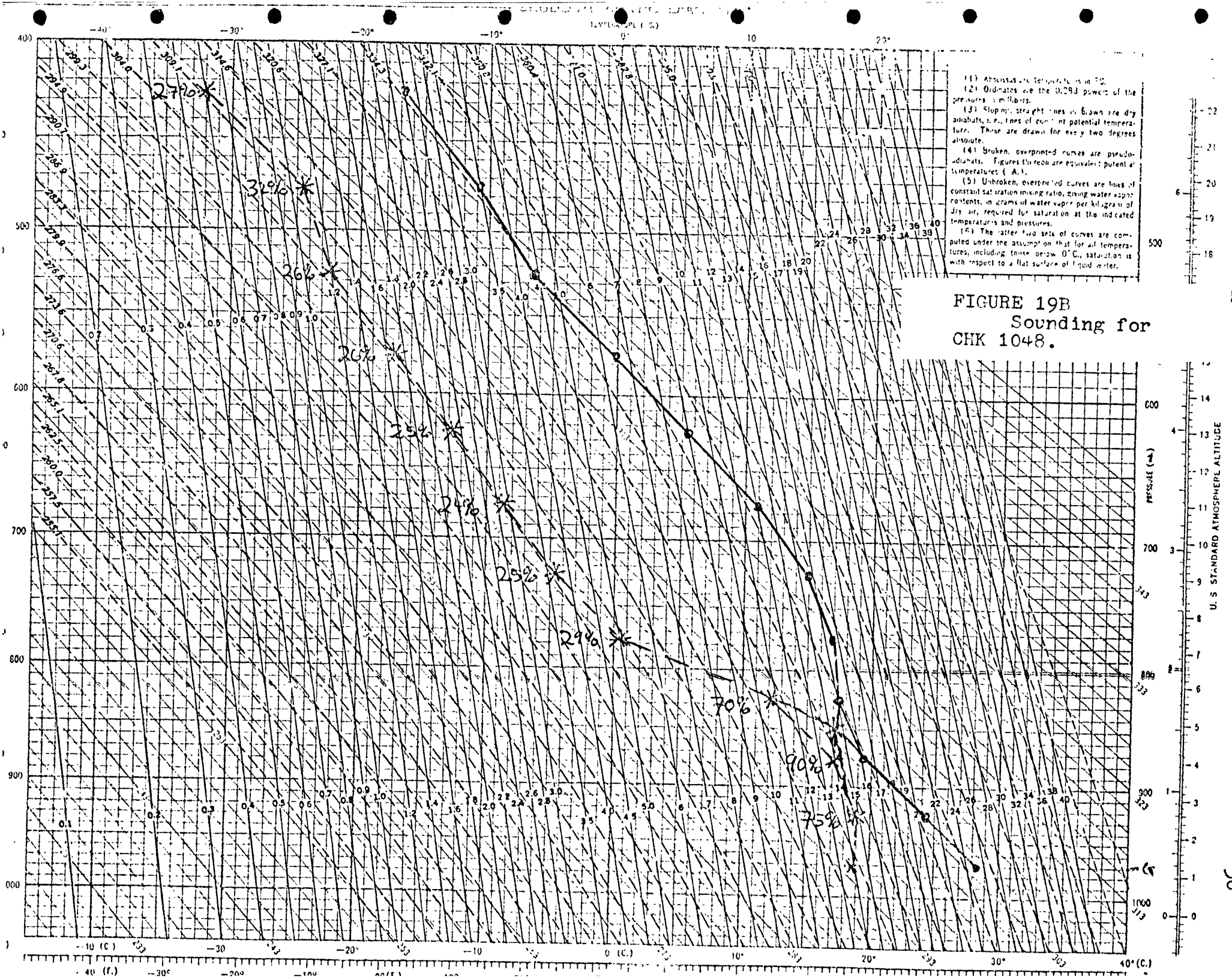

FIGURE 19B
Sounding for
CHK 1048.

FIGURE 20A
Same as figure 17A
except for CHK 1400.

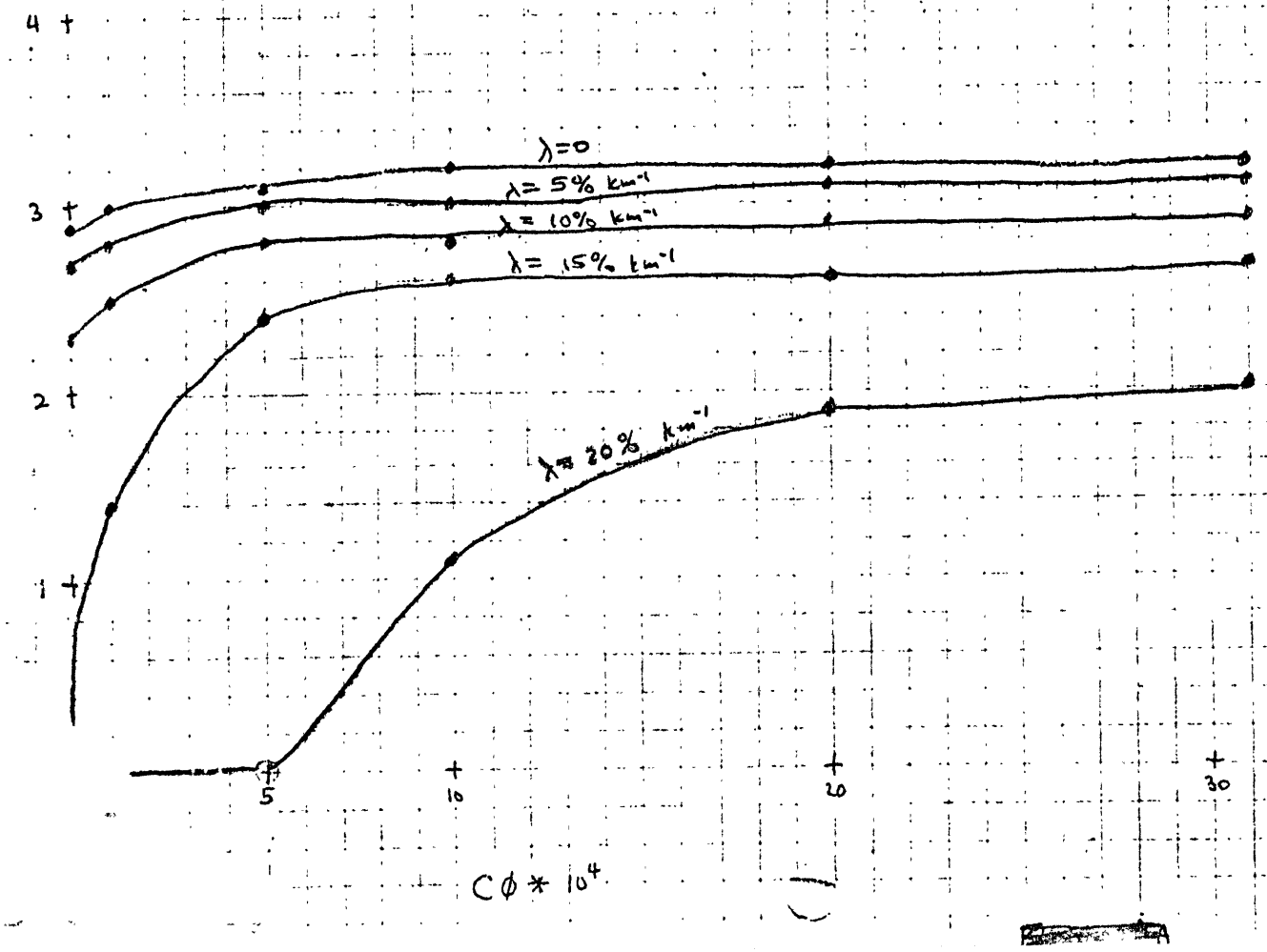

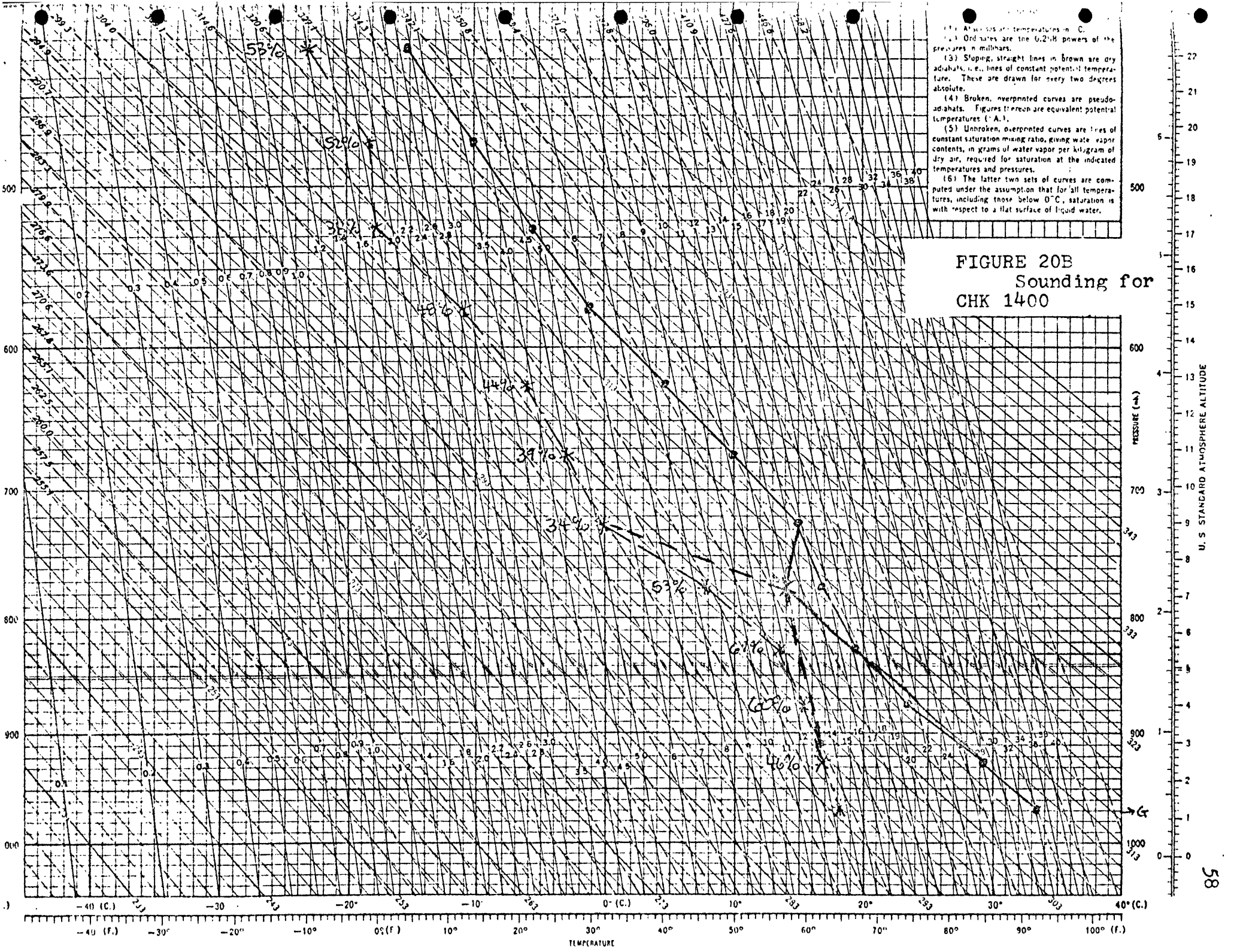

FIGURE 20B
Sounding for
CHK 1400

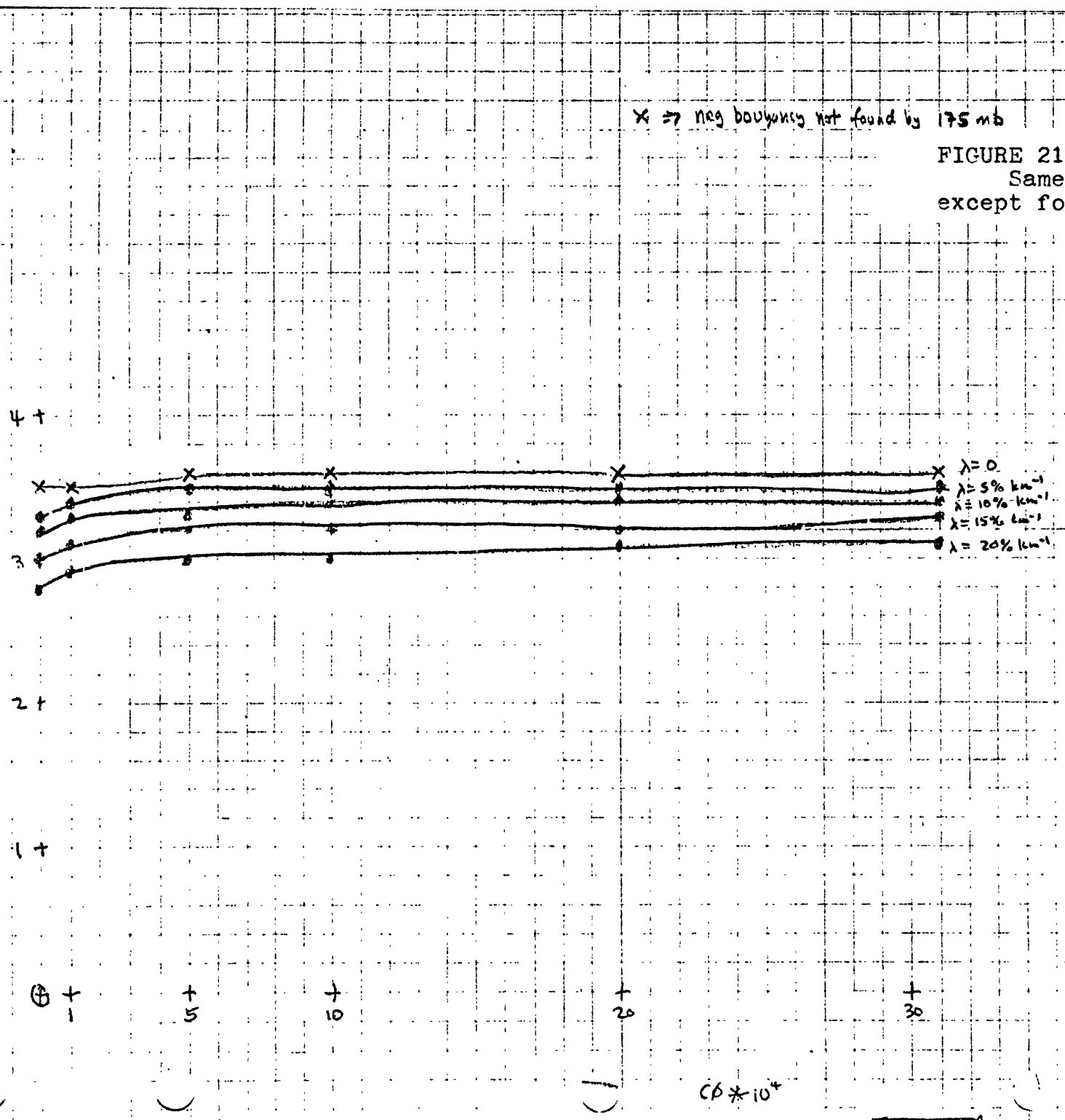

FIGURE 21A
Same as figure 17A except for CHK 1536.

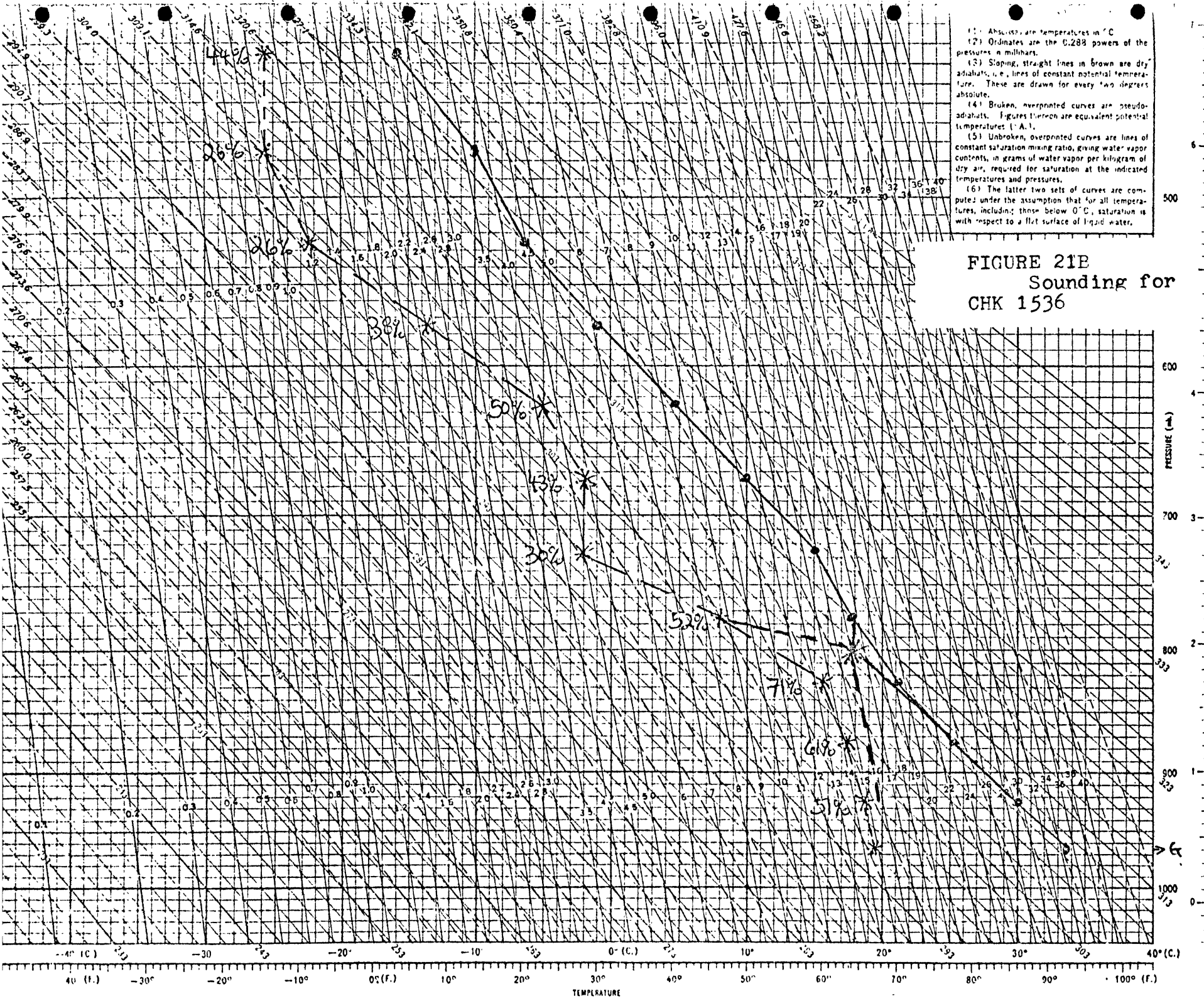

FIGURE 21B
Sounding for
CHK 1536

FIGURE 22A
Same as figure 16A except for WAT 1105, and without data above 325 mb.

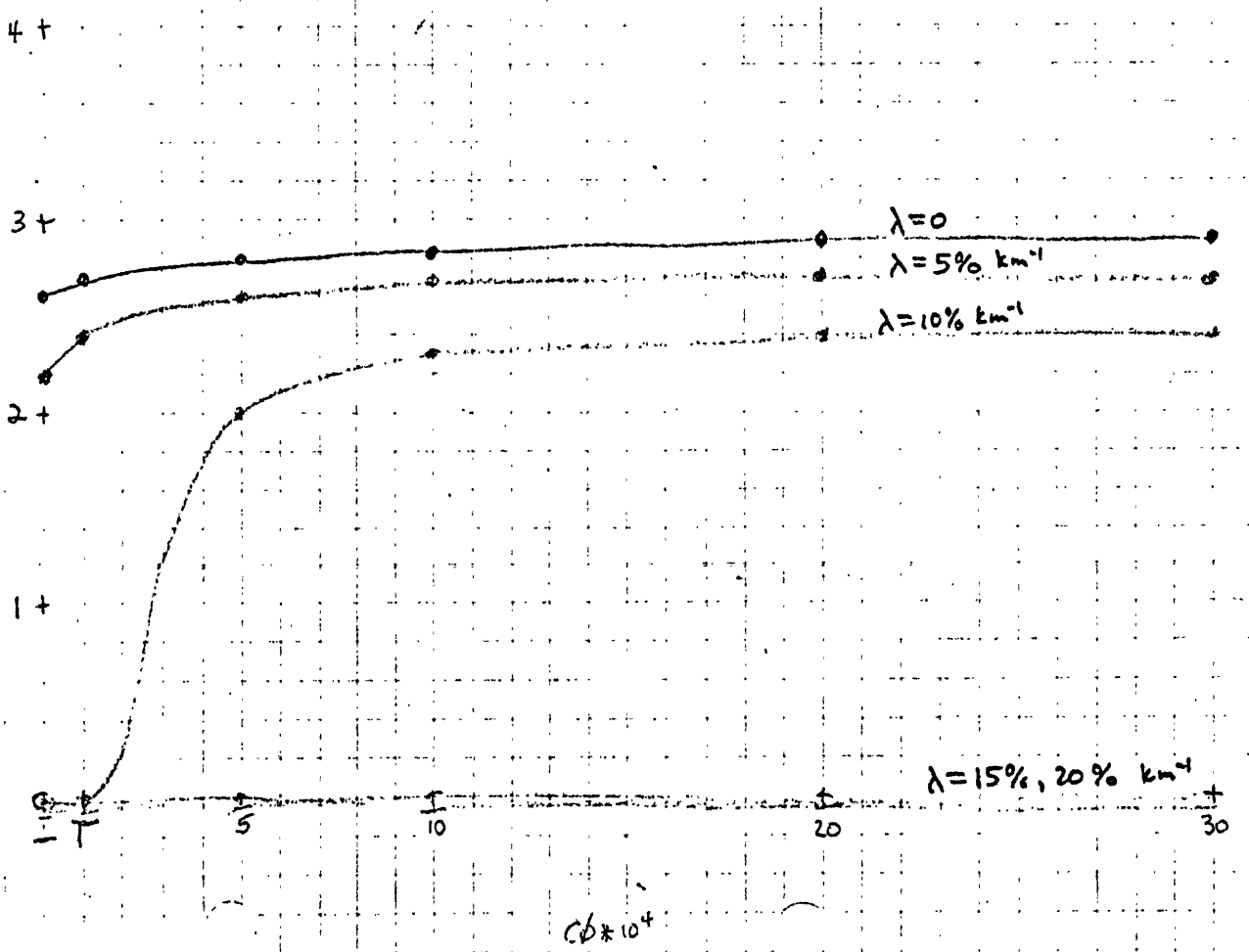

By CWF

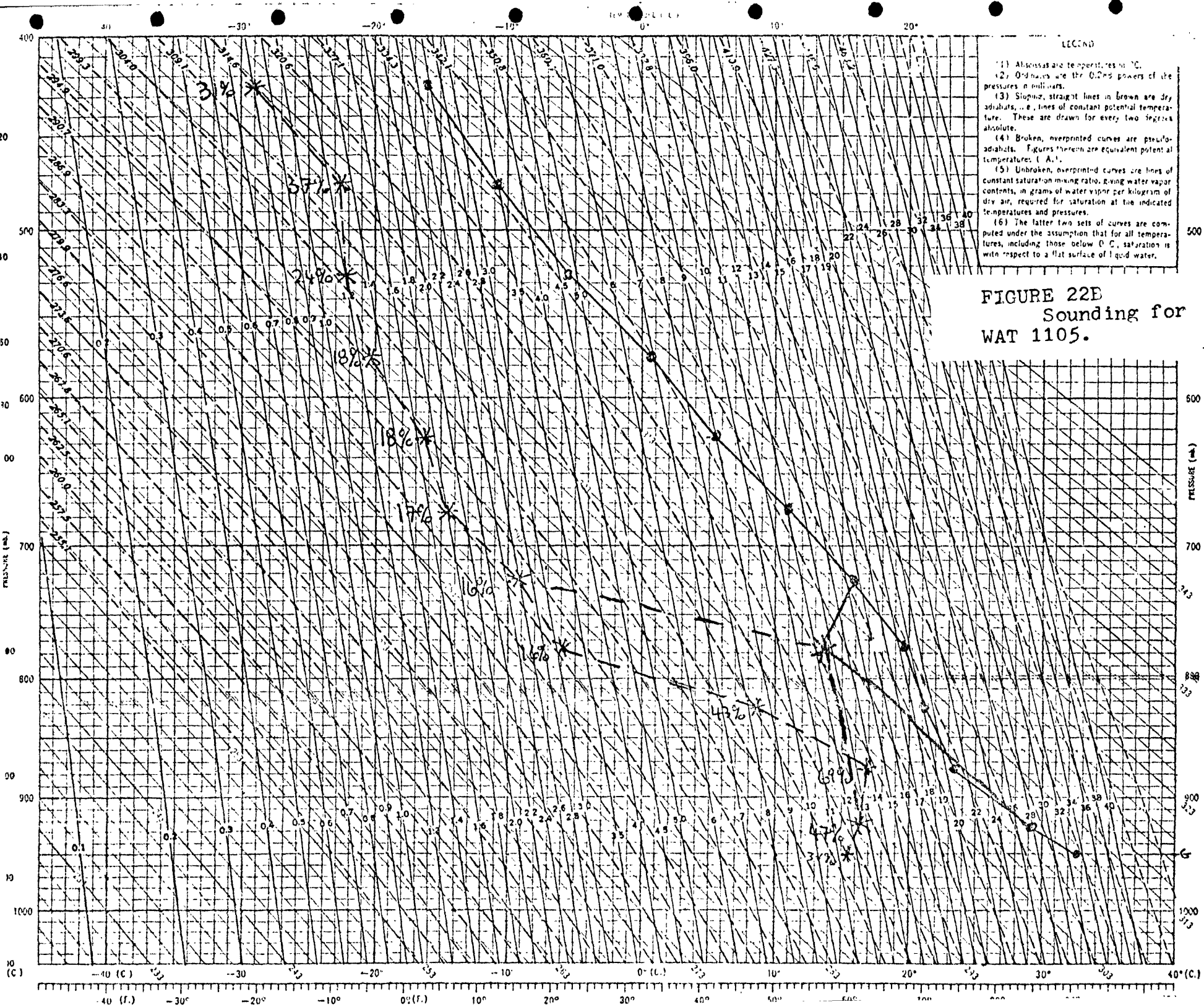
LEGEND
(1) Abscissas are temperatures in °C.
(2) Ordinates are the 0.286 powers of the pressures in millibars.
(3) Sloping, straight lines in brown are dry adiabats, i.e., lines of constant potential temperature. These are drawn for every two degrees absolute.
(4) Broken, overprinted curves are pseudo-adiabats. Figures thereon are equivalent potential temperatures (°A.).
(5) Unbroken, overprinted curves are lines of constant saturation mixing ratio, giving water vapor contents, in grams of water vapor per kilogram of dry air, required for saturation at the indicated temperatures and pressures.
(6) The latter two sets of curves are computed under the assumption that for all temperatures, including those below 0°C, saturation is with respect to a flat surface of liquid water.
FIGURE 22B
Sounding for
WAT 1105.
PRESSURE (mb.)
U. S. STANDARD ATMOSPHERE ALTITUDE
(C.)
(F.)

FIGURE 23A
Same as figure 17A
except for COR 1400.

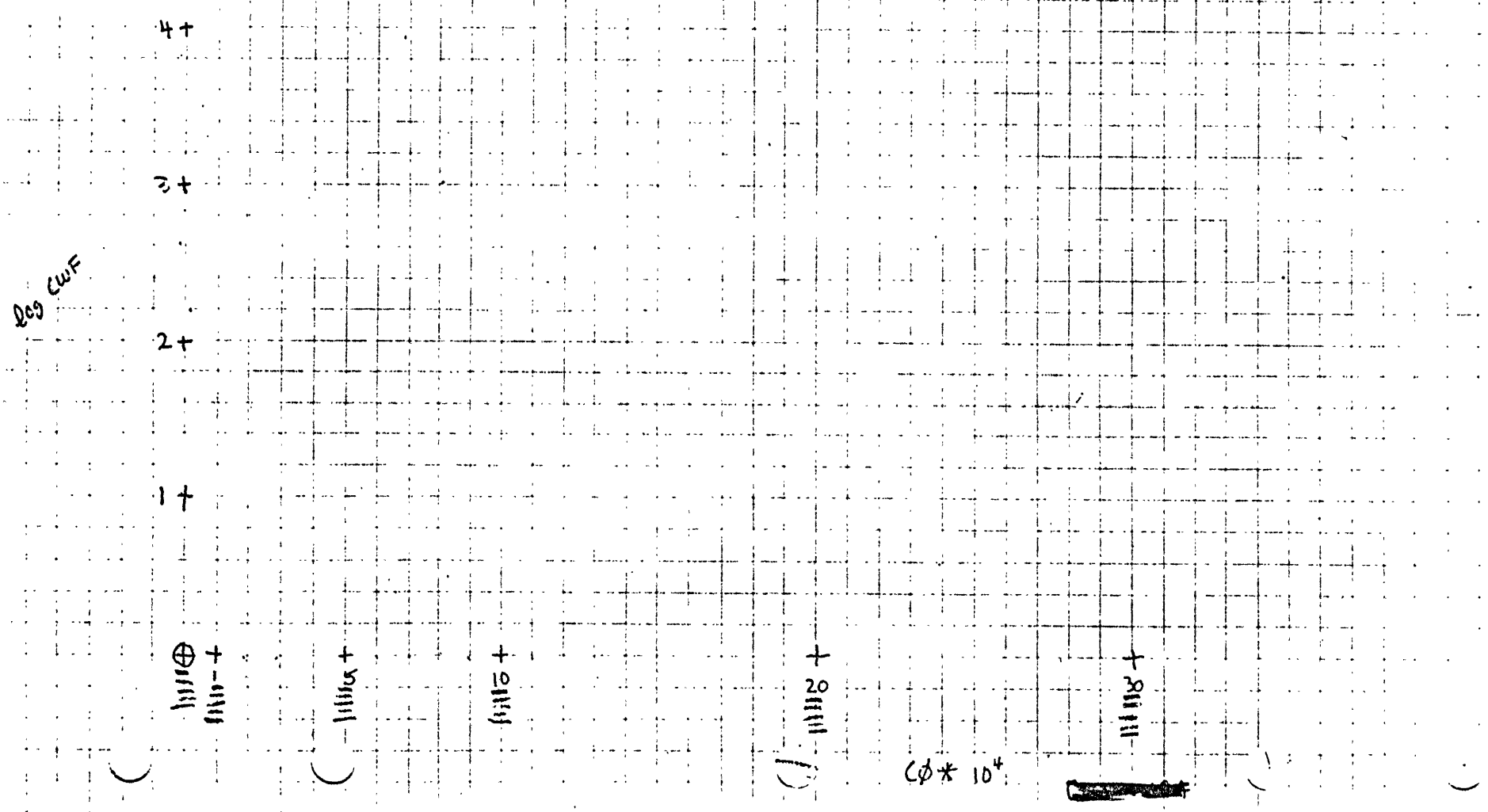
4+
3+
Log CWF
2+
1+
+
+

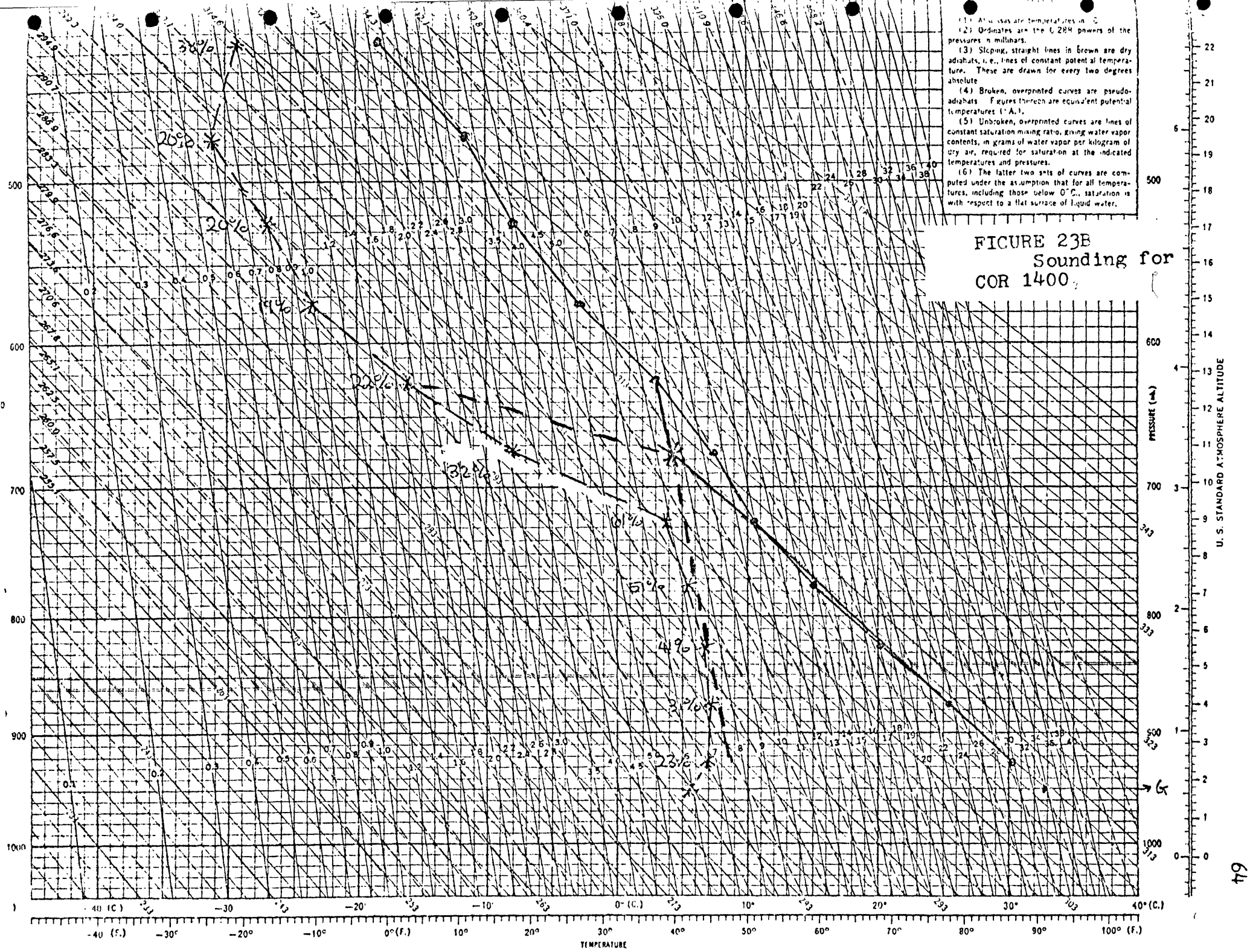

FIGURE 23B
Sounding for
COR 1400

FIGURE 24A
Same as figure 17A
except for WAT 1526.

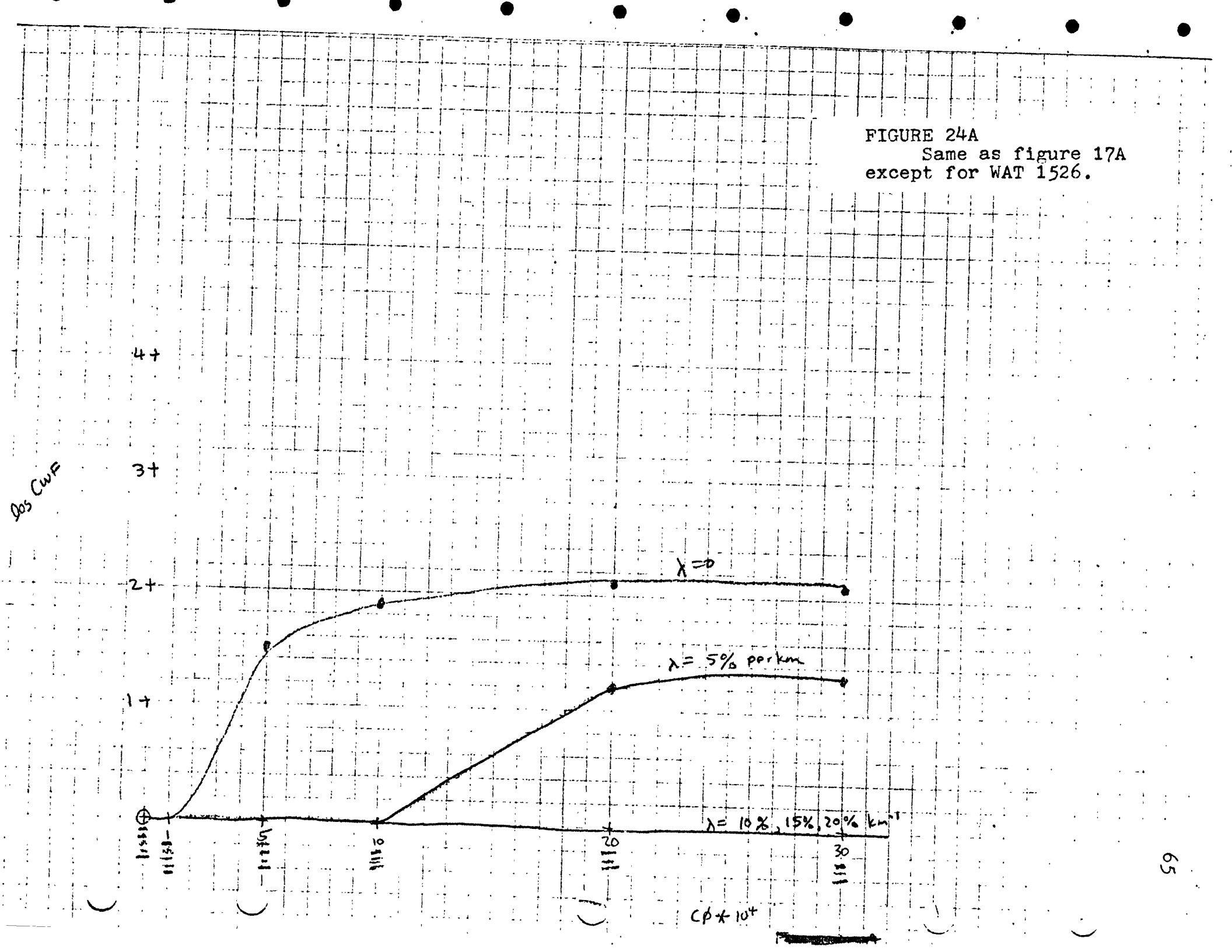

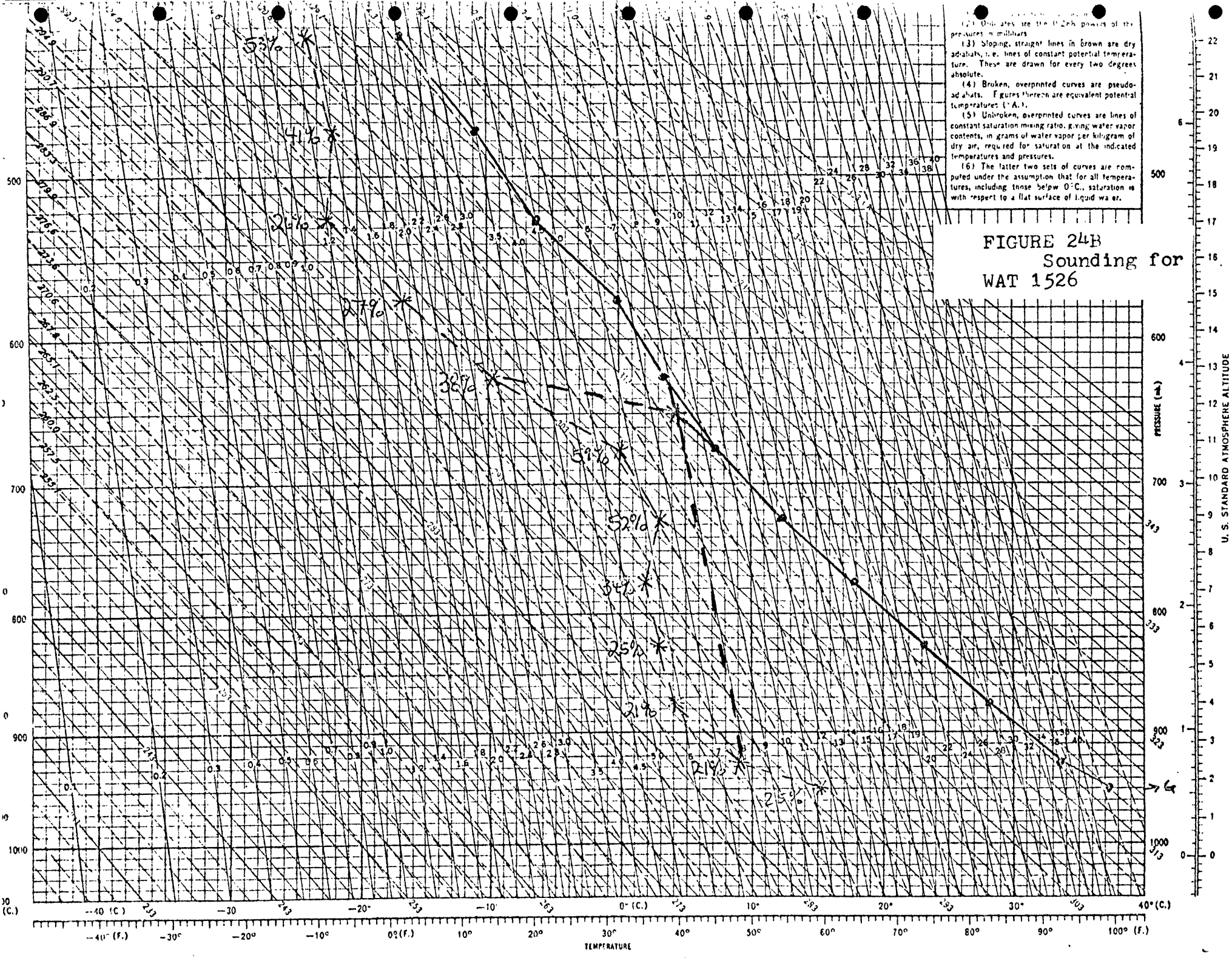
(2) Ordinates are the 0.286 powers of the pressures in millibars.
(3) Sloping, straight lines in brown are dry adiabats, i.e. lines of constant potential temperature. These are drawn for every two degrees absolute.
(4) Broken, overprinted curves are pseudo-adiabats. Figures thereon are equivalent potential temperatures (°A.).
(5) Unbroken, overprinted curves are lines of constant saturation mixing ratio, giving water vapor contents, in grams of water vapor per kilogram of dry air, required for saturation at the indicated temperatures and pressures.
(6) The latter two sets of curves are computed under the assumption that for all temperatures, including those below 0°C., saturation is with respect to a flat surface of liquid water.
FIGURE 24B
Sounding for
WAT 1526
PRESSURE (mb.)
U. S. STANDARD ATMOSPHERE ALTITUDE
TEMPERATURE
-40 (C.)
-30
-20
-10
0° (C.)
10°
20°
30°
40° (C.)
-40° (F.)
-30°
-20°
-10°
0° (F.)
10°
20°
30°
40°
50°
60°
70°
80°
90°
100° (F.)

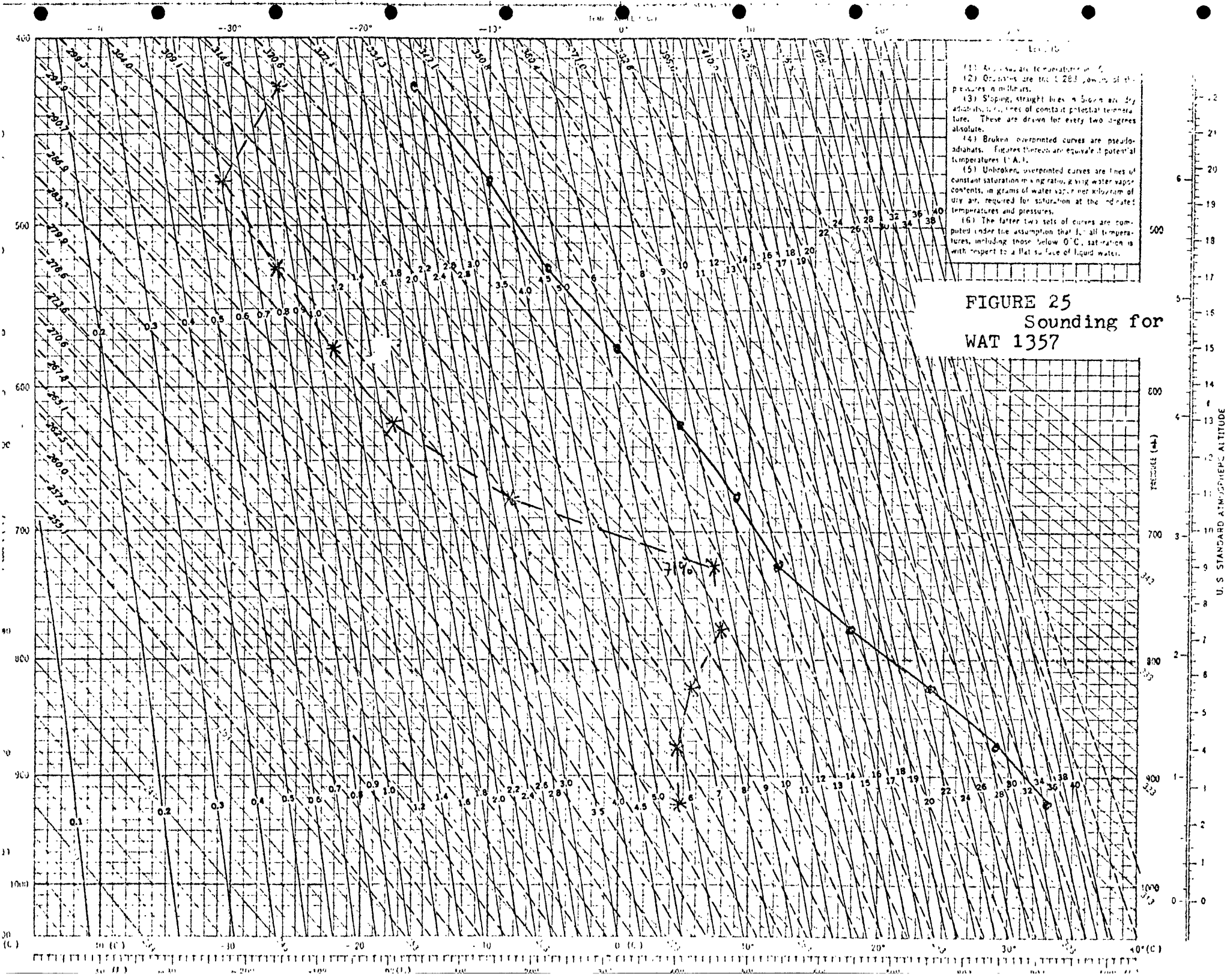

FIGURE 25
Sounding for
WAT 1357

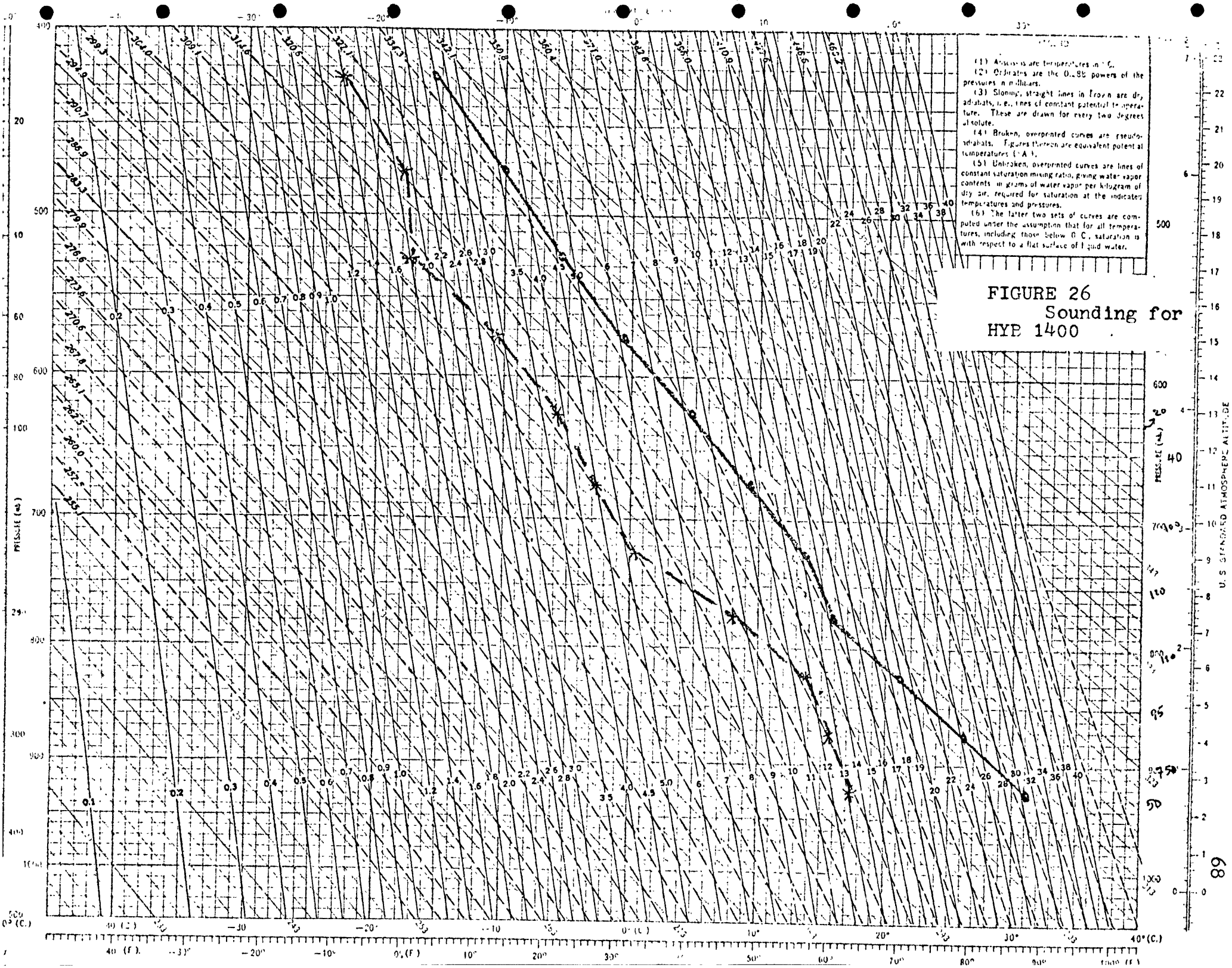

FIGURE 26
Sounding for
HYP 1400

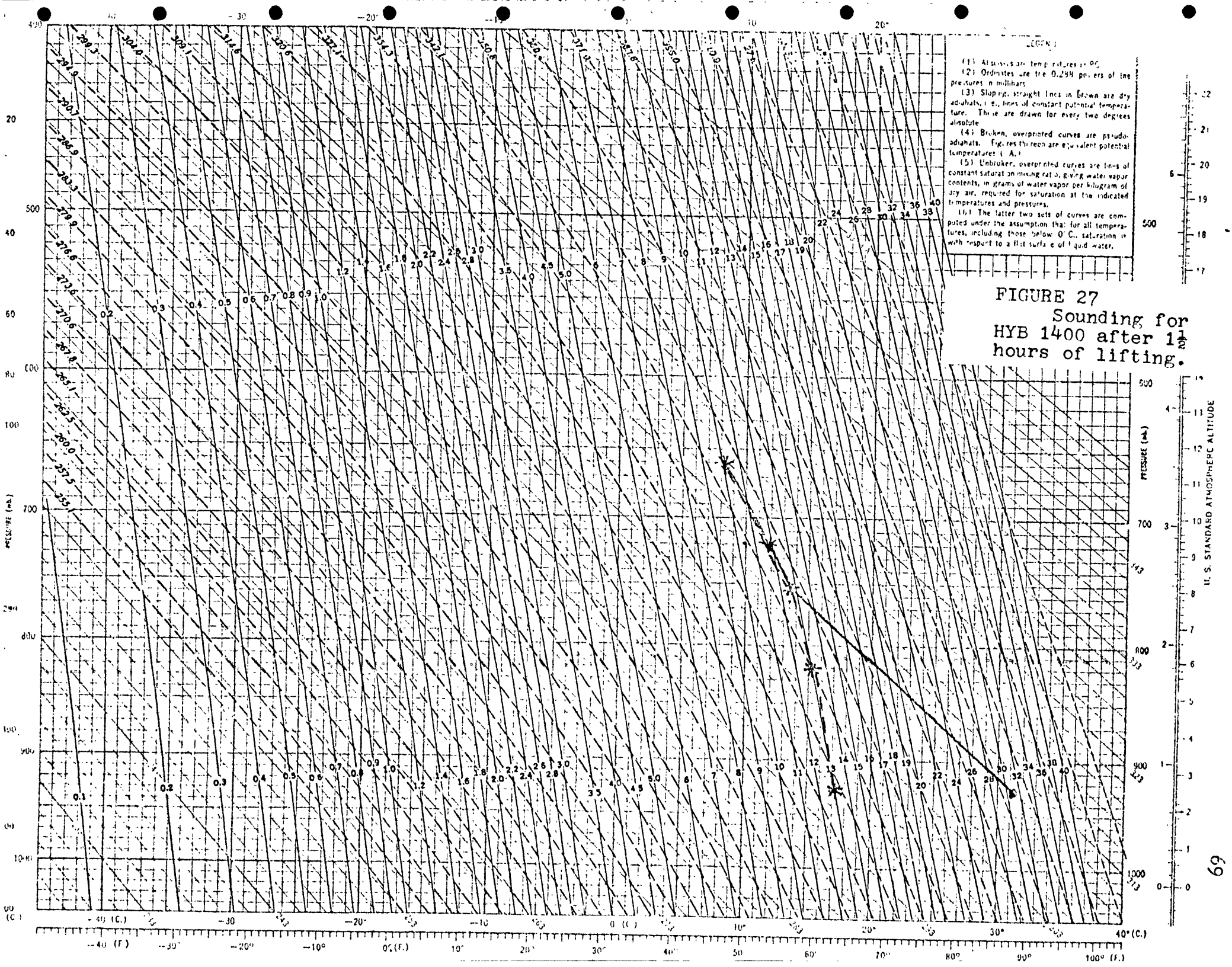

FIGURE 27
Sounding for HYB 1400 after 1½ hours of lifting.

FIGURE 28A
Same as figure 17A
except for HYB 1530

all CWF showed + Bouyancy from Clouds

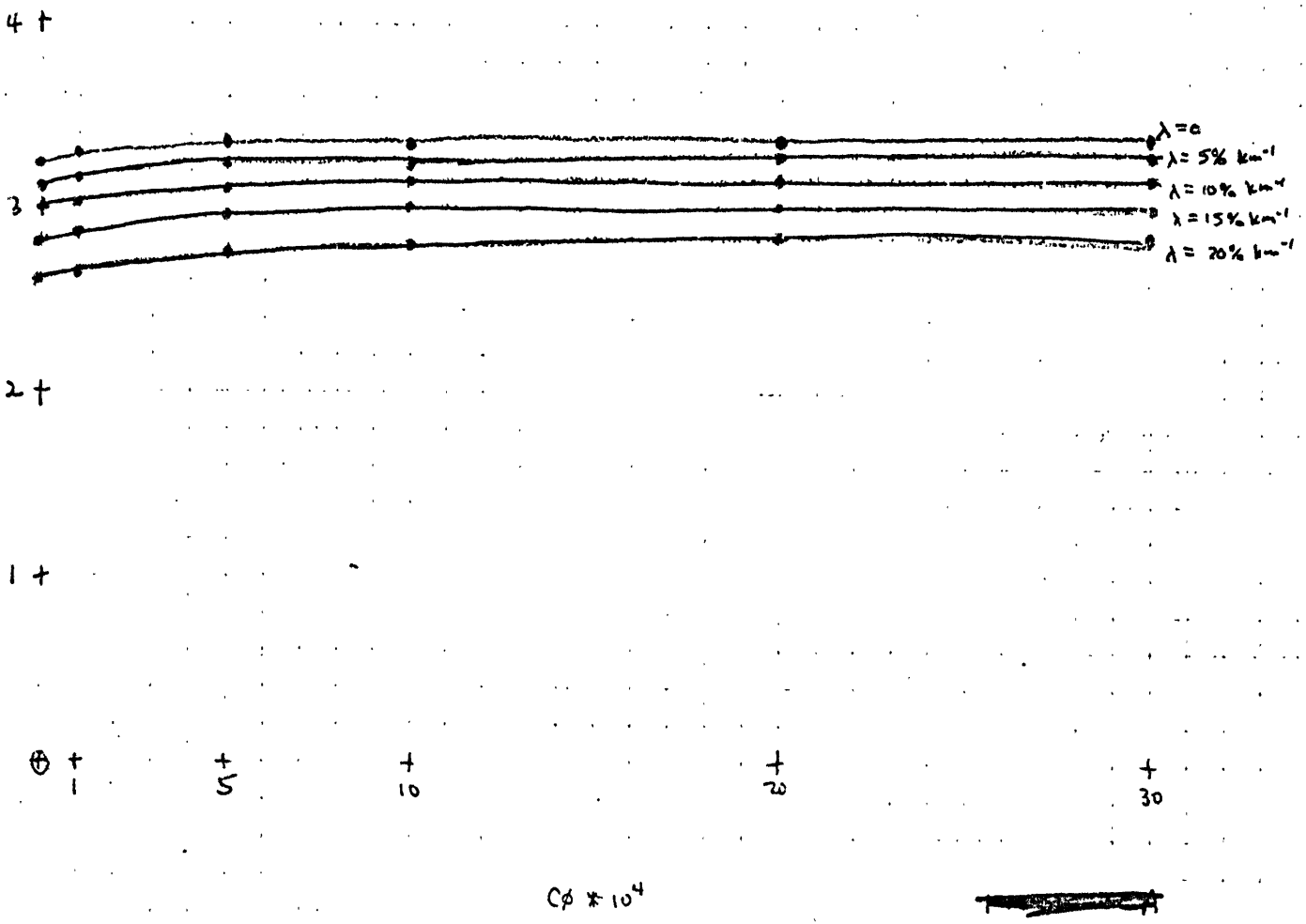

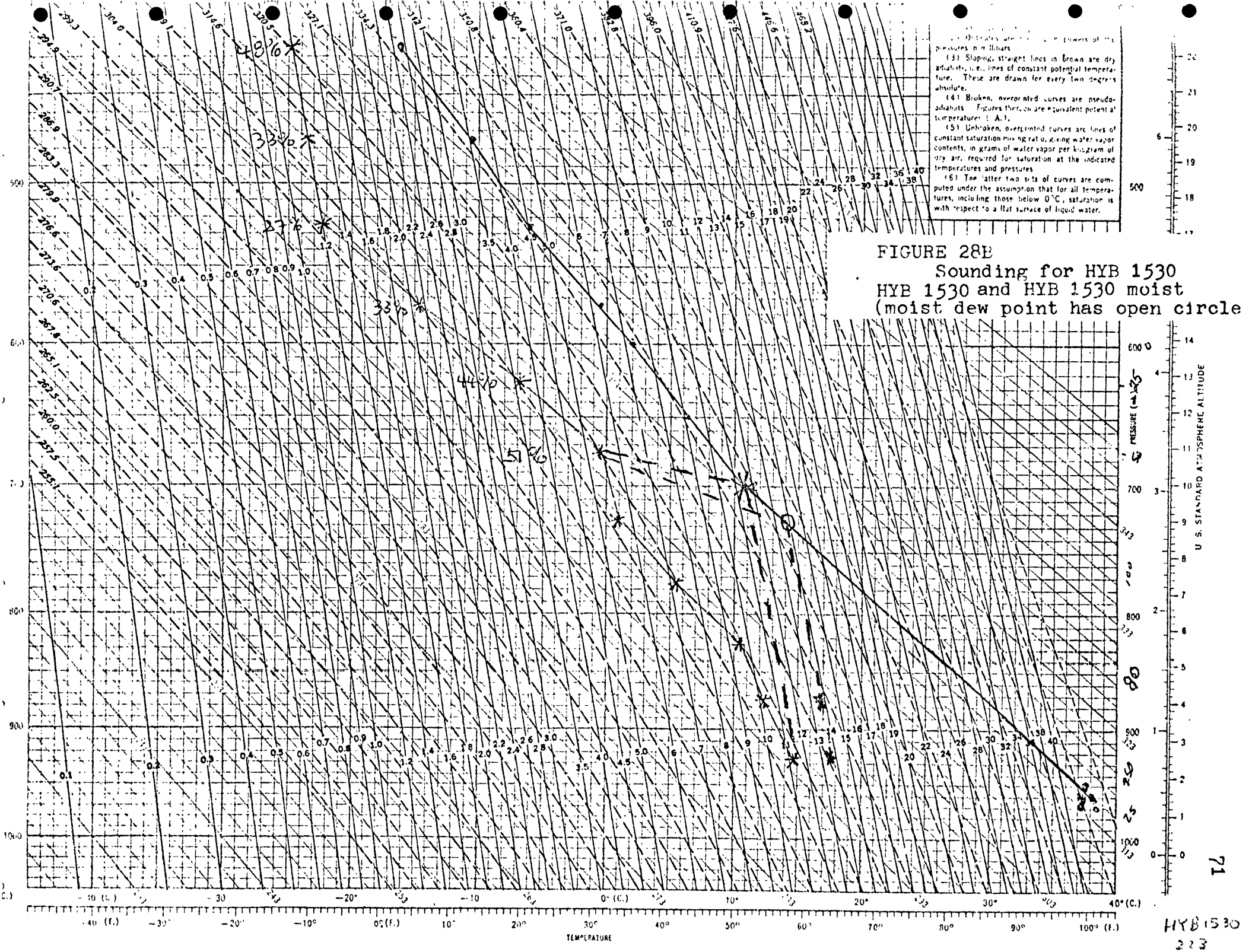

FIGURE 28B
Sounding for HYB 1530
HYB 1530 and HYB 1530 moist
(moist dew point has open circle

HYB 1530
223

FIGURE 28C
Same as figure 17A
except for HYB 1530 moist.

X ⇒ Negative Buoyancy not found

all CWF showed + buoyancy
from cloudbase

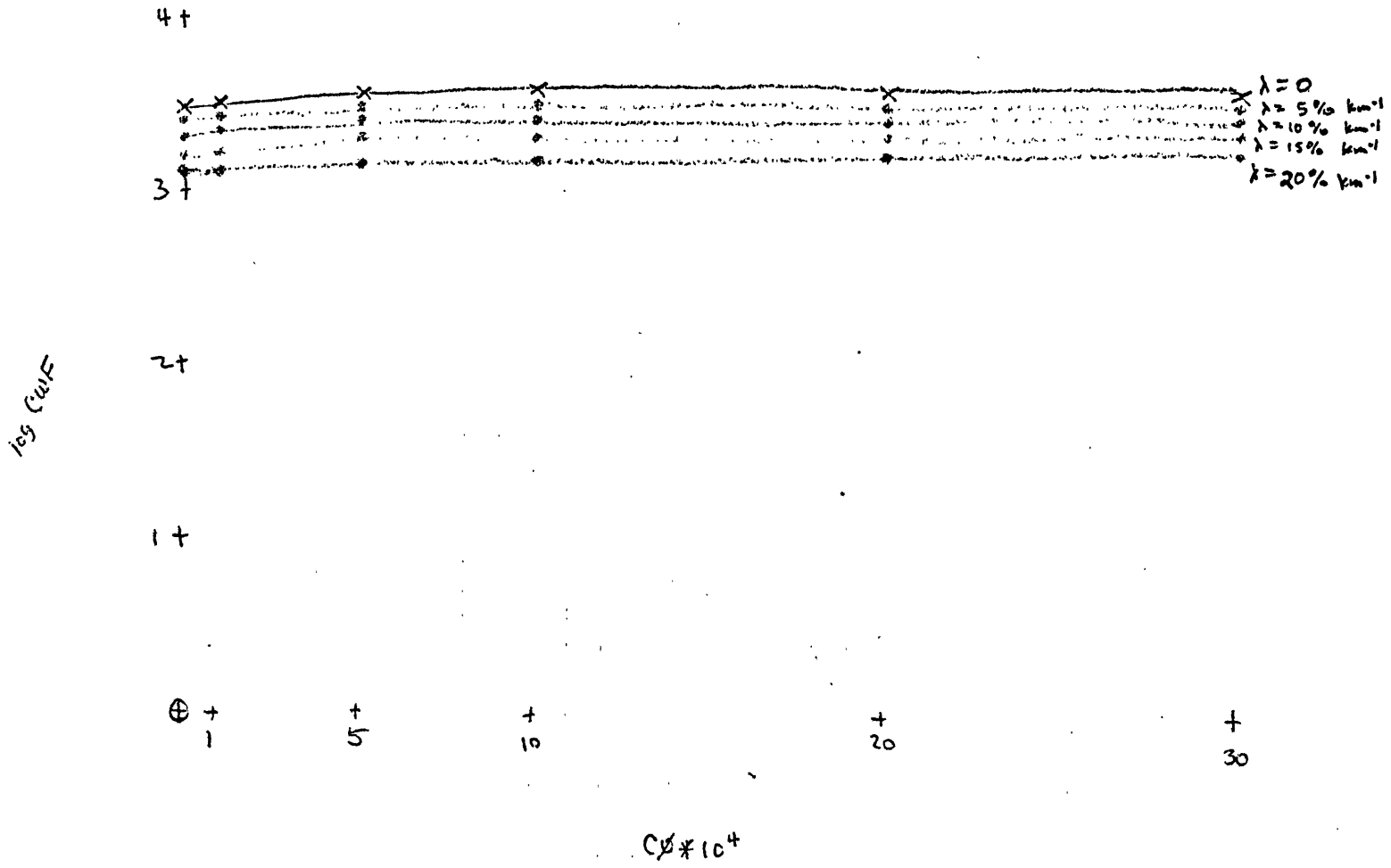

FIGURE 28D
Plot of cloud tops as defined in text for two lambdas, as a function of CØ, for the HYB 1530 and HYB 1530 moist soundings.

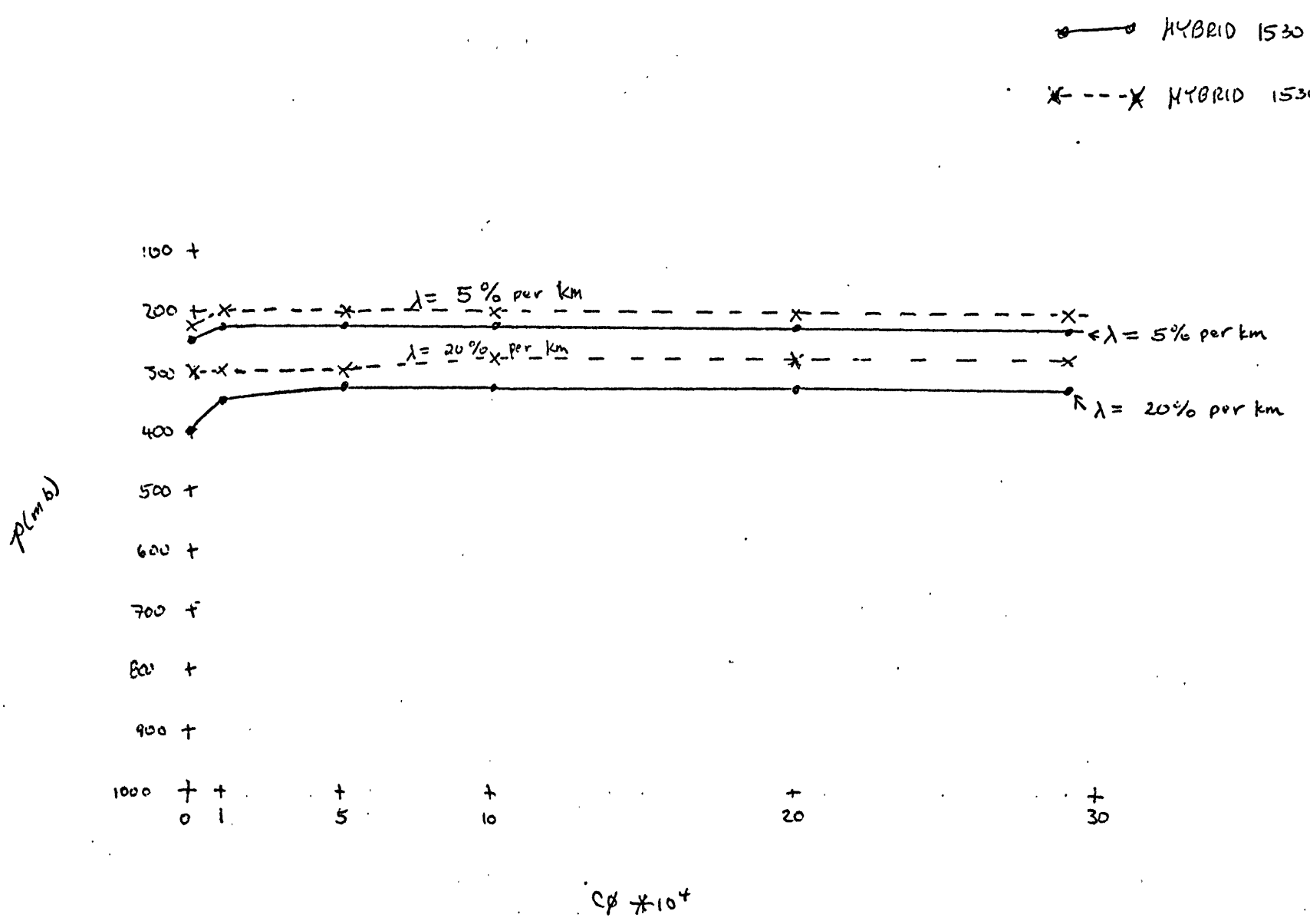

FIGURE 29A
Same as figure 17A
except for LTS 1527
all + bouyant from cloud base

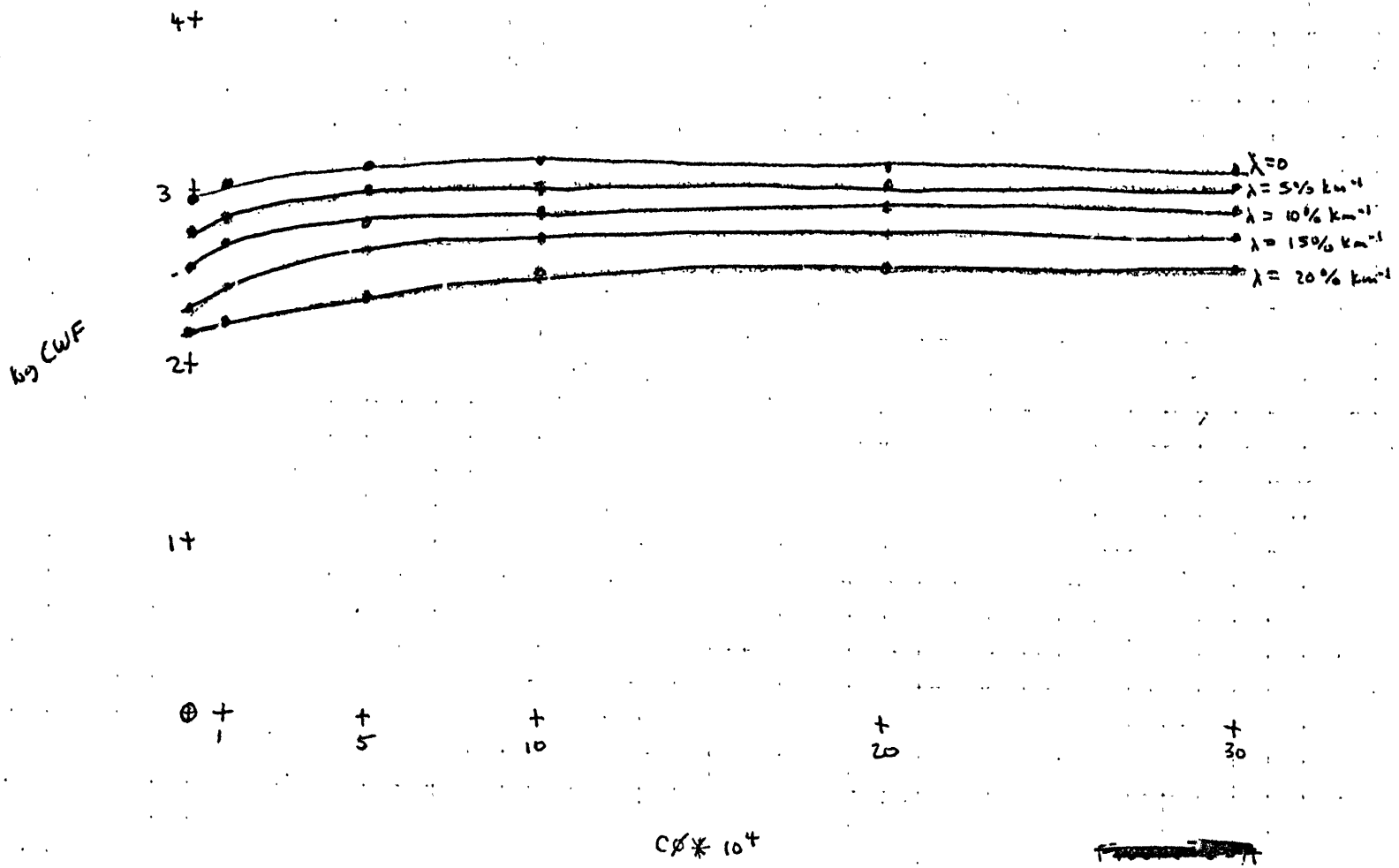

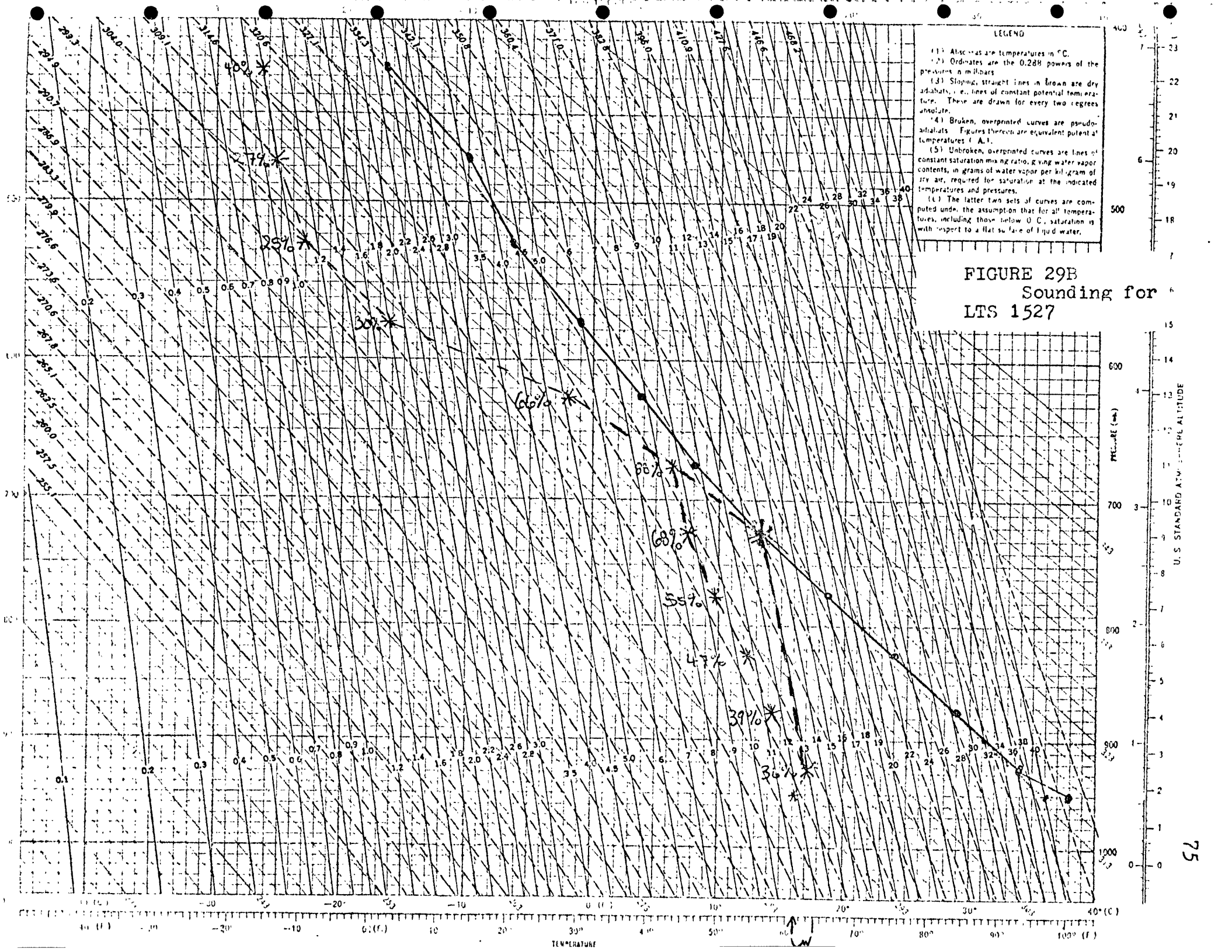

FIGURE 29B
Sounding for
LTS 1527

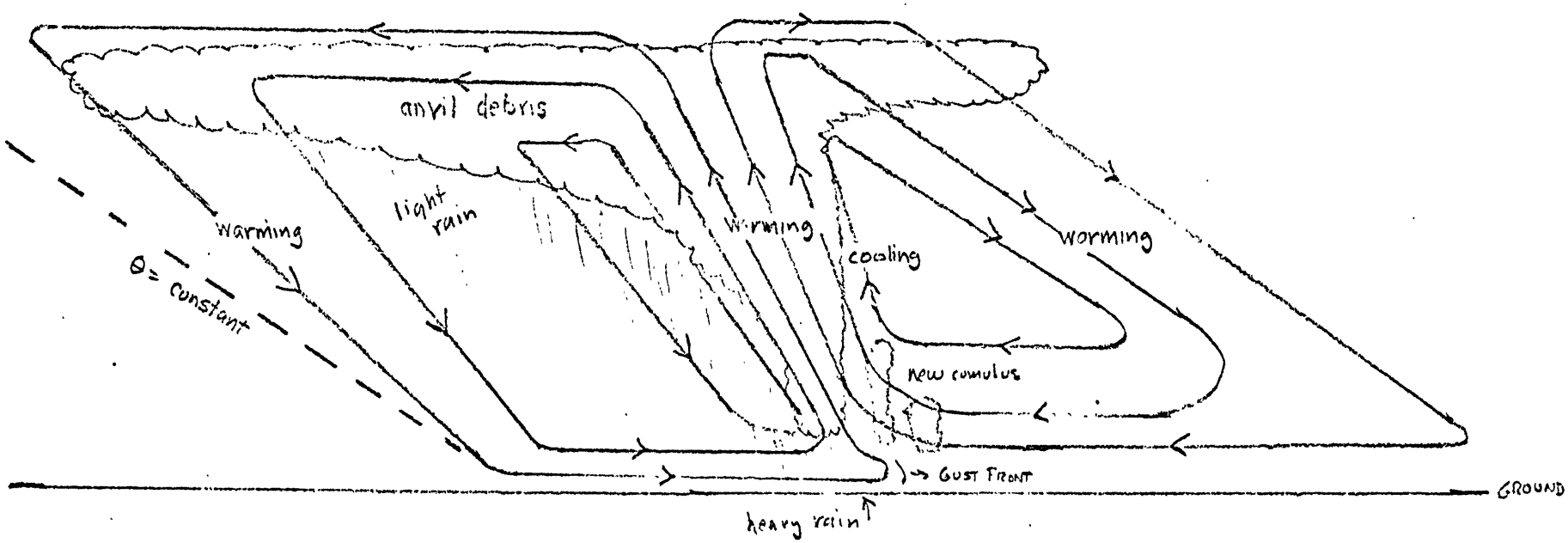

FIGURE 30

Schematic of mesoscale circulation associated with a squall line. Taken from Emanuel (1978). Streamlines are solid curves with arrows. Cloud outline is scalloped. Rain is shaded, the density of which indicates heaviness of rain.

FIGURE 31A
Stability analysis for 1100, 1400 CST.
Areas of $\nabla^2 > 0$ are shaded in black.
Boundary layer analysis meaningless (see Appendix).

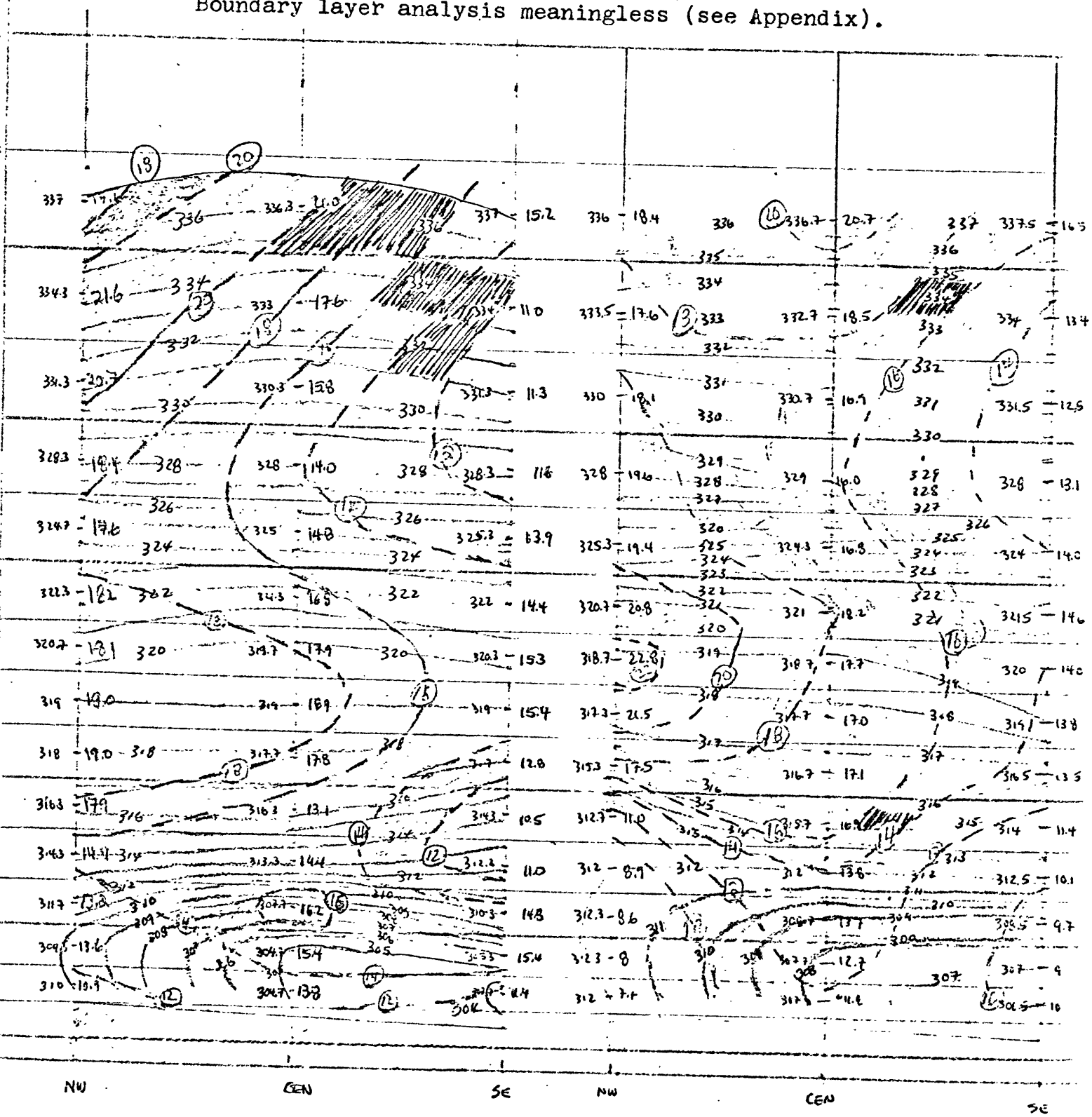

FIGURE 31B
Same as figure 31A, except for 1530, 1700 CST.

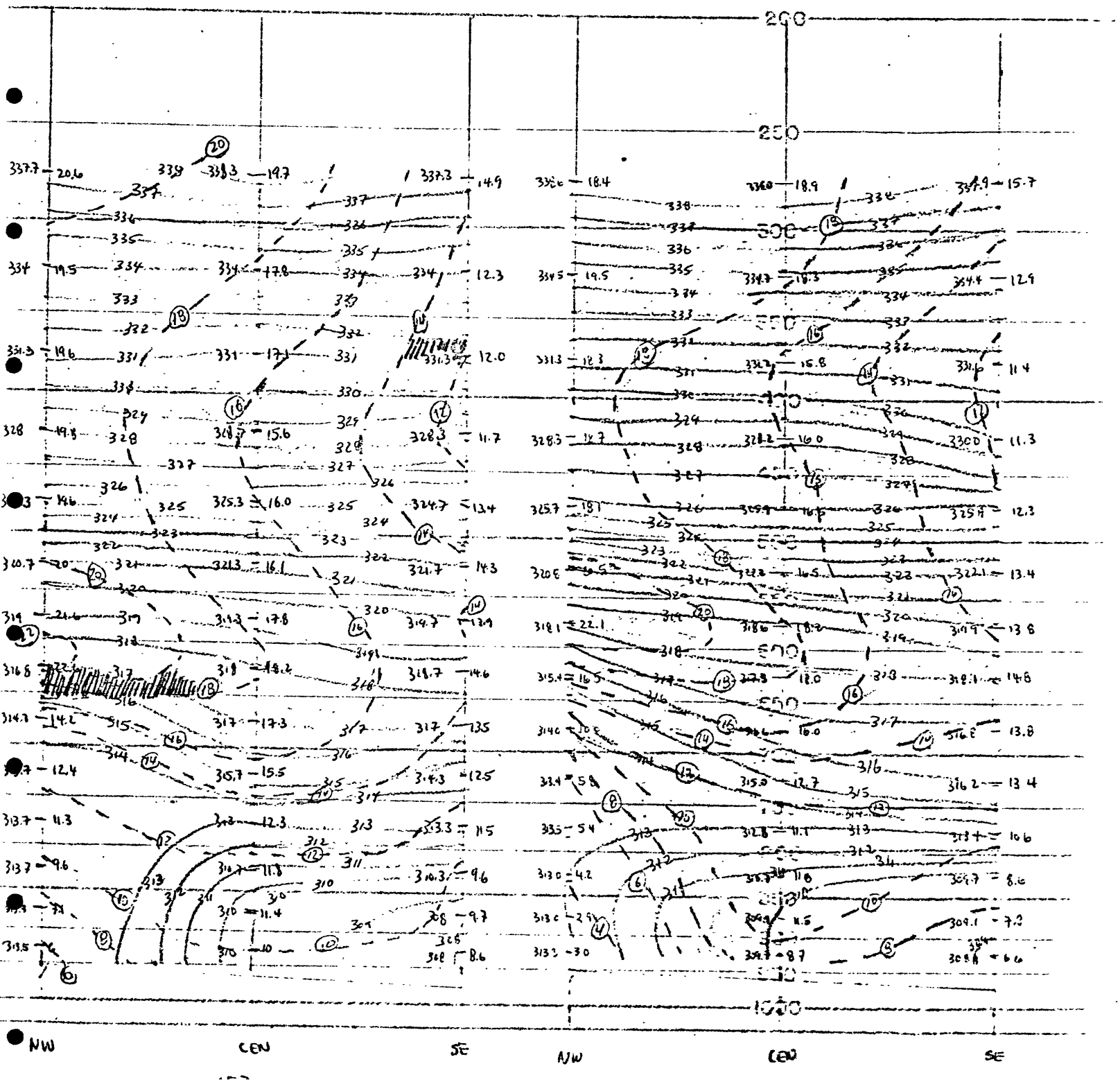

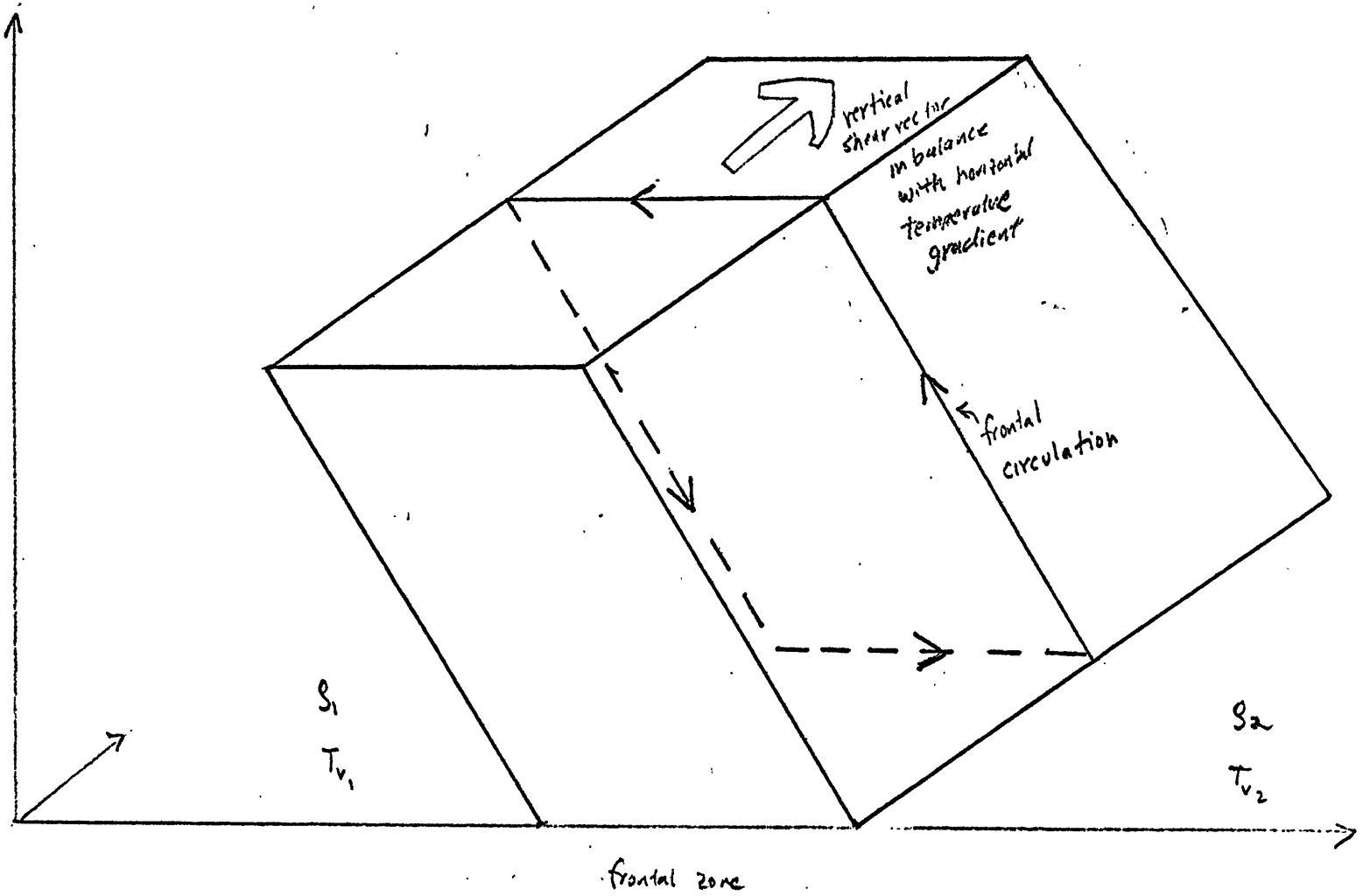

$\rho_1 > \rho_2$

or

$T_{v_1} < T_{v_2}$

FIGURE 32

Sketch of frontal circulation in 3-D. Arrows show direction of flow. Hollow arrow shows sense of vertical shear associated with the horizontal temperature gradient.

FIGURE 33
Time evolution of CWFs for one choice of lambda and CØ. Plotted on a log scale versus time.

λ = 10% per km $C\phi = 2 \times 10^{-3}\ m^{-1}$

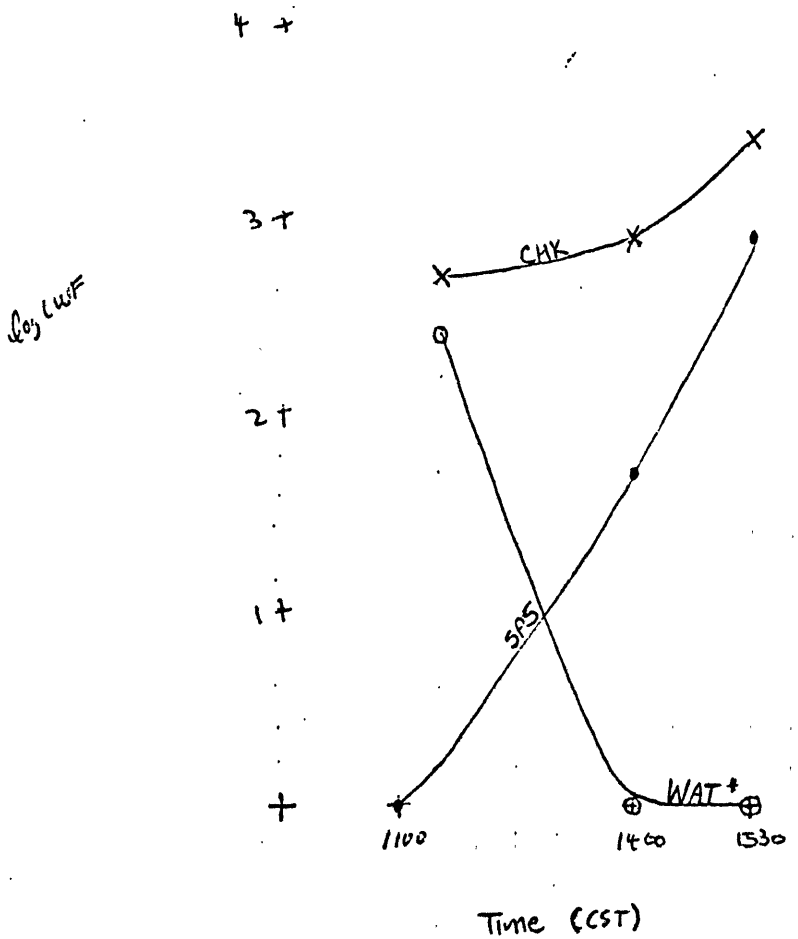

*→ WAT includes COR 1400
Since WAT 1400 was not complete

FIGURE 34
Results of divergence calculation done at 1500 CST. Details are in text.

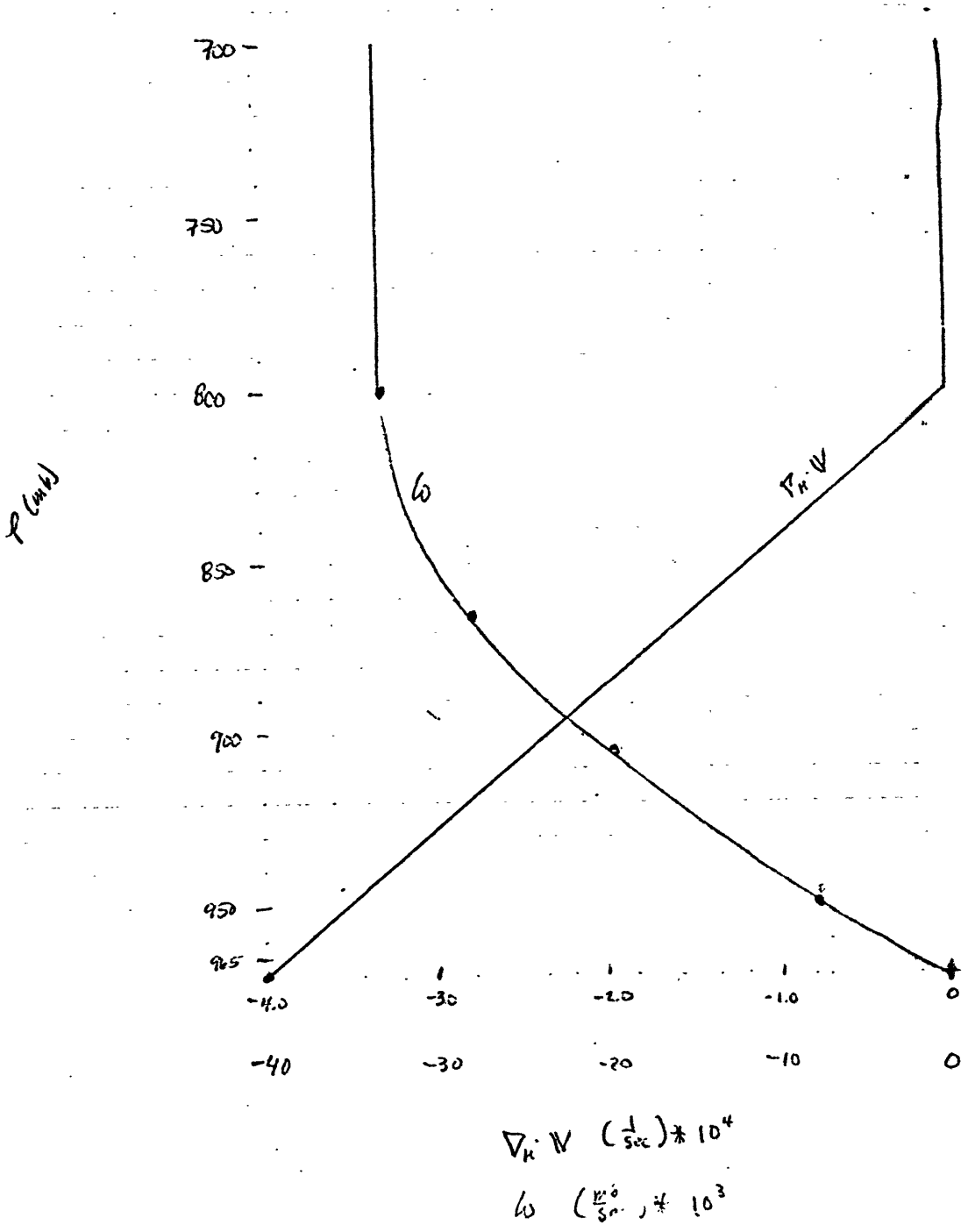

BIBLIOGRAPHY

Anthes, R.A., 1978: "The height of the planetary boundary layer and the production of circulation in a sea breeze model", J.A.S., v. 35, pp 1231-1239.

Arakawa, A., and W.H.Schubert, 1974: "Interaction of a cumulus cloud ensemble with the large-scale environment", Part I, J.A.S., v. 31, pp 674-701.

Barnes, S.L.,J.H.Henderson, and R.J.Ketchum, 1971: Rawinsonde Observation and Processing Techniques at the National Severe Storms Laboratory, NOAA technical Memorandum, ERL NSSL-53.

Eisen, P.A., 1972: "A mesoscale study of the Oklahoma squall line of 8 and 9 June 1966", M.S. Thesis, Dept. of Meteorology, Pennsylvania State University, 88pp.

Emanuel, K., 1978: "Inertial stability and mesoscale convective systems", Ph.D. thesis, Dept. of Meteorology, M.I.T., 207pp.

Fankhauser, J.C., 1974: "The derivation of consistent fields of wind and geopotential height from mesoscale rawinsonde data", J.A.M., v. 13, pp 637-646.

Hoskins, B.J., and F.P. Bretherton, 1972: "Atmospheric frontogenesis models: mathematical formulation and solution", J.A.S., v. 29, pp 11-37.

Johnson, et al., 1977: "In site measurement of moist adiabatic ascent in developing cumulus congestus in northeastern Colorado by coordinated instrumented aircraft", Preprints of the 10th conference on Severe Local Storms, Omaha, pp. 120-125.

Lewis, J.M.,S.C. Bloom and J.D. Gray, 1976: "Organization of a prefrontal squall line by mesoscale processes", Preprints of the 6th Conference on Weather Forecasting and Analysis, Albany, pp 213-220.

Ogura, Y. and Y.-L. Chen: "A life history of an intense mesoscale convective storm in Oklahoma", J.A.S., v 34, pp 1458-1476.

Raymond, O.J., 1977: "Instability of the low level jet and severe storm formation", Preprints of the 10th Conference on Severe Local Storms, Omaha, pp. 515-520.

Schaeffer, J.T., 1975: "Nonlinear, biconstituent diffusion; a possible trigger of convection", J.A.S., v.32, pp. 2278-2284.

Silverman, B.A. and M. Glass: "A numerical simulation of warm cumulus clouds: part I, parameterization vs non-parameterization of micro physics", J.A.S., v. 30, p1620.

Tepper, M. 1950: "A proposed mechanism of squall lines: the pressure jump line," Journal of Meteorology, v. 7, pp 21-29.

Teweles, S. 1970: "A spurious diurnal variation in radiosonde humidity records", Bulletin of the A.M.S., v. 51, pp 836-840.